

#### LIBRARY Michigan State University

This is to certify that the dissertation entitled

## NONLINEAR RESONANT PHENOMENA IN MULTILEVEL QUANTUM SYSTEMS

presented by

**Christian Hicke** 

has been accepted towards fulfillment of the requirements for the

Ph.D. degree in Physics & Astronomy

G. Dyburau

Major Professor's Signature

04/15/2008

Date

MSU is an affirmative-action, equal-opportunity employer

**PLACE IN RETURN BOX** to remove this checkout from your record. **TO AVOID FINES** return on or before date due. **MAY BE RECALLED** with earlier due date if requested.

| DATE DUE | DATE DUE | DATE DUE |
|----------|----------|----------|
|          |          |          |
|          |          |          |
|          |          |          |
|          |          |          |
|          |          |          |
|          |          |          |
|          |          |          |
| A        | -        |          |
|          |          |          |
|          |          |          |
|          |          |          |

5/08 K:/Proj/Acc&Pres/CIRC/DateDue indd

## NONLINEAR RESONANT PHENOMENA IN MULTILEVEL QUANTUM SYSTEMS

By

Christian Hicke

#### A DISSERTATION

Submitted to
Michigan State University
in partial fulfillment of the requirements
for the degree of

DOCTOR OF PHILOSOPHY

Department of Physics and Astronomy

2008

#### ABSTRACT

## NONLINEAR RESONANT PHENOMENA IN MULTILEVEL QUANTUM SYSTEMS

By

#### Christian Hicke

We study nonlinear resonant phenomena in two-level and multilevel quantum systems. Our results are of importance for applications in the areas of quantum control, quantum computation, and quantum measurement.

We present a method to perform fault-tolerant single-qubit gate operations using Landau-Zener tunneling. In a single Landau-Zener pulse, the qubit transition frequency is varied in time so that it passes through the frequency of a radiation field. We show that a simple three-pulse sequence allows eliminating errors in the gate up to the third order in errors in the qubit energies or the radiation frequency.

We study the nonlinear transverse response of a spin S > 1/2 with easy-axis anisotropy. The coherent transverse response displays sharp dips or peaks when the modulation frequency is adiabatically swept through multiphoton resonance. The effect is a consequence of a certain conformal property of the spin dynamics in a magnetic field for the anisotropy energy  $\propto S_z^2$ . The occurrence of the dips or peaks is determined by the spin state. Their shape strongly depends on the modulation amplitude. Higher-order anisotropy breaks the symmetry, leading to sharp steps in

the transverse response as function of frequency. The results bear on the dynamics of molecular magnets in a static magnetic field.

We show that a modulated large-spin system has special symmetry. In the presence of dissipation it leads to characteristic nonlinear effects. They include abrupt switching between transverse magnetization branches with varying modulating field without hysteresis and a specific pattern of switching in the presence of multistability and hysteresis. Along with steady forced vibrations the transverse spin components can display transient vibrations at a combination of the Larmor frequency and a slower frequency determined by the anisotropy energy. The analysis is based on a microscopic theory that takes into account relaxation mechanisms important for single-molecule magnets and other large-spin systems. We find how the Landau-Lifshitz model should be modified in order to describe the classical spin dynamics. The occurrence of transient oscillations depends on the interrelation between the relaxation parameters.

We extend the analysis to the quantum regime by developing a formalism which allows to transform the system's quantum kinetic operator equation into a partial differential equation of motion of the system's probability density distribution in the spin coherent state representation. Using the spin density distribution, we analyze the quantum corrections of classical limit cycles. We show that the stationary distribution of the system coincides with the positions of stable stationary states in the semiclassical limit. We discuss the mechanism of quantum activation and show that it leads to switching in the system, where the transition between globally stable states happens in a comparatively small range of the parameter space. We analyze the quantum behavior of switching in the absence of hysteresis and Hamiltonian-like dynamics.

#### ACKNOWLEDGMENTS

I would like to express my deep gratitude to my advisor and teacher Mark Dykman for his outstanding support during the last five years at Michigan State University. Apart from having been a constant source of insight into scientific techniques at the highest level, Mark was always very supportive in personal matters, for which I am very grateful.

I would also like to thank my Dissertation Committee members, Norman Birge, Bhanu Mahanti, Carlo Piermarocchi, and C.-P. Yuan, who have been enthusiastic about my work and helpful with their comments.

The staff at the Physics and Astronomy Department and at the Office for International Students and Scholars helped to make the stay at Michigan State University a very pleasant experience.

Many thanks go to Dmitry Ryvkin and Lea Santos, with whom I was lucky to share the office as well as to my long-time roommate, Johannes Grote, without whom the time in Michigan would have been only half the fun.

Special thanks go to my wife, Mina, my son, Marvin, and my parents, Gabriele and Hans-Georg, my brothers, Martin and Konstantin, my parents-in-law, Young Ja Kim and Suk Doo Yoon, and all my friends and family members in East Lansing, back in Germany, and in many other corners of the world for all the beautiful moments in between.

## TABLE OF CONTENTS

| LIST OF FIGURES                                                      |           |  |
|----------------------------------------------------------------------|-----------|--|
| 1 Introduction                                                       | 1         |  |
| 2 Fault-Tolerant Landau-Zener Quantum Gates                          | 9         |  |
| 2.1 Introduction                                                     | 9         |  |
| 2.2 Landau-Zener transformation in the modified adiabatic basis      | 12        |  |
| 2.3 Rotation matrix representation                                   | 16        |  |
| 2.4 Composite Landau-Zener pulses                                    | 18        |  |
| 2.4.1 Error compensation with $\pi$ -pulses                          | 19        |  |
| 2.4.2 Maximal error of the three-pulse sequence                      | 22        |  |
| 2.5 Conclusions                                                      | 25        |  |
| 3 Multiphoton Antiresonance in Large-Spin Systems                    | 28        |  |
| 3.1 Introduction                                                     | 28        |  |
| 3.2 Low-field susceptibility crossing                                | 32        |  |
| 3.2.1 The quasienergy spectrum                                       | 32        |  |
| 3.2.2 Susceptibility and quasienergy crossing                        | 35        |  |
| 3.3 Antiresonance of the transverse multiphoton response             | 36        |  |
| 3.3.1 Two-photon resonance                                           | 40        |  |
| 3.4 Susceptibility crossing for a semiclassical spin                 | 41        |  |
| 3.4.1 Conformal property of classical trajectories                   | 43        |  |
| 3.4.2 The WKB picture in the neglect of tunneling                    | 44        |  |
| 3.5 Degeneracy lifting by higher order terms in $S_z$                | 46        |  |
| 3.6 Conclusions                                                      | 47        |  |
| 4 Hysteresis, Transient Oscillations, and Nonhysteretic Switching in | a         |  |
| Resonantly Modulated Large-Spin Systems                              | <b>52</b> |  |
| 4.1 Introduction                                                     | 52        |  |
| 4.2 The model                                                        | 56        |  |
| 4.2.1 Rotating wave approximation                                    | 58        |  |
| 4.2.2 Quantum kinetic equation                                       | 59        |  |
| 4.3 Classical motion of the modulated spin                           | 61        |  |
| 4.3.1 Stationary states in the rotating frame for weak damping       | 63        |  |
| 4.3.2 Saddle-node bifurcations                                       | 65        |  |
| 4.3.3 Periodic states and Hopf bifurcations                          | 68        |  |
| 4.4 Hamiltonian-like motion at exact resonance                       | 69        |  |
| 4.5 Spin dynamics in the absence of limit cycles                     | 71        |  |

| 4.5.1 Hysteresis of spin response in the absence of limit cycles            | 72         |
|-----------------------------------------------------------------------------|------------|
| 4.5.2 Interbranch switching without hysteresis                              | 74         |
| 4.6 Spin dynamics in the presence of limit cycles                           | 75         |
| 4.6.1 Phase portrait far from the astroid                                   | 77         |
| 4.6.2 Other bifurcations of limit cycles                                    | 79         |
| 4.6.3 Hysteresis of spin response in the presence of limit cycles           | 82         |
| 4.7 Conclusions                                                             | 85         |
| 5 Quantum-Classical Transition and Quantum Activation in Modu               | -          |
| lated Large-Spin Systems                                                    | 88         |
| 5.1 Introduction                                                            | 88         |
| 5.2 Dynamics of modulated large-spin systems                                | 90         |
| 5.2.1 Some properties of spin coherent states                               | 91         |
| 5.2.2 The master equation in the spin coherent state representation and its | 00         |
| semiclassical limit                                                         | 92         |
| 5.2.3 Dynamics of the system in the presence of limit cycles                | 96         |
| 5.3 The stationary limit of modulated large-spin systems                    | 101<br>102 |
| 5.3.1 The stationary distribution in the quasienergy representation         |            |
| 5.3.2 Switching and hysteresis                                              | 106<br>108 |
| 5.4 Conclusions                                                             | 110        |
| 5.4 Conclusions                                                             | 110        |
| 6 Conclusions                                                               | 114        |
| APPENDICES                                                                  | 119        |
| A Symmetry of classical spin dynamics: a feature of the conforma            | 1          |
| mapping                                                                     | 120        |
| B Energy change near a Hopf bifurcation                                     | 123        |
| C Spin Coherent State Representation of the Master Equation                 | 126        |
| RIBLIOGRAPHY                                                                | 129        |



## LIST OF FIGURES

| 2.1 | System of spatially separated qubits with individually tunable energies . | 10 |
|-----|---------------------------------------------------------------------------|----|
| 2.2 | Landau-Zener transitions                                                  | 14 |
| 2.3 | Trajectory of system on modified Bloch sphere                             | 17 |
| 2.4 | Rotation angles as function of the control parameter                      | 18 |
| 2.5 | Landau-Zener composite pulse sequence                                     | 21 |
| 2.6 | Gate error of Landau-Zener pulse sequences                                | 25 |
| 2.7 | Gate error of composite on-resonance pulse sequences                      | 27 |
| 3.1 | Three-photon resonance in a spin-2 system                                 | 30 |
| 3.2 | Quasienergies of a spin-2 system as a function of the detuning            | 34 |
| 3.3 | Level anticrossing and antiresonance of the susceptibilities              | 38 |
| 3.4 | Scaling of the multiphoton susceptibility splitting                       | 39 |
| 3.5 | Quasienergy surface in the semiclassical limit                            | 42 |
| 3.6 | Susceptibility of a spin with quartic anisotropy                          | 48 |
| 3.7 | Independence of hysteresis steps on transverse field                      | 51 |
| 4.1 | Phase portraits of the spin                                               | 64 |
| 4.2 | Saddle-node bifurcation lines in the limit of zero damping                | 67 |
| 4.3 | Hysteresis of spin response in the absence of periodic states             | 74 |
| 4.4 | Non-hysteretic switching                                                  | 75 |

| 4.5  | Saddle-node and Hopf bifurcation lines                                     | 76  |
|------|----------------------------------------------------------------------------|-----|
| 4.6  | Full bifurcation diagram in the zero damping limit                         | 80  |
| 4.7  | Hopf, saddle-node, and saddle-loop bifurcation point                       | 81  |
| 4.8  | Hysteresis of the spin dynamics in the presence of limit cycles            | 83  |
| 5.1  | Spin density distribution of a limit cycle in a spin 10 system             | 97  |
| 5.2  | Spin density distribution of a limit cycle in a spin 30 system             | 98  |
| 5.3  | Cross section through spin density distribution (spin 10)                  | 99  |
| 5.4  | Cross section through spin density distribution (spin 30)                  | 100 |
| 5.5  | Stationary distribution over quasienergy levels I                          | 102 |
| 5.6  | Hysteresis of the magnetization for different values of $S$ (fixed points) | 104 |
| 5.7  | Hysteresis of the magnetization for different values of $S$ (limit cycles) | 105 |
| 5.8  | Switching in the presence of hysteresis                                    | 107 |
| 5.9  | Hysteresis in the case of small damping                                    | 108 |
| 5.10 | Stationary distribution over quasienergy levels II                         | 109 |
| 5.11 | Switching in the absence of hysteresis                                     | 110 |
| 5.12 | Spin density distribution in the range of non-hysteretic switching         | 111 |
| Δ 1  | Contour of integration                                                     | 122 |

## Chapter 1

## Introduction

The investigation of modulated multilevel quantum systems with almost equidistant energy levels has attracted much theoretical and experimental interest in recent years. In such systems damping is often weak and even a comparatively small resonant field can lead to interesting nonlinear effects. This happens because the field is in resonance with many transitions at a time. Due to the nonlinear character of these multilevel systems, different states of forced vibrations can coexist. Quantum and classical fluctuations cause transitions between the stable states. This makes the analysis of modulated systems far more complicated than of systems at thermal equilibrium. Their dynamics remains poorly understood. It is therefore important to improve the theoretical understanding of these systems in order to find new effects, explain the existing experiments, give guidance to new experiments, and to find new applications.

The multilevel character of the energy spectrum leads to often unexpected and unusual coherent and incoherent effects. Coherent effects are of immediate interest for quantum control and quantum computation. Understanding them significantly extends the current theory of coherent quantum processes, which is largely focused on the dynamics of two-level systems. At the same time, understanding incoherent

effects, and in particular phenomena related to switching between classically stable vibrational states, would substantially contribute to the broad field of quantum physics far from thermal equilibrium. It has become clear recently that the mechanism of interstate switching opens a new and very promising approach to sensing and in particulat to quantum measurements.

In this study we concentrate our investigation on single-spin systems which are modulated by an external radiation field. We start with the analysis of a spin S=1/2 system and investigate how its operation as a quantum gate can be made robust under the influence of an environment that exerts low frequency noise on the qubit. We then move to large spin systems, where S>1/2, and investigate multiphoton resonant phenomena and nonlinear dissipative effects which play an important role in the research field of molecular magnets and other large spin systems.

In many proposed implementations of a quantum computer single-qubit operations are performed by applying pulses of radiation. These pulses cause resonant transitions between qubit states, that is between the two states of a two-level system. The operation is determined by the pulse amplitude and duration. In many proposals, particularly in the proposed scalable condensed-matter based systems [1], control pulses will be applied globally, to many qubits at a time. A target qubit can be addressed individually by tuning it in resonance with the radiation. The corresponding gate operations invariably involve errors which come from the underlying errors in the radiation frequency, amplitude, and length of the radiation pulse as well as in the qubit transition frequency tuning.

Improving the accuracy of quantum gates and reducing their sensitivity to errors

from different sources is critical for a successful operation of a quantum computer. Much progress has been made to reduce the impact of the errors on the gate operation fidelity by using active control and the design of composite pulse sequences [2, 3, 4, 5, 6].

Of special interest are frequency offset errors in the qubit energy and radiation frequency,  $\varepsilon$ . Such errors come from various sources. An example is provided by systems where the qubit-qubit interaction is not turned off, and therefore the transition energy of a qubit depends on the state of other qubits. Typically, the error affects the fidelity of the gate operation linearly. The goal is to find ways to increase the fidelity of the gate. For conventional single-qubit gate implementations, where the qubit transition frequency, ideally, stays in exact resonance with the radiation pulse for a specified period of time, the best known error compensating pulses still produce errors that scale as  $\varepsilon^2$  [7].

Here, we will investigate gate operations that are based on a non-standard way of operating qubits, where the qubit transition frequency is swept through resonance with a radiation field. This process is well known as Landau-Zener crossing [8, 9] and plays an important role in different areas of quantum physics. Far away from resonance the interaction between qubit and radiation field is weak. At the same time, for a sufficiently broad range over which the transition frequency is swept, even in the presence of an unknown frequency offset, the system will always go through resonance. Therefore, one may expect that Landau-Zener crossings have an advantage over conventional on-resonance gates. In turn, this may lead to better composite pulses and a far more efficient error correction. In this study we will show that this is indeed the case.

Large-spin systems have been attracting much attention recently. Examples are S = 3/2 and S = 5/2 Mn impurities in semiconductors as well as nuclear spins I = 3/2 where radiation-induced quantum coherence between the spin levels was observed [10]. The interest in nuclear spins has renewed in view of their possible use in quantum computing [11].

An important class of large-spin systems is single-molecule magnets (SMMs). SMMs display an extremely rich behavior and have been attracting much attention in recent years. A variety of SMMs has already been discovered and investigated theoretically and experimentally [12, 13, 14, 15, 16, 17, 18, 19, 20, 21] (see Refs. [22, 23, 24] for a review) and new systems are being found [25, 26]. Mn- and Fe-based molecular magnets exhibit electron spins of S = 10 and higher.

In a broader sense, the interest in quantum spin dynamics comes also from field theory. The dynamics is closely related to the Lipkin-Meshkov-Glick model [27, 28, 29, 30], which is used in various areas, from condensed matter physics to nuclear theory.

Large-spin systems have a finite but comparatively large number of quantum states. Therefore, a single system can be used to study a broad range of phenomena, from purely quantum to semiclassical where the spin behaves almost like a classical top. An important feature of large-spin systems is that, in a strong static magnetic field, their energy levels become almost equidistant, with level spacings close to  $\hbar\omega_0$ , where  $\omega_0$  is the Larmor frequency. As a result, radiation at frequency  $\approx \omega_0$  is resonant simultaneously for many interlevel transitions. This leads to new quantum and classical nonlinear resonant effects.

The effects of a strong resonant field on systems with nearly equidistant energy levels, in the absence of dissipation, have been studied for weakly nonlinear oscillators [31, 32, 33, 34]. However, spins are qualitatively different from oscillators. The number of spin states is finite, 2S + 1, and the algebra of spin operators differs from that of the oscillator operators.

An outstanding question is whether the coherent semiclassical spin dynamics has conformal properties. Such properties may lead to interesting observable consequences. As we show, the model with uniaxial anisotropy, which describes many systems of current interest, indeed has such properties. This provides an explanation to a number of experiments on molecular magnets, where an unexpected hysteretic behavior was observed [16] (see Fig. 3.7 below).

The classical dynamics of a large-spin system in a resonant field would be expected to have similarities with the dynamics of a modulated magnetic nanoparticle near ferromagnetic resonance. It was understood back in the 1950's [35, 36] that the response near ferromagnetic resonance becomes strongly nonlinear already for a comparatively weak radiation strength due to the magnetization dependence of the effective magnetic field. The resonant response may become multivalued as a function of the modulating field amplitude [37, 38]. A detailed analysis of nonlinear magnetization dynamics in uniaxial nanoparticles modulated by a strong circularly polarized periodic field was done recently [39]. These studies as well as many other studies of magnetization dynamics in ferromagnets were based on the phenomenological Landau-Lifshitz-Gilbert equation.

In contrast to magnetic nanoparticles, for large-spin systems quantum effects are substantial. A distinction which remains important in the classical limit concerns relaxation mechanisms. Spin relaxation occurs via transitions between discrete energy levels with emission, absorption, or inelastic scattering of excitations of a thermal

reservoir to which the spin is coupled. Relevant relaxation mechanisms depend on the specific system but as we show, even in the classical limit relaxation is generally not described by the Landau-Lifshitz damping. As a result the classical spin dynamics strongly differs from the dynamics of a magnetic nanoparticle.

The microscopic analysis of relaxation is simplified by the near equidistance of the energy levels in a strong static magnetic field. As a consequence, excitations of the thermal bath emitted, for example, in transitions within different pairs of neighboring levels have almost the same energies. Therefore, relaxation is described by a small number of constants independent of the form of the weighted with the interaction density of states of the bath, and the analysis applies for an arbitrary ratio between the level nonequidistance and their relaxational broadening [40].

Large-spin systems are of great interest for the study of quantum to classical transitions. The inverse size of the spin, 1/S, can be seen as an effective Planck number which controls the "quantumness" of the system. Of particular interest in this context is hysteresis in a modulated large spin system, which occurs in the classical limit.

Switching between coexisting stable states underlies many phenomena in physics, from diffusion in solids to protein folding. For classical systems in thermal equilibrium switching is often described by the activation law, with the switching probability being  $W \propto \exp(-\Delta U/kT)$ , where  $\Delta U$  is the activation energy. As temperature is decreased, quantum fluctuations become more and more important, and below a certain crossover temperature switching occurs via tunneling [41, 42, 43]. The behavior of systems away from thermal equilibrium is far more complicated. Still, for classical systems switching is often described by an activation type law, with the tempera-

ture replaced by the characteristic intensity of the noise that leads to fluctuations [44, 45, 46, 47, 48, 49, 50, 51, 52]. Quantum nonequilibrium systems can also switch via tunneling between classically accessible regions of their phase space [32, 53, 33, 54].

Decay of a metastable state is usually considered as resulting from tunneling or thermal activation. Besides classical activation and quantum tunneling, nonequilibrium systems have another somewhat counterintuitive mechanism of transitions between stable states. This mechanism is called quantum activation and has been explained recently for the cases of a parametrically driven oscillator [55] and a nonlinear oscillator [56]. It describes escape from a metastable state due to quantum fluctuations that accompany relaxation of the system [57]. These fluctuations lead to diffusion away from the metastable state and, ultimately, to transitions over the classical "barrier", that is, the boundary of the basin of attraction of the metastable state in phase space. Quantum activation is often more probable than tunneling even at zero temperature.

The counterintuitive nature of the effect of quantum activation requires studying whether this effect occurs in systems other than an oscillator. Large-spin systems provide an ideal example. They are particularly interesting and challenging because they may display features that have no counterpart for oscillators. One of such features is the onset of periodic states in the rotating frame, which has been previously found in the phenomenological analysis of magnetic nanoparticles [39].

It is a challenge to find limit cycles for large spins in the classical limit, using a microscopic model of coupling to a bath, and to determine the conditions where they emerge. The natural next step is to investigate the smearing of the cycles by quantum fluctuations and the study of quantum activation in systems with limit cycles.

The thesis is organized as follows. In chapter 2 we develop a theory that allows us to analyze single-qubit operations where the qubit transition frequency  $\omega_0(t)$  is swept through the frequency of the resonant field  $\omega_F$  and by that inducing Landau-Zener tunneling in the qubit. We propose a composite Landau-Zener pulse sequence and demonstrate that it compensates energy offset errors to a much higher degree than conventional quantum gates. In chapter 3 we study the quasienergy spectrum and the response of a modulated large spin with quadratic in  $S_z$  anisotropy energy. We show that, at multiphoton resonance, the susceptibilities in the resonating states display an interesting coherent antiresonant behavior. In chapter 4 we study the dynamics of such a spin in the semiclassical limit in the presence of relaxation and present a stability analysis which predicts a rich hysteretic behavior. In chapter 5 we extend the analysis from the semiclassical limit to the the quantum regime by introducing a formalism that makes use of spin coherent states and the stationary quasienergy distribution. We explain how classical limit cycles are manifested in the quantum regime and show that in modulated large spin system switching occurs via quantum activation.

## Chapter 2

## Fault-Tolerant Landau-Zener

## Quantum Gates

#### 2.1 Introduction

In many proposed implementations of a quantum computer (QC) single-qubit operations are performed by applying pulses of radiation. The pulses cause resonant transitions between qubit states, that is between the states of the system that comprises a qubit. The operation is determined by the pulse amplitude and duration. In many proposals, particularly in the proposed scalable condensed-matter based systems [1], control pulses will be applied globally, to many qubits at a time. A target qubit is chosen by tuning it in resonance with the radiation. The corresponding gate operations invariably involve errors which come from the underlying errors in the frequency, amplitude, and length of the radiation pulse as well as in the qubit tuning.

Improving the accuracy of quantum gates and reducing their sensitivity to errors from different sources is critical for a successful operation of a QC. Much progress has been made recently in this direction by using radiation pulses of special shape and composite radiation pulses [2]. In the analysis or resonant pulse shape it is usually assumed that the qubit transition frequency is held constant during the pulse.

An alternative approach to single-qubit operations is based on Landau-Zener tunneling (LZT) [8, 9]. In this approach the qubit transition frequency  $\omega_0(t)$  is swept through the frequency of the resonant field  $\omega_F$  [58]. The change of the qubit state depends on the field strength and the speed at which  $\omega_0(t)$  is changed when it goes through resonance [59]. The LZT can be used also for a two-qubit operation in which qubit frequencies are swept past each other leading to excitation swap [58, 60, 61].

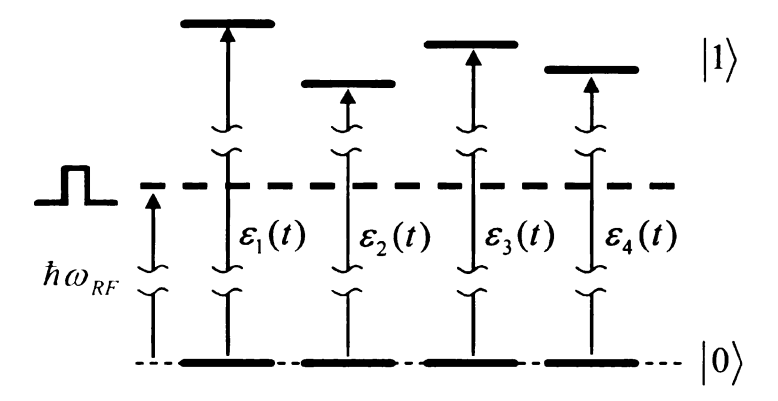


Figure 2.1: System of spatially separated qubits with individually tunable energies. In between operations transition frequencies are detuned to avoid excitation hopping.

In this chapter we study the robustness of the LZT-based gate operations. We develop a simple pulse sequence that is extremely stable against errors in the qubit transition frequency or equivalently, the radiation frequency. Such errors come from various sources. An example is provided by systems where the qubit-qubit interaction is not turned off, and therefore the transition energy of a qubit depends on the state of other qubits. Much effort has been put into developing means for correcting them using active control [4, 5, 6].

An advantageous feature of LZT is that the change of the qubit state populations

depends on the radiation amplitude and the speed of the transition frequency change  $\dot{\omega}_0$ , but not on the exact instant of time when the frequency coincides with the radiation frequency,  $\omega_0(t) = \omega_F$ . However, the change of the phase difference between the states depends on this time. Therefore an error in  $\omega_0$  or  $\omega_F$  leads to an error in the phase difference, i.e., a phase error. This error has two parts: one comes from the phase accumulation before crossing the resonant frequency, and the other after the crossing. Clearly, they have opposite signs.

A natural way of reducing a phase error is to make the system accumulate the appropriate opposite in sign phases before and after the "working" pulse. To do this, we first apply a strong radiation pulse that swaps the states, which can be done with exponentially high efficiency using LZT. Then we apply the "working" pulse, and then another swapping pulse. The swapping pulses effectively change the sign of the accumulated phase. As we show, by adjusting their parameters we can compensate phase errors with a high precision.

In Sec. II below we give the scattering matrix for LZT in a modified adiabatic basis which turns out to be advantageous compared to the computational basis. The scattering matrix describes the quantum gate. In Sec. III it is presented in more conventional for quantum computation terms of the qubit rotation matrix. In Sec. IV, which is the central part of the chapter, we propose a simple composite Landau-Zener (LZ) pulse and demonstrate that it efficiently compensates energy offset errors even where these errors are not small. Sec. V contains concluding remarks.

# 2.2 Landau-Zener transformation in the modified adiabatic basis

A simple implementation of the LZ gate is as follows. The amplitude of the radiation pulse is held fixed, while the difference between the qubit transition frequency and the radiation frequency

$$\Delta = \Delta(t) = \omega_F - \omega_0(t) \tag{2.1}$$

is swept through zero. If  $\omega_0(t)$  is varied slowly compared to  $\omega_F$ , i.e.,  $|\dot{\omega}_0| \ll \omega_F^2$ , the qubit dynamics can be described in the rotating wave approximation, with Hamiltonian

$$H = H(t) = \begin{pmatrix} \Delta/2 & \gamma \\ \gamma & -\Delta/2 \end{pmatrix}. \tag{2.2}$$

Here,  $\gamma$  is the matrix element of the radiation-induced interstate transition. The Hamiltonian H is written in the so-called computational basis, with wave functions  $|0\rangle = \begin{pmatrix} 1 \\ 0 \end{pmatrix}$  and  $|1\rangle = \begin{pmatrix} 0 \\ 1 \end{pmatrix}$ .

We assume that well before and after the frequency crossing the values of  $|\Delta|$  largely exceed  $\gamma$  and  $\Delta$  slowly varies in time,  $|\dot{\Delta}/\Delta^2| \ll 1$ . Then the wave functions of the system are well described by the adiabatic approximation, i.e., by the instantaneous eigenfunctions of the Hamiltonian (2.2),

$$|\psi_0\rangle = \begin{bmatrix} \cos(\theta/2) \\ \sin(\theta/2) \end{bmatrix}, \qquad |\psi_1\rangle = \begin{bmatrix} -\sin(\theta/2) \\ \cos(\theta/2) \end{bmatrix}, \qquad (2.3)$$

$$\theta = (\operatorname{sgn}\Delta)\cos^{-1}\frac{|\Delta|}{2E}, \qquad E = \left(\frac{\Delta^2}{4} + \gamma^2\right)^{1/2},$$

where  $\Delta \equiv \Delta(t)$  and  $(-1)^n E \operatorname{sgn}\Delta$  is the adiabatic energy of the states  $|\psi_n\rangle = |\psi_{0,1}\rangle$ . The adiabatic approximation for E and  $\theta$  is accurate to  $\gamma^2 \dot{\Delta}/\Delta^3$  and  $\gamma \dot{\Delta}/\Delta^3$ ,

respectively.

In contrast to the standard adiabatic approximation, we chose the states  $|\psi_{0,1}\rangle$  and their energies in such a way that  $|\psi_0\rangle$  and  $|\psi_1\rangle$  go over into  $|0\rangle$  and  $|1\rangle$ , respectively, for  $|\Delta|/\gamma \to \infty$ . As a result  $\theta$  is discontinuous as a function of  $\Delta$  for  $\Delta = 0$ , but the adiabatic approximation does not apply for such  $\Delta$  anyway.

For the future analysis it is convenient to introduce the Pauli matrices X, Y, Z in the basis (2.3), with

$$Z|\psi_n\rangle = (1-2n)|\psi_n\rangle, \qquad X|\psi_n\rangle = |\psi_{1-n}\rangle \quad (n=0,1),$$

and Y = iXZ. In these notations, the operator of the adiabatic time evolution  $U(t_f, t_i) = T \exp[-i \int_{t_i}^{t_f} dt H(t)]$  has the form

$$U(t_f, t_i) = \exp\left[-i\left(\operatorname{sgn}\Delta\right)Z\int_{t_i}^{t_f} E(t)\,dt\right],\tag{2.4}$$

with  $\operatorname{sgn} \Delta \equiv \operatorname{sgn} \Delta(t_i) \equiv \operatorname{sgn} \Delta(t_f)$  [the sign of  $\Delta(t)$  is not changed in the range where Eq. (2.4) applies].

The LZ transition can be thought of as occurring between the states (2.3). Following the standard scheme [8, 9] we take two values  $\Delta_{1,2}$  of  $\Delta(t)$  such that they have opposite signs,  $\Delta_1\Delta_2 < 0$ . We choose  $|\Delta_{1,2}|$  sufficiently large, so that the adiabatic approximation (2.3) applies for  $\Delta(t_i) = \Delta_i$ , i = 1, 2. At the same time,  $|\Delta_{1,2}|$  are sufficiently small, so that  $\Delta(t)$  can be assumed to be a linear function of time between  $\Delta_1$  and  $\Delta_2$ ,

$$\Delta(t) \approx -\eta(t - t_c), \qquad \eta = -\dot{\Delta}(t_c),$$
 (2.5)

where the crossing time  $t_c$  is given by the condition  $\Delta(t_c) = 0$ . The adiabaticity for  $t = t_{1,2}$  requires that  $|\Delta_{1,2}| \gg \gamma$ ,  $\eta^{1/2}$ . We will consider the LZ transition first for the case  $\Delta_1 > 0$  and  $\Delta_2 < 0$ , when  $\eta > 0$ .

The modified adiabatic basis (2.3) is advantageous, because in this basis the transition matrix S has a particularly simple form. For  $\Delta(t)$  of the form (2.5) the error in S is determined by the accuracy of the adiabatic approximation itself and is of order  $\gamma/\eta^2|t_{1,2}-t_c|^3$ , in contrast to the computational basis, where the error is  $\sim O(\gamma/\eta|t_{1,2}-t_c|)$ . This latter error is comparatively large for the values of  $\gamma/|\Delta_{1,2}|$  of interest for quantum computing. It leads to the well-known oscillations of the transition amplitude with increasing  $|\Delta|$  [59], whereas in the basis (2.3) such oscillations do not arise, see Fig.2.2.

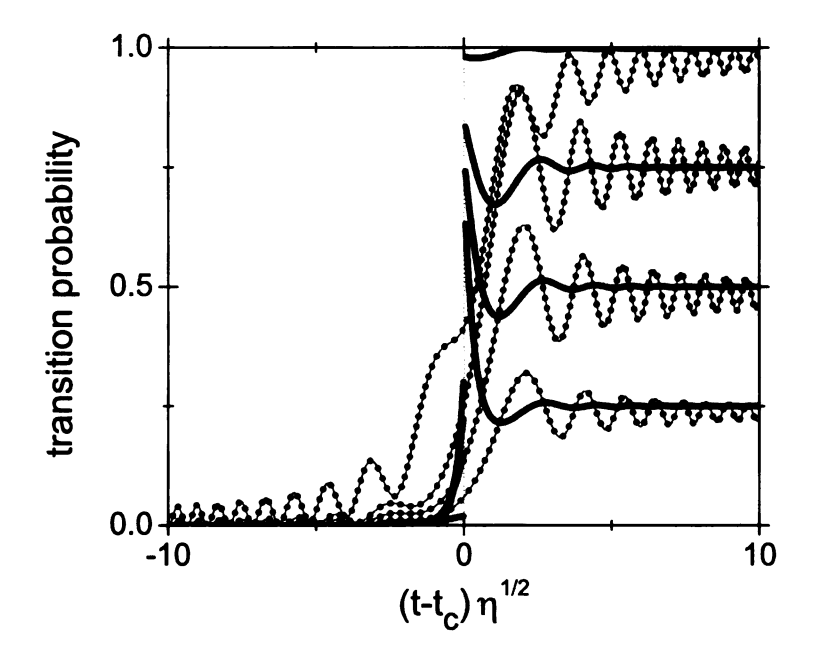


Figure 2.2: Landau-Zener transitions  $|\psi_0\rangle \to |\psi_1\rangle$  and  $|0\rangle \to |1\rangle$  in the modified adiabatic basis (2.3) and in the computational basis for linear  $\Delta(t)$  (2.5). Solid and dotted lines show the squared amplitude of the initially empty states  $|\psi_1\rangle$  and  $|1\rangle$ , respectively. The lines refer to g=1,0.47,0.33, and 0.21, in the order of decreasing transition probability for  $(t-t_c)\eta^{1/2}=10$ . As long as  $\Delta(t)$  is large and negative, the system stays in the initially occupied adiabatic state  $|\psi_0\rangle$ , and therefore the solid curves for different g cannot be resolved for  $(t-t_c)\eta^{1/2}\lesssim -1$ . For large  $(t-t_c)\eta^{1/2}$  the solid lines quickly approach the Landau-Zener probabilities  $1-e^{-2\pi g^2}$ .

The energy detuning  $|\Delta_{1,2}|$  cannot be made too large, because this would make the

gate operation long. If we characterize the overall error of the adiabatic approximation as the sum  $\sum_{i=1,2} \gamma/\eta^2 |t_i - t_c|^3$  and impose the condition that the overall duration of the operation  $t_2 - t_1$  be minimal, we see that the error is minimized when the pulses  $\Delta(t)$  are symmetrical,  $t_2 - t_c = t_c - t_1$ , i.e.,  $|\Delta_1| = |\Delta_2|$ .

The matrix  $S(t_2, t_1) \equiv S$  in the basis (2.3) can be obtained using the parabolic cylinder functions that solve the Schrödinger equation with the Hamiltonian (2.2), (2.5),

$$S(t_{2}, t_{1}) = \begin{pmatrix} S_{11} & S_{12} \\ S_{21} & S_{22} \end{pmatrix},$$

$$S_{11} = \exp\left[-\pi g^{2} + i(\varphi_{2} - \varphi_{1})\right],$$

$$S_{12} = -\frac{(2\pi)^{1/2}}{g\Gamma(ig^{2})} \exp\left[-\frac{\pi}{2}g^{2} - i\frac{\pi}{4} + i(\varphi_{1} + \varphi_{2})\right],$$

$$S_{21} = \frac{(2\pi)^{1/2}}{g\Gamma(-ig^{2})} \exp\left[-\frac{\pi}{2}g^{2} + i\frac{\pi}{4} - i(\varphi_{1} + \varphi_{2})\right],$$

$$S_{22} = \exp\left[-\pi g^{2} - i(\varphi_{2} - \varphi_{1})\right],$$

$$(2.6)$$

where  $\Gamma(x)$  is the gamma function.

The dimensionless coupling parameter  $g = \gamma/|\eta|^{1/2}$  in Eq. (2.6) is the major parameter of the theory, it determines the amplitude of the  $|\psi_n\rangle \to |\psi_{1-n}\rangle$  transition. The phases  $\varphi_{1,2}$  are

$$\varphi_i = \frac{\Delta_i^2}{4|\eta|} + g^2 \ln\left(\frac{|\Delta_i|}{|\eta|^{1/2}}\right) + \frac{g^4|\eta|}{2\Delta_i^2}, \qquad i = 1, 2.$$
(2.7)

Here we have disregarded the higher order terms in  $|\Delta_{1,2}|^{-1}$ . The constants in  $\varphi_{1,2}$  are chosen so as to match the corresponding constants in the parabolic cylinder functions [62].

The matrix S for a transition from the initial state with  $\Delta_1 < 0$  to the final state with  $\Delta_2 > 0$  is given by the transposed matrix (2.6) in which the phases  $\varphi_1$  and  $\varphi_2$ 

are interchanged. In this case  $\eta < 0$  in Eq. (2.5); the expressions for  $\varphi_{1,2}$  and g do not change.

### 2.3 Rotation matrix representation

The LZ transition can be conveniently described using the standard language of gate operations in quantum computing. To do this we express the transition matrix in terms of the operators  $R_X(\theta) = \exp(-i\theta X/2)$  and  $R_Z(\theta) = \exp(-i\theta Z/2)$  of rotation about x and z axes in the basis (2.3). The rotation matrices can be written using the "adiabatic" phases  $\phi(t_i)$  that accumulate between the time  $t_i$  and the time  $t_c$  at which the levels would cross in the absence of coupling. From Eq. (2.7)

$$\varphi_{i} = \phi(t_{i}) + \varphi_{0} \quad (i = 1, 2), \qquad t_{1} < t_{c} < t_{2},$$

$$\phi(t_{i}) = \left| \int_{t_{c}}^{t_{i}} E \, dt \right|, \qquad \varphi_{0} = \frac{1}{2} g^{2} (\ln g^{2} - 1), \tag{2.8}$$

where we have disregarded corrections  $\propto |\Delta_{1,2}|^{-4}$ , in agreement with the approximations made in obtaining Eq. (2.6).

For the case  $\Delta_1 > 0 > \Delta_2$  the dependence of the transition matrix S (2.6) on the phases  $\phi(t_{1,2})$  has the form

$$S(t_2, t_1) = R_z \left[ -2\phi(t_2) \right] S' R_z \left[ 2\phi(t_1) \right]. \tag{2.9}$$

A direct calculation shows that the matrix S' is

$$S' = R_z(\Phi)R_x(\alpha)R_z(-\Phi). \tag{2.10}$$

The rotation angles  $\Phi$ ,  $\alpha$  are given by the expressions

$$\Phi = -2\varphi_0 + \arg\Gamma(ig^2) + \frac{3\pi}{4},$$

$$\alpha = 2\cos^{-1}\left[\exp(-\pi g^2)\right].$$
(2.11)

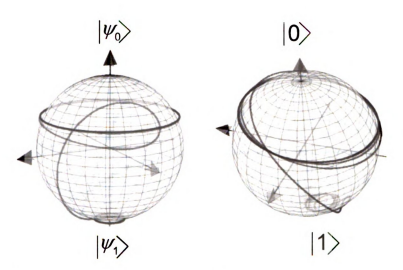


Figure 2.3: Trajectory of system in  $|\psi_0\rangle$ ,  $|\psi_1\rangle$  and  $|0\rangle$ ,  $|1\rangle$  basis, respectively. Initial state:  $|\psi_1\rangle = \sqrt{0.01} |\psi_0\rangle + \sqrt{0.99} |\psi_1\rangle$ , g = 0.5. Note that instead of using basis (2.3) the slightly different basis  $|\psi_0\rangle = 1/\sqrt{1+\gamma^2/\Delta^2} (1,\gamma/\Delta)^T$ ,  $|\psi_1\rangle = 1/\sqrt{1+\gamma^2/\Delta^2} (-\gamma/\Delta, 1)^T$  was used to draw the figure. For large values of  $\gamma/|\Delta|$  this basis is asymptotically the same as the original basis (2.3). The benefit of using this basis is solely for illustration purposes; in contrast to using basis (2.3) the trajectories of the system have no discontinuity at  $\Delta = 0$  (cf. Fig. 2.2).

A minor modification of these equations allows using them also for the case  $\Delta_1 < 0 < \Delta_2$  when the frequency difference is increased in time in order to bring the states in resonance. It was explained below Eq. (2.7) how to relate the matrix S in this case to the matrix S for  $\Delta_1 > 0 > \Delta_2$ . Following this prescription we obtain

$$S(t_2, t_1) = R_z \left[ 2\phi(t_2) - \Phi \right] R_x(\alpha) R_z \left[ -2\phi(t_1) + \Phi \right]. \tag{2.12}$$

In the rotation matrix representation, the only difference from the S matrix from the case of decreasing  $\Delta(t)$  is that  $\Phi$  and  $\phi(t_{1,2})$  change signs. Eqs. (2.9)-(2.12) express the LZ transition matrix in the form of rotation operators in the basis of the modified adiabatic states  $|\psi_0\rangle$  and  $|\psi_1\rangle$  (2.3). For strong coupling,  $\exp(-\pi g^2) \ll 1$ , the rotation angle  $\alpha$  approaches  $\pi$ , which corresponds to a population swap between the adiabatic states. It is well known from the LZ theory [8, 9] that the swap operation

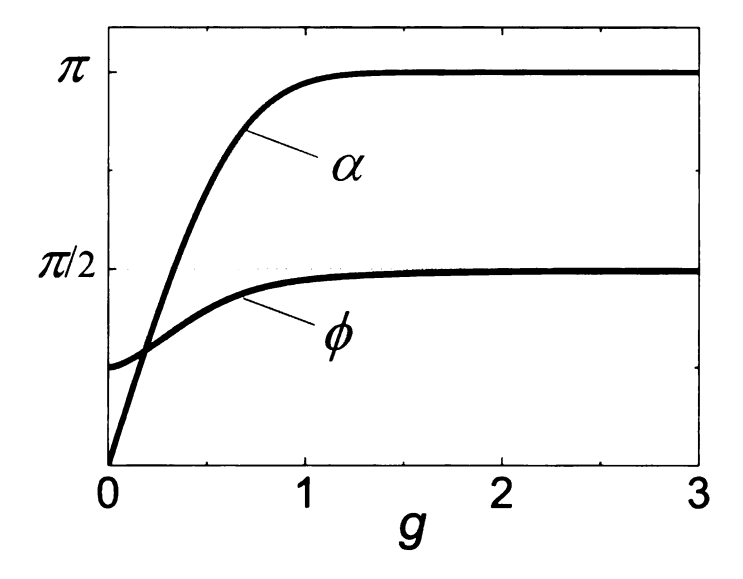


Figure 2.4: The rotation angles  $\alpha$  (solid line) and  $\Phi$  (dashed line) in the rotation-matrix representation of the Landau-Zener gate operation as functions of the control parameter g. The  $\pi/2$  gate,  $\alpha = \pi/2$ , requires  $g = [\ln 2/(2\pi)]^{-1/2} \approx 0.33$ .

is exponentially efficient,  $\pi - \alpha \approx 2 \exp(-\pi g^2)$  for large g. In the opposite limit of weak coupling,  $g \ll 1$ , the change of the state populations is small,  $\alpha \approx (8\pi)^{1/2}g$ . In addition to the change of state populations there is also a phase shift that accumulates during an operation. The dependence of the angles  $\alpha$  and  $\Phi$  on the coupling parameter g is shown in Fig.2.4.

## 2.4 Composite Landau-Zener pulses

For many models of quantum computers an important source of errors are errors in qubit transition frequencies  $\omega_0$ . They may be induced by a low-frequency external noise that modulates the interlevel distance. They may also emerge from errors in the control of the qubit-qubit interaction: if the interaction is not fully turned off between operations, the interlevel distance is a function of the state of other qubits.

In addition there are systems where the interaction is not turned off at all, like in liquid state NMR-based QC's. In all these systems it is important to be able to perform single-qubit gate operations that would be insensitive to the state of other qubits.

The rotation-operator representation suggests a way to develop fault tolerant composite LZ pulses with respect to errors in the qubit transition frequency  $\omega_0$  and in the radiation frequency  $\omega_F$ . We will assume that there is a constant error  $\varepsilon$  in the frequency difference  $\Delta(t) = \omega_F - \omega_0(t)$ , but that no other errors occur during the gate operation. From Eq. (2.5), the renormalization  $\Delta(t) \to \Delta(t) + \varepsilon$  translates into the change of the adiabatic energy E and the crossing time  $t_c$ , with  $t_c \to t_c + \varepsilon/\eta$ . As a result the phases  $\phi(t_{1,2})$  as given by Eq. (2.8) are incremented by

$$\delta\phi(t_i) = \frac{E(t_i)\Delta(t_i)}{|\eta\Delta(t_i)|}\varepsilon + \frac{|\Delta(t_i)|}{8|\eta|E(t_i)}\varepsilon^2, \qquad i = 1, 2,$$
(2.13)

to second order in  $\varepsilon$ .

#### 2.4.1 Error compensation with $\pi$ -pulses

A simple and robust method of compensating errors in  $\phi$  is based on a composite pulse that consists of the desired pulse sandwiched between two auxiliary pulses. Using  $\pi$ -pulses in which  $\Delta(t)$  is linear in t, as shown in Fig. 2.5, it is possible to eliminate errors of first and second order in  $\varepsilon$ . The goal is to compensate the factors  $R_z[\pm 2\delta\phi(t_{1,2})]$  in the S-matrix (2.9). We note that all other factors in S are not changed by the energy change  $\varepsilon$ , which is one of the major advantageous features of the LZ gate operation. A  $\pi$ -pulse is obtained if  $\exp(\pi g^2) \gg 1$ , which is met already for not too large g: for example,  $\exp(-\pi g^2) < 10^{-5}$  for g > 1.92.

Disregarding corrections  $\sim \exp(-\pi g^2)$  we can write the S-matrix for the  $\pi$ -pulse as

$$S_{\pi}(t',t) \approx -iXR_{z}[2\phi_{\pi}(t) + 2\phi_{\pi}(t') - 2\Phi]$$
  

$$\equiv -iR_{z}[-2\phi_{\pi}(t) - 2\phi_{\pi}(t') + 2\Phi]X, \qquad (2.14)$$

where t, t' are the initial and final times, and the subscript  $\pi$  indicates that the corresponding quantities refer to a  $\pi$ -pulse. We assume that  $\Delta(t) > 0 > \Delta(t')$ .

The overall gate operation is now performed by a composite pulse

$$S_c(t_2', t_1') = S_{\pi}(t_2', t_2)S(t_2, t_1)S_{\pi}(t_1, t_1'). \tag{2.15}$$

In writing this expression we assumed that the system is switched instantaneously between the states that correspond to the end (beginning) of the correcting pulse and the beginning (end) of the working pulse  $S(t_2, t_1)$ . The overall composite pulse is shown in Fig. 2.5. The first and the second  $\pi$ -pulses correct the errors  $\delta \phi$  (2.13) in the phases  $\phi(t_1)$  and  $\phi(t_2)$ , respectively. We show how it works for  $\phi(t_2)$ . From Eqs. (2.9), (2.14), the error in  $\phi(t_2)$  will be compensated if

$$\delta\phi_{\pi}(t_2') + \delta\phi_{\pi}(t_2) - \delta\phi(t_2) = 0.$$

To second order in  $\varepsilon$ , the errors  $\delta \phi$  here are given by Eq. (2.13) with appropriate  $t_i$ . The total error will be equal to zero provided

$$\frac{E_{\pi}(t_2')}{\eta_{\pi}} - \frac{E(t_2)}{\eta} - \frac{E_{\pi}(t_2)}{\eta_{\pi}} = 0,$$

$$\frac{|\Delta_{\pi}(t_2')|}{\eta_{\pi}E_{\pi}(t_2')} - \frac{|\Delta(t_2)|}{\eta E(t_2)} + \frac{\Delta_{\pi}(t_2)}{\eta_{\pi}E_{\pi}(t_2)} = 0.$$
(2.16)

Equations (2.16) are simplified if we keep only the lowest order terms with respect to  $\gamma^2/\Delta^2$ , in which case  $E(t_i) \approx |\Delta(t_i)|/2$  both for the working and the correcting

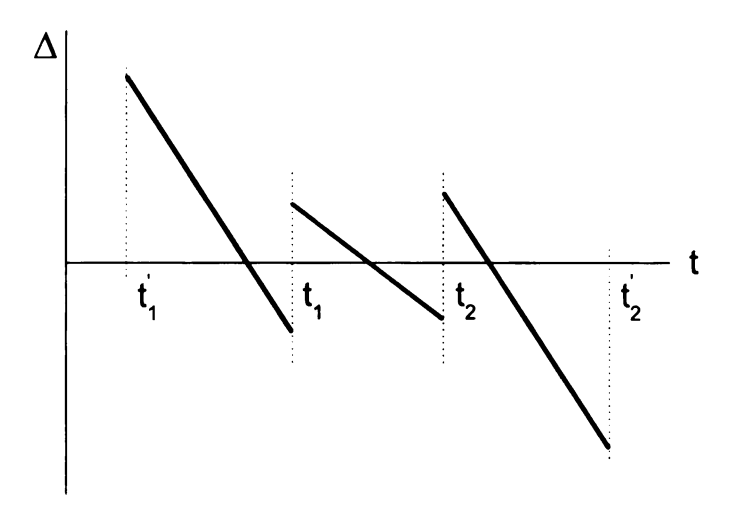


Figure 2.5: An idealized composite pulse. The first and third pulses are  $\pi$ -pulses, the pulse in the middle performs the required gate operation. The overall pulse compensates errors in the qubit energy to 3rd order.

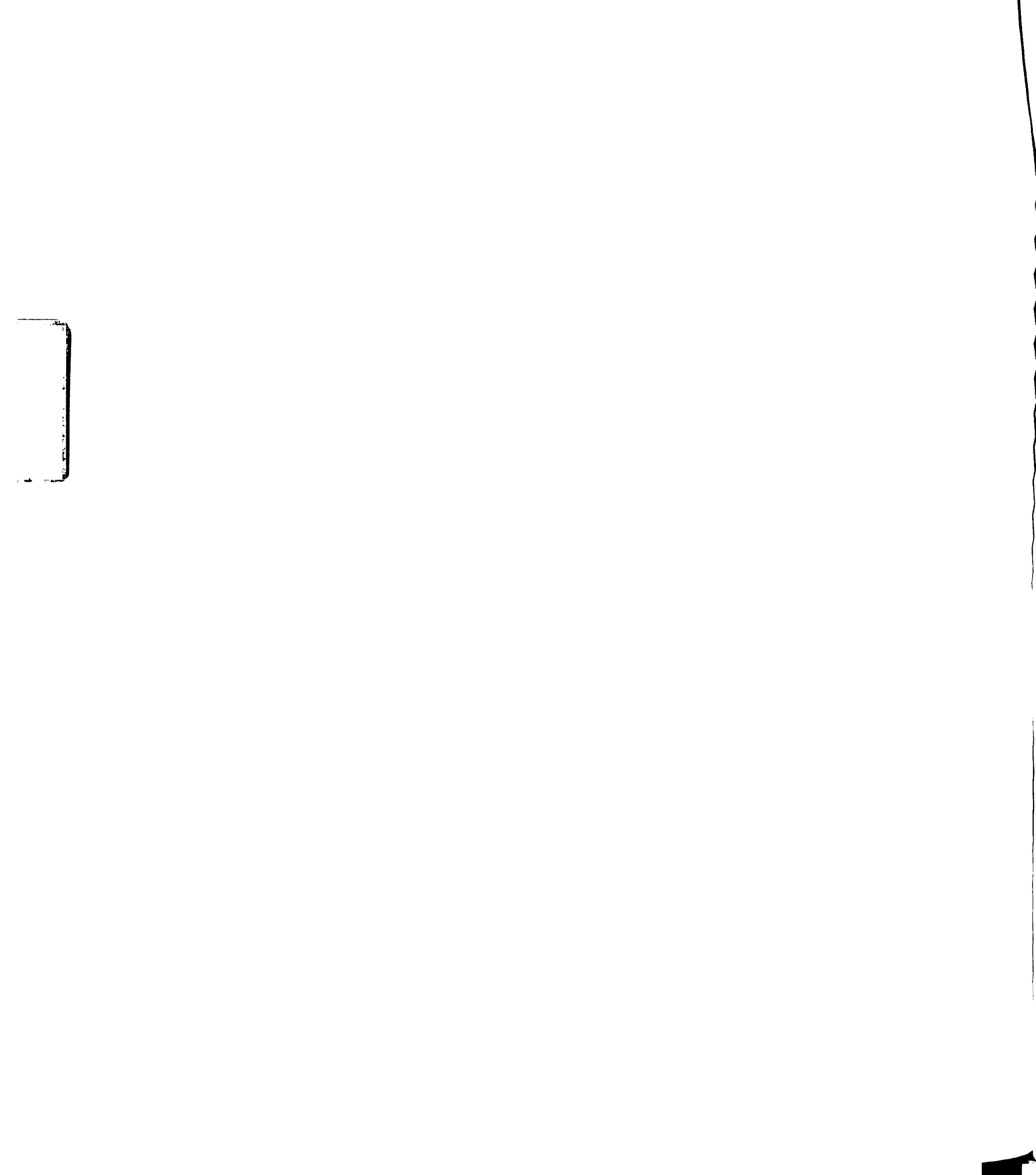
pulse. This gives

$$\eta_{\pi} = 2\eta, \qquad |\Delta_{\pi}(t_2')| - 2|\Delta(t_2)| - \Delta_{\pi}(t_2) = 0.$$
(2.17)

An immediate consequence of Eq. (2.17) is that the coupling constant  $\gamma_{\pi}$  for the  $\pi$ pulse should exceed the value of  $\gamma$  for the working pulse, because  $g_{\pi} \geq g$  and  $\eta_{\pi} > \eta$ .

Another consequence is that the  $\pi$ -pulse amplitude should exceed that of the working pulse. If we choose  $\Delta_{\pi}$  so that the error of the adiabatic approximation in the  $\pi$ -pulse does not exceed that of the working pulse,  $\gamma_{\pi}\eta_{\pi}/|\Delta_{\pi}|^3 \leq \gamma\eta/|\Delta(t_2)|^3$ , we obtain from Eq. (2.17) the condition  $\Delta_{\pi}(t_2) \geq |\Delta(t_2)| 2^{1/2} (g_{\pi}/g)^{1/3}$ .

We note that the correcting pulse is asymmetric, with  $|\Delta_{\pi}(t_2')| > \Delta_{\pi}(t_2), 2|\Delta(t_2)|$ , as shown in Fig. 2.5. Another important comment is that the proposed simple single pulse does not allow us to correct errors of higher order in  $\varepsilon$ . It is straightforward to see that the equation for  $\Delta_{\pi}(t_2), \Delta_{\pi}(t_2')$  that follows from the condition that the error  $\sim \varepsilon^3$  vanishes is incompatible with Eqs. (2.17). However, the terms  $\propto (\varepsilon/\gamma)^3$ 



contain a small factor  $g^2\gamma/\Delta(t_{1,2})^3\ll 1$ . The higher-order terms in  $\varepsilon/\gamma$  contain higher powers of the parameter  $\gamma/\Delta(t_{1,2})$ . This is why compensating errors only up to the second order in  $\varepsilon$  turns out efficient.

The analysis of the first correcting  $\pi$ -pulse,  $S_{\pi}(t_1, t'_1)$ , is similar to that given above. The amplitude of this pulse also exceeds the amplitude of the working pulse. The duration of the correcting pulses is close to the duration of the working pulse, for  $g \sim 1$  and  $g_{\pi} \gtrsim 2$ .

The pulse sequence (2.15) is written assuming that the radiation is switched off between the pulses and that the switching between the working and correcting pulses is instantaneous. A generalization to a more realistic case of a nonzero switching time is straightforward. The time evolution between the pulses can be described by extra terms in the phases  $\phi_{\pi}(t_1)$ ,  $\phi_{\pi}(t_2)$ , leading to the appropriate modification of the equations for error compensation (2.16). The analysis can be also extended to the case where  $\Delta(t)$  is a nonlinear function of time and the coupling g depends on time. This extension requires numerical analysis; we have found for several types of  $\Delta(t)$ , g(t) that good error correction can still be achieved with a three-pulse sequence.

#### 2.4.2 Maximal error of the three-pulse sequence

In order to demonstrate the error correction we will consider single working pulses  $S(t_2, t_1)$  with the overall phases  $\Phi - 2\phi(t_{1,2}) \equiv 0 \pmod{2\pi}$  in the absence of errors, which we will denote by  $S^{(0)}(t_2, t_1)$ . Such pulses describe transformations between the states (2.3) with no extra phase, that is pure X rotations. We will also choose the correcting  $\pi$ -pulses with the overall phase  $2\phi_{\pi}(t) + 2\phi(t') - 2\Phi \equiv 0 \pmod{2\pi}$  in the absence of errors, with t, t' being  $t'_1, t_1$  and  $t_2, t'_2$  for the first and second pulse, respectively. Then in the absence of errors the overall gate is either not affected by

the correcting pulse or its sign is changed.

The restriction on the phases provides extra constraints on the parameters of the correcting pulses. First of all, it "discretizes" the total duration of the pulses. For the correcting pulses we still have a choice of  $\Delta_{\pi}(t_2)$  and  $\Delta_{\pi}(t_1)$ . They will be chosen maximally close to  $|\Delta(t_2)|2^{1/2}(g_{\pi}/g)^{1/3}$  and  $\Delta(t_1)2^{1/2}(g_{\pi}/g)^{1/3}$ , respectively, in order to minimize the error of the adiabatic approximation (2.3) and to minimize the overall pulse duration.

We will characterize the gate error  $\mathcal{E}$  by the spectral norm of the difference of the operator S in the presence of errors and the "ideal" gate operator  $S^{(0)}$ ,

$$\mathcal{E} = ||S - S^{(0)}||_2. \tag{2.18}$$

Here,  $||A||_2$  is the square root of the maximal eigenvalue of the operator  $A^{\dagger}A$ . For uncorrected pulses  $S = S(t_2, t_1)$ , whereas for corrected pulses  $S = S_c(t'_2, t'_1)$ . For simple symmetric composite pulses described below, the overall sign of the composite pulse is opposite to that of the original pulse in the absence of errors. In this case we set  $S = -S_c(t'_2, t'_1)$  in Eq. (2.18).

For uncorrected pulses we have

$$\mathcal{E} = 2^{1/2} |1 - n_{x1} n_{x2} - n_{u1} n_{u2} \cos \alpha|^{1/2}, \tag{2.19}$$

where  $\mathbf{n}_i = (\cos[\delta\phi(t_i)], \sin[\delta\phi(t_i)])$  is an auxiliary 2D unit vector (i = 1, 2). Eq. (2.18) applies also in the case of corrected pulses, but now we have to replace in the definition of the  $\mathbf{n}_1$  vector

$$\delta\phi(t_1) \to \delta\phi(t_1) - \delta\phi_{\pi}(t_1) - \delta\phi_{\pi}(t_1'). \tag{2.20}$$

A similar replacement must be done in the definition of the vector  $\mathbf{n}_2$ .

For small phase errors  $|\delta\phi(t_{1,2})|$  the function  $\mathcal E$  for uncorrected pulses is linear in the error. In particular, to first order in  $\varepsilon$  for a symmetric pulse we have  $|\delta\phi(t_1)| \approx$ 

 $|\delta\phi(t_2)| \approx \varepsilon E(t_1)/\eta$ , and  $\mathcal{E} \approx 2|\varepsilon|E(t_1)\eta^{-1}\sin(\alpha/2)$ . In contrast, by applying the same arguments to a corrected pulse, we see that the gate error is  $\propto \varepsilon^3$ . As noted above, the terms  $\propto \varepsilon^3$  and higher-order terms in  $\varepsilon$  contain a small factor. They become very small already for not too small  $\varepsilon$ .

To illustrate how the composite pulse works we compare in Fig. 2.6 the error of an uncorrected LZ gate with the gate error of the composite pulse. The data refer to different values of g of the working pulse; the corresponding values of  $\alpha$  are given in Fig. 2.4. We used  $\Delta(t_1) = -\Delta(t_2) \approx 10\eta^{1/2}$  [the precise value of  $\Delta(t_{1,2})$  was adjusted to make  $S(t_2, t_1)$  an X-rotation,  $S(t_2, t_1) = R_x(\alpha)$ ]. The compensating  $\pi$ -pulses where modeled by pulses with  $g_{\pi} = 3$ . Based on the arguments provided at the end of Sec. IV A, we took  $\Delta_{\pi}(t_2) \approx |\Delta(t_2)| 2^{1/2} (g_{\pi}/g)^{1/3}$ , whereas  $\Delta_{\pi}(t_2')$  was found from Eq. (2.16); we used  $\Delta_{\pi}(t_1') = -\Delta_{\pi}(t_2')$  and  $\Delta_{\pi}(t_1) = -\Delta_{\pi}(t_2)$ .

It is seen from Fig. 2.6 that the proposed composite pulses are extremely efficient for compensating gate errors. Even for the energy error  $\varepsilon = \gamma$ , where the error of an uncorrected pulse is close to 1, for the composite pulse  $\mathcal{E} \lesssim 10^{-3}$ . For  $g \lesssim 1$  the error of the single pulse scales as  $\varepsilon$ , whereas the error of the composite pulse scales as  $\varepsilon^3$ , in agreement with the theory. For large g, when the gate is almost an X-gate ( $\pi$ -pulse), in the case of symmetric pulses that we discuss, the coefficients at the terms  $\propto \varepsilon$  and  $\propto \varepsilon^3$  become small; they become equal to zero for  $\alpha = \pi$ . Therefore for large g and for not too small  $\varepsilon$  the errors of single and composite pulses scale as  $\varepsilon^2$  and  $\varepsilon^4$ , respectively. On the other hand, for  $\varepsilon/\gamma$  close to 1, errors of the composite pulses with larger g are larger than for smaller g. This is because the calculations in Fig. 2.6 refer to the same  $\Delta/\eta^{1/2}$ , in which case the errors  $\propto \varepsilon^3$ ,  $\varepsilon^4$  are proportional to  $g^2$ .

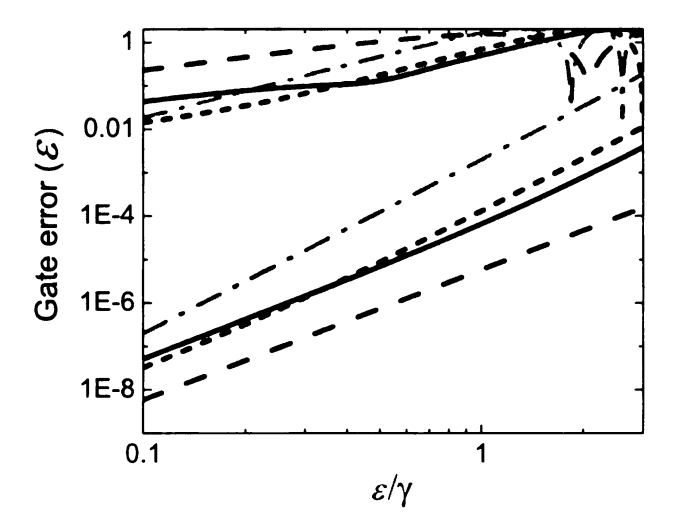


Figure 2.6: Gate errors  $\mathcal{E}$  for Landau-Zener pulses as a function of the frequency error  $\mathcal{E}$ . The upper and lower curves refer to the single LZ pulse and the composite pulse, respectively. The dash-dotted, dotted, solid, and dashed lines show  $\mathcal{E}$  for g = 2, 1.2, 1, and 0.3.

#### 2.5 Conclusions

In this chapter we have developed a theory of quantum gates based on LZ pulses. In these pulses the control dc field is varied in such a way that the qubit frequency passes through the frequency of the external radiation field. In the adiabatic basis an LZ gate can be expressed in a simple explicit form in terms of rotation matrices. Our central result is that already a sequence of three LZ pulses can be made fault-tolerant. The error of the corresponding composite pulse  $\mathcal{E}$  scales with the error  $\varepsilon$  in the qubit energy or radiation frequency at least as  $\varepsilon^3$ . In addition, the coefficient at  $\varepsilon^3$  has an extra parametrically small factor. The duration of the 3-pulse sequence is about 4 times the duration of the single pulse, for the parameters that we used.

Fault tolerance of LZ gates is partly due to the change of state populations being independent of precise frequency tuning. In particular, LZ tunneling makes it

possible to implement simple  $\pi$ -pulses with an exponentially small error in the state population.

The approach developed here can be easily generalized to more realistic smooth pulses, as mentioned above. It can be applied also to two-qubit gate operations in which the frequencies of interacting qubits are swept past each other, leading to excitation transfer [58]. Such operations are complementary to two-qubit phase gates and require a different qubit-qubit interaction.

LZ pulses provide an alternative to control pulses where qubits stay in resonance with radiation for a specified time [2]. In this more conventional approach it is often presumed that qubits are addressed individually by tuning their frequencies. In contrast to this technique, LZ pulses do not require stabilizing the frequency at a fixed value during the operation. As a consequence, calibration of LZ pulses is also different, which may be advantageous for some applications, in particular in charge-based systems [60, 63]. The explicit expressions discussed above require that the qubit transition frequency vary linearly with time, but the linearity is needed only for a short time when the qubit and radiation frequencies are close to each other, as seen from Fig.2.2, which should not be too difficult to achieve.

For pulses based on resonant tuning for a fixed time, much effort has been put into developing fault-tolerant pulse sequences, see Ref. [3] and papers cited therein. In particular, for energy offset errors it has been shown that a three-pulse sequence can reduce the error to  $\mathcal{E} \sim \varepsilon^2$  [7] (the fidelity F evaluated in Ref. [7] is related to  $\mathcal{E}$  discussed in Ref. [3] and in this chapter by the expression  $1 - F \propto \mathcal{E}^2$  for small  $\mathcal{E}$ ; therefore an error  $\mathcal{E} \sim \varepsilon^2$  corresponds to the estimate [7]  $1 - F \sim \varepsilon^4$ ). As illustrated in Fig.2.7, this error is parametrically larger, for small  $\varepsilon$ , than the error of the three-pulse sequence proposed here,  $\mathcal{E} \propto \varepsilon^3$ . We note that, with two correcting pulses of a

more complicated form, it is possible to eliminate errors of higher order in  $\varepsilon$ . It follows

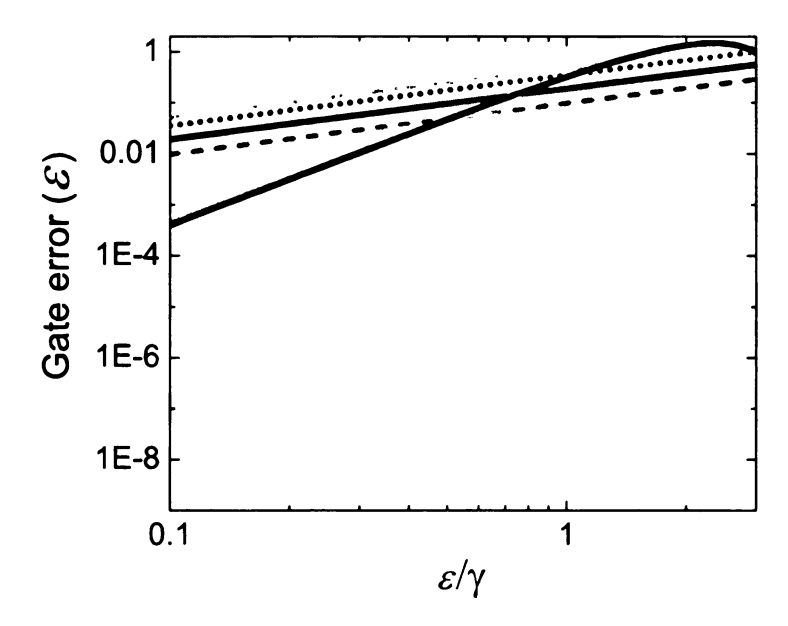


Figure 2.7: Gate errors  $\mathcal{E}$  for CORPSE pulses [7] as a function of the off-resonance error  $\varepsilon$ . The upper and lower curves refer to uncorrected pulses and composite pulses, respectively. The dash-dotted, dotted, solid, and dashed lines show  $\mathcal{E}$  for rotation angles  $\theta = \pi, \pi/2, \pi/4$ , and  $\pi/8$ . Here, the ideal gate operation, related to the ideal Hamiltonian  $H = \gamma X$ , is  $U = R_x(\theta)$ , where  $\theta = 2\gamma T$  and T is the duration of the pulse. Off-resonance errors lead, as in the case of Landau-Zener gates, to  $H \to H' = H + \varepsilon Z/2$ . As a consequence,  $U \to U' = R_{\vec{n}}(\theta')$ , where  $\vec{n} = 1/\sqrt{1+\varepsilon^2/4\gamma^2} (1,0,\varepsilon/2\gamma)^{\rm T}$  and  $\theta' = \theta\sqrt{1+\varepsilon^2/4\gamma^2}$ . Note that in the displayed range of  $\varepsilon/\gamma$ , the error of the composite pulse is practically independent of  $\theta$  (which is not the case for smaller values of  $\varepsilon/\gamma$ ). The CORPSE composite pulse sequence has the form  $U = R_x(\theta_3)R_{-x}(\theta_2)R_x(\theta_1)$ , where  $\theta_1 = 2\pi + \theta/2 - \sin^{-1}(\sin(\theta/2)/2)$ ,  $\theta_2 = 2\theta_1 - 2\pi - \theta$ , and  $\theta_3 = \theta_1 - 2\pi$ .

from the results of this chapter that fault-tolerant LZ gates can be implemented using the standard repertoire of control techniques and may provide a viable alternative to the conventional single qubit gates.

## Chapter 3

## Multiphoton Antiresonance in

## Large-Spin Systems

#### 3.1 Introduction

Large-spin systems have been attracting much attention recently. Examples are S=3/2 and S=5/2 Mn impurities in semiconductors and Mn- and Fe-based molecular magnets with electron spin S=10 and higher. Nuclear spins I=3/2 have been also studied, and radiation-induced quantum coherence between the spin levels was observed [10]. An important feature of large-spin systems is that their energy levels may be almost equidistant. A familiar example is spins in a strong magnetic field in the case of a relatively small magnetic anisotropy, where the interlevel distance is determined primarily by the Larmor frequency. Another example is low-lying levels of large-S molecular magnets for small tunneling. As a consequence of the structure of the energy spectrum, external modulation can be close to resonance with many transitions at a time. This should lead to coherent nonlinear resonant effects that have no analog in two-level systems.

The effects of a strong resonant field on systems with nearly equidistant energy levels have been studied for weakly nonlinear oscillators. These studies concern both coherent effects, which occur without dissipation [31, 32, 33], and incoherent effects, in particular those related to the oscillator bistability and transitions between coexisting stable states of forced vibrations. In the absence of dissipation, a nonlinear oscillator may display multiphoton antiresonance in which the susceptibility displays a dip or a peak as a function of modulation frequency [34].

In this chapter we study resonantly modulated spin systems with S > 1/2. Of primary interest are systems with uniaxial magnetic anisotropy, with the leading term in the anisotropy energy of the form of  $-DS_z^2/2$ . We show that the coherent transverse response of such spin systems displays peaks or dips when the modulation frequency adiabatically passes through multiphoton resonances. The effect is nonperturbative in the field amplitude. It is related to the special conformal property of the spin dynamics in the semiclassical limit. It should be noted that the occurrence of antiresonance for a spin does not follow from the results for the oscillator. A spin can be mapped onto a system of two oscillators rather than one; the transition matrix elements for a spin and an oscillator are different as are also the energy spectra.

We show that the coherent transverse response of a spin is sensitive to terms of higher order in  $S_z$  in the anisotropy energy. In addition, there is a close relation between the problem of resonant high-frequency response of a spin and the problem of static spin polarization transverse to the easy axis. Spin dynamics in a static magnetic field has been extensively studied both theoretically and experimentally [12, 13, 14, 15, 16, 17, 18, 19, 20, 21]. One of the puzzling observations on magnetization switching in molecular magnets, which remained unexplained except for the low-order perturbation theory, is that the longitudinal magnetic field at which the switching

occurs is independent of the transverse magnetic field [16]. The analysis presented below provides an explanation which is nonperturbative in the transverse field and also predicts the occurrence of peaks or dips in the static polarization transverse to the easy axis as the longitudinal magnetic field is swept through resonance.

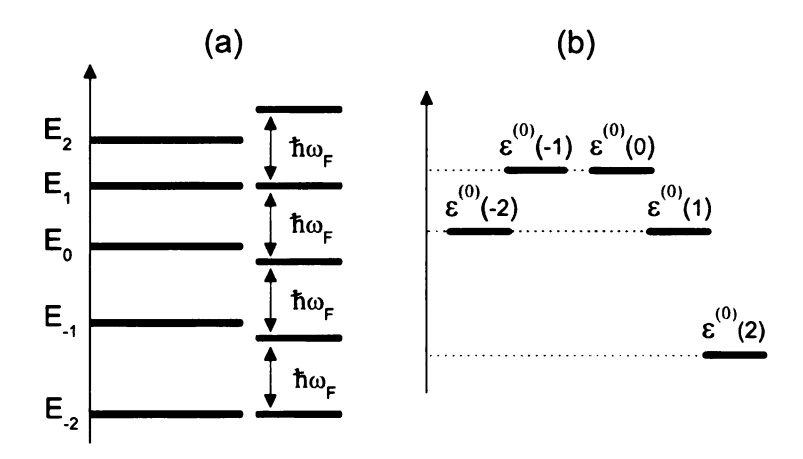


Figure 3.1: Three-photon resonance in a S=2 system in the limit of a weak ac field. (a) Spin energy levels  $E_m$  and n-photon energies  $n\hbar\omega_F$ . (b) Quasienergies in the limit of zero modulation amplitude,  $\varepsilon^{(0)}(m) = E_m - m\hbar\omega_F$ ; the pairwise degenerate levels correspond to one- and three-photon resonance, respectively.

The onset of strong nonlinearity of the transverse response due to near equidistance of the energy levels can be inferred from Fig. 3.1(a). It presents a sketch of the Zeeman levels of a spin  $E_m$  ( $-S \le m \le S$ ) in a strong magnetic field along the easy magnetization axis  $\hat{\mathbf{z}}$ . The spin Hamiltonian is

$$H_0 = \omega_0 S_z - \frac{1}{2} D S_z^2 \qquad (\hbar = 1),$$
 (3.1)

where  $\omega_0$  is the Larmor frequency. For comparatively weak anisotropy,  $DS \ll \omega_0$ , the interlevel distances  $E_{m+1} - E_m$  are close to each other and change linearly with m.

A transverse periodic field leads to transitions between neighboring levels. An interesting situation occurs if the field frequency  $\omega_F$  is close to  $\omega_0$  and there is

multiphoton resonance in the mth state:  $N\omega_F$  coincides with the energy difference  $E_{m+N} - E_m$ , N > 1. The amplitude of the resonant N-photon transition in this case is comparatively large, because the transition goes via N sequential one-photon virtual transitions which are all almost resonant. Therefore one should expect a comparatively strong multiphoton Rabi splitting already for a moderately strong field.

A far less obvious effect occurs in the coherent transverse response of the system, that is in the magnetization at the modulation frequency or, equivalently, the susceptibility. As we show, the expectation value of the susceptibility displays sharp spikes at multiphoton resonance. The shape of the spikes very strongly depends on the field amplitude.

The chapter is organized as follows. In Sec. II we study the quasienergy spectrum and the transverse response of a spin with quadratic in  $S_z$  anisotropy energy. We show that, at multiphoton resonance, not only multiple quasienergy levels are crossing pairwise, but the susceptibilities in the resonating states are also crossing. In Sec. III we show that multiphoton transitions, along with level repulsion, lead to the onset of spikes in the susceptibility and find the shape and amplitude of the spikes as functions of frequency and amplitude of the resonant field. In Sec. IV we present a WKB analysis of spin dynamics, which explains the simultaneous crossing of quasienergy levels and the susceptibilities beyond perturbation theory in the field amplitude. In Sec. V the role of terms of higher order in  $S_z$  in the anisotropy energy is considered. Section VI contains concluding remarks.

#### 3.2 Low-field susceptibility crossing

#### 3.2.1 The quasienergy spectrum

We first consider a spin with Hamiltonian  $H_0$  (3.1), which is additionally modulated by an almost resonant ac field. The modulation can be described by adding to  $H_0$ the term  $-S_x A \cos \omega_F t$ , where A characterizes the amplitude of the ac field. As mentioned above, we assume that the field frequency  $\omega_F$  is close to  $\omega_0$  and that  $\omega_F, \omega_0 \gg D, A, |\omega_F - \omega_0|$ .

It is convenient to describe the modulated system in the quasienergy, or Floquet representation. The Floquet eigenstates  $|\psi_{\varepsilon}(t)\rangle$  have the property  $|\psi_{\varepsilon}(t+\tau_F)\rangle = \exp(-i\varepsilon\tau_F)|\psi_{\varepsilon}(t)\rangle$ , where  $\tau_F = 2\pi/\omega_F$  is the modulation period and  $\varepsilon$  is quasienergy. For resonant modulation, quasienergy states can be found by changing to the rotating frame using the canonical transformation  $U(t) = \exp(-i\omega_F S_z t)$ . In the rotating wave approximation the transformed Hamiltonian is

$$H = -\delta\omega S_z - \frac{1}{2}DS_z^2 - \frac{1}{2}AS_x,$$

$$\delta\omega = \omega_F - \omega_0.$$
(3.2)

Here we disregarded fast-oscillating terms  $\propto A \exp(\pm 2i\omega_F t)$ .

The Hamiltonian H has a familiar form of the Hamiltonian of a spin in a scaled static magnetic field with components  $\delta \omega$  and A/2 along the  $\hat{\mathbf{z}}$  and  $\hat{\mathbf{x}}$  axes, respectively. Much theoretical work has been done on spin dynamics described by this Hamiltonian in the context of molecular magnets.

The eigenvalues of H give quasienergies of the modulated spin. In the weak modulating field limit,  $A \to 0$ , the quasienergies are shown in Fig.3.1(b). In this limit spin states are the Zeeman states, i.e., the eigenstates  $|m\rangle^{(0)}$  of  $S_z$ , with  $-S \le m \le 1$ 

S. The interesting feature of the spectrum, which is characteristic of the magnetic anisotropy of the form  $DS_z^2$ , is that several states become simultaneously degenerate pairwise for A = 0 [16, 17]. From Eq. (3.2), the quasienergies  $\varepsilon^{(0)}(m)$  and  $\varepsilon^{(0)}(m+N)$  are degenerate if the modulation frequency is

$$\delta\omega = \delta\omega_{m:N}, \qquad \delta\omega_{m:N} = -D\left(m + \frac{1}{2}N\right).$$
 (3.3)

The condition (3.3) is simultaneously met for all pairs of states with given 2m + N. It coincides with the condition of N-photon resonance  $E_{m+N} - E_m = N\omega_F$ . In what follows N can be positive and negative. There are 4S-1 frequency values that satisfy the condition (3.3) for a given S.

The field  $\propto A$  leads to transitions between the states  $|m\rangle^{(0)}$  and to quasienergy splitting. The level splitting for the Hamiltonian (3.2) was calculated earlier [17]. For multiphoton resonance, it is equal to twice the multiphoton Rabi frequency  $\Omega_R(m; N)$ ,

$$\Omega_R(m; N) = |A/2D|^{|N|} |D| 
\times \left[ \frac{(S+m+N)!(S-m)!}{(S+m)!(S-m-N)!} \right]^{\frac{1}{2} \operatorname{sgn} N} \frac{1}{2(|N|-1)!^2}$$
(3.4)

The N-photon Rabi frequency (3.4) is  $\propto A^{|N|}$ , as expected. We note that the amplitude A is scaled by the anisotropy parameter D, which characterizes the nonequidistance of the energy levels and is much smaller than the Larmor frequency. Therefore  $\Omega_R$  becomes comparatively large already for moderately weak fields  $A \sim D$ .

We denote the true quasienergy states as  $|\nu\rangle$ , with integer or half-integer  $\nu$  such that  $-S \leq \nu \leq S$ . The quasienergies  $\varepsilon_{\nu}$  do not cross. One can enumerate the states  $|\nu\rangle$  by thinking of them as the adiabatic states for slowly increasing  $\delta\omega$ , starting from large negative  $\delta\omega$ . For  $-\delta\omega/DS \gg 1$ , |A|/D the states  $|\nu\rangle$  are very close to the Zeeman states  $|\nu\rangle^{(0)}$ , with  $\nu$  being the eigenvalue of  $S_z$ . This then specifies the values of  $\nu$  for all  $\delta\omega$ .

If the field is weak, the states  $|\nu\rangle$  are close to the corresponding Zeeman states,  $|\nu\rangle \approx |m\rangle^{(0)}$ , for all  $\delta\omega$  except for narrow vicinities of the resonant values  $\delta\omega_{m:N}$  given by Eq. (3.3). The relation between the numbers  $\nu$  and m for  $|\nu\rangle \approx |m\rangle^{(0)}$  is

$$\nu = m + \sum_{N}' \theta (\delta \omega - \delta \omega_{m;N}) \operatorname{sgn} N, \tag{3.5}$$

where N runs from -S-m to S-m; the term N=0 is eliminated, which is indicated by the prime over the sum;  $\theta(x)$  is the step function. In obtaining Eq. (3.5) we took into account that, for weak fields, only neighboring quasienergy levels  $\varepsilon_{\nu}$  and  $\varepsilon_{\nu\pm 1}$ come close to each other. Eq. 3.5) defines the state enumerating function  $m(\nu)$ .

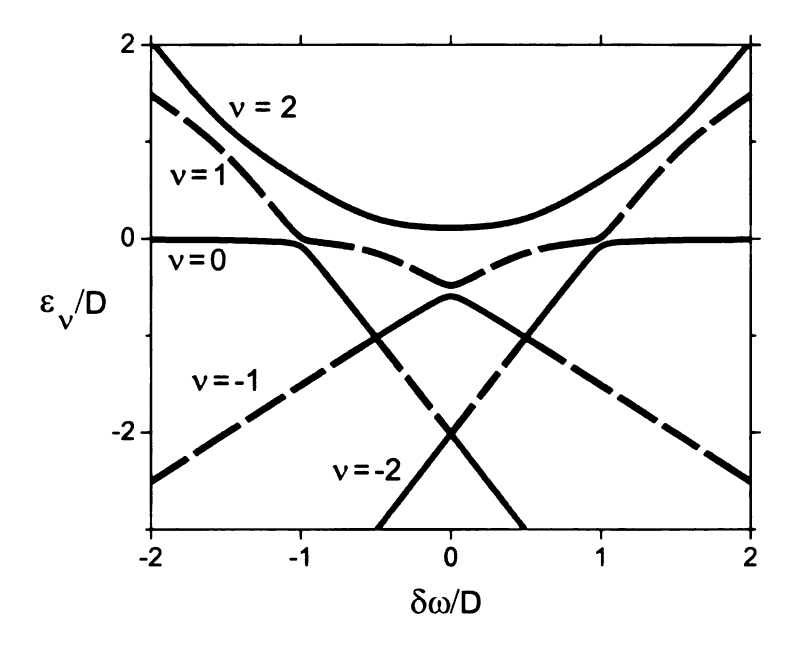


Figure 3.2: Quasienergy levels  $\varepsilon_{\nu}$  for a spin-2 system as functions of detuning  $\delta\omega/D$  for the scaled field amplitude A/D=0.3. The levels anticross pairwise at multiphoton resonances given by Eq. (3.3). The unperturbed quasienergies (the limit A=0) correspond to straight lines  $\varepsilon^{(0)}(m)=-\delta\omega\,m-Dm^2/2$ .

The enumeration scheme and the avoided crossing of the quasienergy levels are illustrated in Fig. 3.2. For the chosen S=2 the anticrossing occurs for 7 frequency values, as follows from Eq. (3.3). The magnitude of the splitting strongly depends

on N: the largest splitting occurs for one-photon transitions. It is also obvious from Fig. 3.2 that several levels experience anticrossing for the same modulation frequency.

#### 3.2.2 Susceptibility and quasienergy crossing

Of central interest to us it the nonlinear susceptibility of the spin. We define the dimensionless susceptibility  $\chi_{\nu}$  in the quasienergy state  $|\nu\rangle$  as the ratio of the expectation value of the appropriately scaled transverse magnetization at the modulation frequency to the modulation amplitude,

$$\chi_{\nu}(\omega_F) = \langle \nu | S_- | \nu \rangle / A. \tag{3.6}$$

In the weak field limit,  $A \to 0$ .

$$\chi_{\nu}(\omega_F) = \frac{m(2\delta\omega + Dm) + DS(S+1)}{4(\delta\omega + Dm)^2 - D^2}$$
(3.7)

where m and  $\nu$  are related by Eq. (3.5); in fact, Eq. (3.7) gives the susceptibility in the perturbed to first order in A Zeeman state  $|m\rangle^{(0)}$ .

A remarkable feature of Eq. (3.7) is the susceptibility crossing at multiphoton resonance. The susceptibilities in Zeeman states  $|m\rangle^{(0)}$  and  $|m+N\rangle^{(0)}$  are equal where the unperturbed quasienergies of these states are equal,  $\varepsilon^{(0)}(m) = \varepsilon^{(0)}(m+N)$ , i.e., where the frequency detuning is  $\delta\omega = \delta\omega_{m;N}$ . In terms of the adiabatic states  $|\nu\rangle$ , for such  $\delta\omega$  we have from Eqs. (3.5), (3.7)  $\chi_{\nu}(\omega_F) = \chi_{\nu'}(\omega_F)$  for  $\nu' = \nu + \operatorname{sgn} N$ .

A direct calculation shows that simultaneous crossing of the susceptibilities and quasienergies occurs also in the fourth order of the perturbation theory provided  $N \geq 3$ . Numerical diagonalization of the Hamiltonian (3.2) indicates that it persists in higher orders, too, until level repulsion due to multiphoton Rabi oscillations comes into play.

The susceptibility  $\chi_{\nu}$  is immediately related to the field dependence of the quasienergy  $\varepsilon_{\nu}$ . Since  $\langle \nu | S_{+} | \nu \rangle = \langle \nu | S_{-} | \nu \rangle$ , from the explicit form of the Hamiltonian (3.2) we have

$$\chi_{\nu} = -2A^{-1}\partial\varepsilon_{\nu}/\partial A,\tag{3.8}$$

Simultaneous crossing of the susceptibilities and quasienergies means that, for an Nphoton resonance, the Stark shift of resonating states is the same up to order N-1in A; only in the Nth order the levels  $\varepsilon_{\nu}$  and  $\varepsilon_{\nu+\mathrm{sgn}N}$  become split [by  $2\Omega_{R}(m;N)$ ].
Respectively, the susceptibilities  $\chi_{\nu}$  and  $\chi_{\nu+\mathrm{sgn}N}$  coincide up to terms  $\propto A^{|N|-3}$ .
The physical mechanism of this special behavior is related to the conformal property of the spin dynamics, as explained in Sec. 3.4.

Equation (3.7) does not apply in the case of one-photon resonance, N=1: it gives  $|\chi_{\nu}| \to \infty$  for  $\delta\omega \to \delta\omega_{m;1}$ . This is similar to the case of one-photon resonance in a two-level system, where the behavior of the susceptibility is well understood beyond perturbation theory. Interestingly, the lowest-order perturbation theory does not apply also at exact two-photon resonance,  $\delta\omega = \delta\omega_{m;2}$ , as discussed below, even though Eq. (3.7) does not diverge.

# 3.3 Antiresonance of the transverse multiphoton response

The field-induced anticrossing of quasienergy levels at multiphoton resonance is accompanied by lifting the degeneracy of the susceptibilities. It leads to the onset of a resonant peak and an antiresonant dip in the susceptibilities as functions of frequency  $\delta\omega$ . The behavior of the quasienergy levels and the susceptibilities is seen from Fig. 3.3. For small field amplitude A the multiphoton Rabi frequency  $\Omega_R \propto A^{|N|}$  is small, the quasienergies of interest  $\varepsilon_{\nu}$  and  $\varepsilon_{\nu+1}$  (with  $m(\nu+1)-m(\nu)=N$ ) come very close to each other at resonant  $\delta\omega$ , as do also the susceptibilities  $\chi_{\nu}$  and  $\chi_{\nu+1}$ .

With increasing A the level splitting rapidly increases in a standard way. The behavior of the susceptibilities is more complicated. They cross, but sufficiently close to resonance they repel each other, forming narrow dips (antiresonance) or peaks (resonance). The widths and amplitudes of the dips/peaks display a sharp dependence on the amplitude and frequency of the field.

For weak field it is straightforward to find the splitting of the susceptibilities

$$\Delta \chi_{\nu;N}(\omega_F) = |\chi_{\nu}(\omega_F) - \chi_{\nu+\mathrm{sgn}N}(\omega_F)|$$

close to N-photon resonance between states  $|m\rangle^{(0)}$  and  $|m+N\rangle^{(0)}$ . In this region the frequency detuning from the resonance

$$\Delta\omega(m;N) = N(\delta\omega - \delta\omega_{m;N})/2 \tag{3.9}$$

is small,  $|\Delta\omega(m;N)| \lesssim \Omega_R(m;N)$ . To the lowest order in A but for an arbitrary ratio  $\Omega_R(m;N)/|\Delta\omega(m;N)|$  the quasienergy states  $|\nu\rangle$  and  $|\nu+\operatorname{sgn}N\rangle$  are linear combinations of the states  $|m\rangle^{(0)}$  and  $|m+N\rangle^{(0)}$ . Then from Eq. (3.2) it follows that the splitting of the quasienergies  $\Delta\varepsilon_{\nu;N} = |\varepsilon_{\nu} - \varepsilon_{\nu+\operatorname{sgn}N}|$  is

$$\Delta \varepsilon_{\nu;N} = \left[ \Delta \omega^2(m;N) + 4\Omega_R^2(m;N) \right]^{1/2}. \tag{3.10}$$

From this expression and Eqs. (3.4), (3.8) it follows that the susceptibility splitting is

$$\Delta \chi_{\nu;N} = \frac{8|N|\Omega_R^2(m;N)}{A^2 \left[\Delta \omega^2(m;N) + 4\Omega_R^2(m;N)\right]^{1/2}}.$$
 (3.11)

The splitting  $\Delta \chi_{\nu;N}$  as a function of frequency  $\delta \omega$  is maximal at N-photon resonance,  $\delta \omega = \delta \omega_{m;N}$ . The half-width of the peak of  $\Delta \chi_{\nu;N}$  at half height is determined

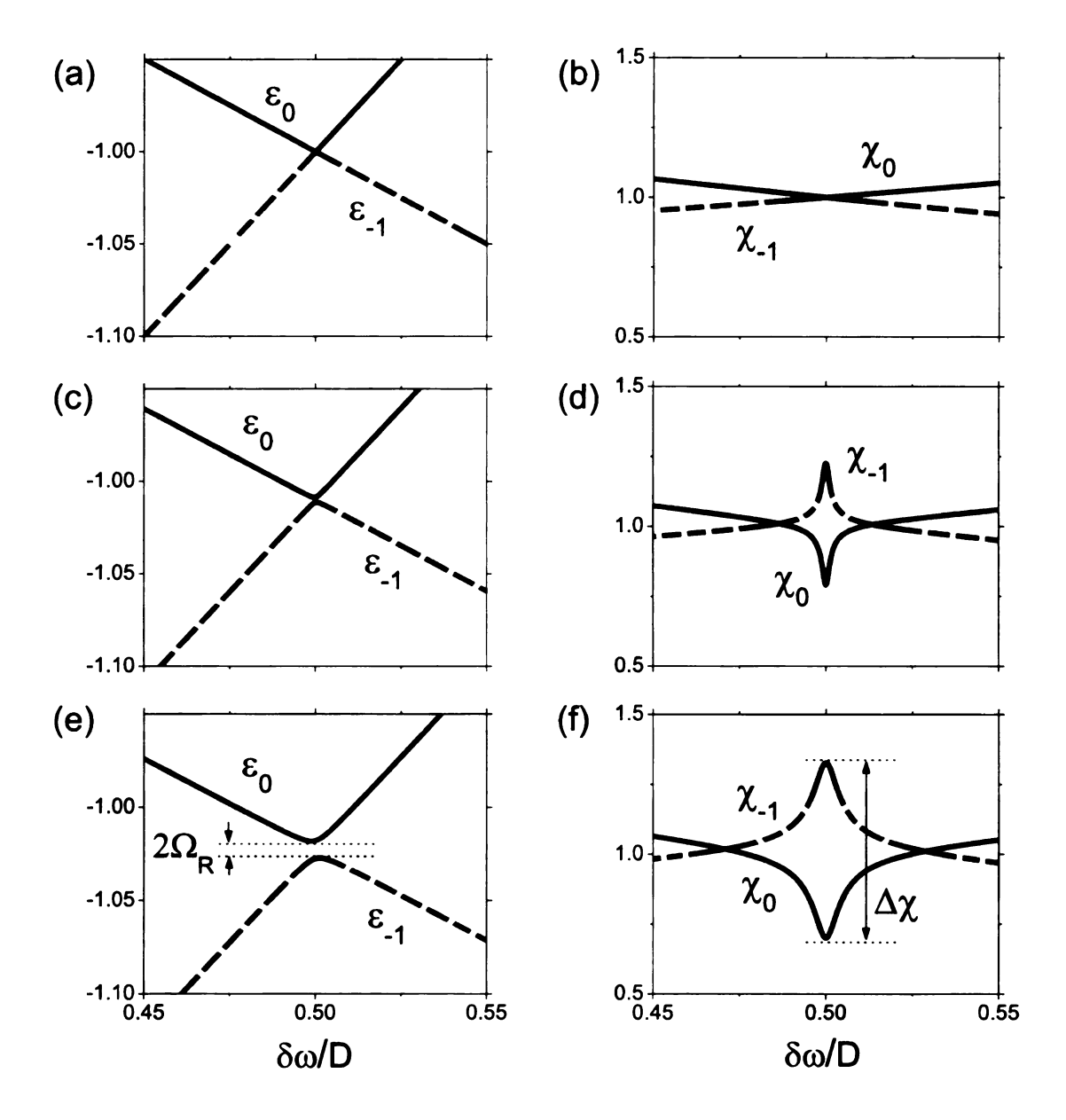


Figure 3.3: Level anticrossing and antiresonance of the susceptibilities. The figure refers to a 3-photon resonance, N=3, in an S=2 system. The involved quasienergy states are  $\nu=-1$  and  $\nu=0$ . The resonating Zeeman states for A=0 are m=-2 and m=1 (the ground and 3rd excited state). Left and right panels show the quasienergies  $\varepsilon_{\nu}$  and susceptibilities  $\chi_{\nu}$  for the same reduced field A/D. Panels (a) and (b), (c) and (d), and (e) and (f) refer to A/D=0, 0.2, and 0.3, respectively.

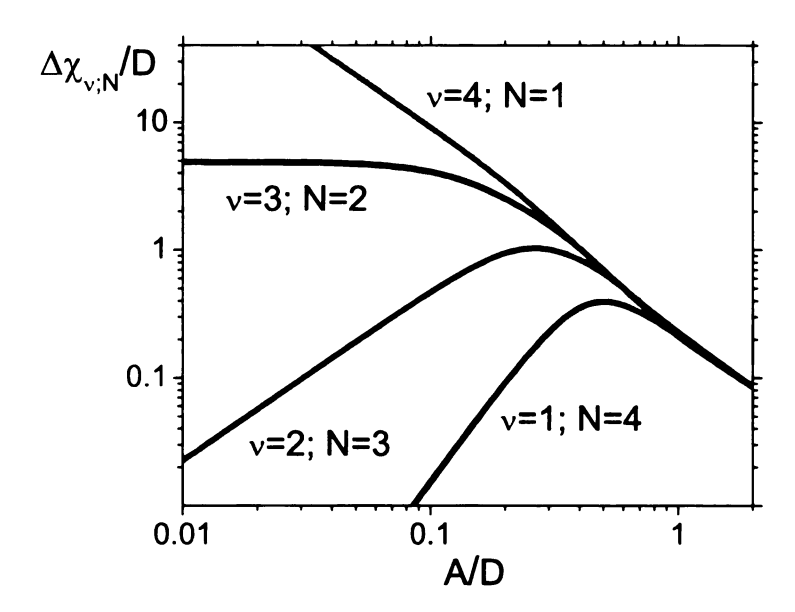


Figure 3.4: The multiphoton susceptibility splitting for S=2. The curves refer to exact N-photon resonances, with  $N=1,\ldots,4$ , for transitions from the ground Zeeman state m=-2 to the excited states  $m=-1,\ldots,2$ , respectively.

by the Rabi splitting and is equal to  $\sqrt{3}\Omega_R/N$ . The peak is strongly non-Lorentzian, it is sharper than the Lorentzian curve with the same half-width. This sharpness is indeed seen in Fig. 3.3. Our numerical results show that Eq. (3.11) well describes the splitting in the whole frequency range  $|\Delta\omega| \lesssim \Omega_R$ .

For small A, the susceptibility splitting is stronger than the level repulsion. It follows from Eqs. (3.10), (3.11) that at exact N-photon resonance  $\Delta\varepsilon \propto A^{|N|}$  whereas  $\Delta\chi \propto A^{|N|-2}$ . This scaling is seen in Fig. 3.4. For  $A/D \gg 1$ , on the other hand, the eigenstates  $|\nu\rangle$  become close to the eigenstates of a spin with Hamiltonian  $-AS_x/2$ . As a result, the susceptibility splitting decreases with increasing A,  $|\Delta\chi_{\nu;N}| \propto A^{-1}$ ; the proportionality coefficient here is independent of N. Therefore, for  $N \geq 3 \Delta\chi_{\nu}$  displays a maximum as a function of A, as seen from Fig. 3.4.

#### 3.3.1 Two-photon resonance

As mentioned above, the lowest order perturbation theory (3.7) does not describe resonant susceptibility for two-photon resonance. Indeed, it follows from Eq. (3.11) that at exact resonance,  $\delta \omega = \delta \omega(m; 2)$ , the susceptibility splitting for weak fields is

$$\Delta \chi_{\nu;2} = D^{-1} [(S - m - 1)(S - m) \times (S + m + 1)(S + m + 2)]^{1/2}.$$
(3.12)

This splitting is independent of A. The expression for the susceptibility (3.7) is also independent of A, yet it does not lead to susceptibility splitting and therefore is incorrect at two-photon resonance.

The inapplicability of the simple perturbation theory (3.7) is a consequence of quantum interference of transitions, the effect known in the linear response of multilevel systems [40]. To the leading order in A, the susceptibility is determined by the squared amplitudes of virtual transitions to neighboring states. For a two-photon resonance,  $\delta\omega = \delta\omega_{m;2}$ , the distances between the levels involved in the transitions  $|m\rangle^{(0)} \to |m+1\rangle^{(0)}$  and  $|m+2\rangle^{(0)} \to |m+1\rangle^{(0)}$  are equal,  $\varepsilon^{(0)}(m+1) - \varepsilon^{(0)}(m) = \varepsilon^{(0)}(m+1) - \varepsilon^{(0)}(m+2)$ . Therefore the transitions resonate and interfere with each other.

To calculate the susceptibility it is necessary to start with a superposition of states  $|m\rangle^{(0)}$  and  $|m+2\rangle^{(0)}$ , add the appropriately weighted amplitudes of transitions  $|m\rangle^{(0)} \to |m+1\rangle^{(0)}$  and  $|m+2\rangle^{(0)} \to |m+1\rangle^{(0)}$ , and then square the result. This gives the correct answer. The independence of the susceptibility splitting from A for two-photon resonance in the range of small A as given by Eq. (3.12) is seen in Fig. 3.4.

#### 3.4 Susceptibility crossing for a semiclassical spin

The analysis of the simultaneous level and susceptibility crossing is particularly interesting and revealing for large spins and for multiphoton transitions with large N. For  $S \gg 1$  the spin dynamics can be described in the WKB approximation. We will start with the classical limit. In this limit it is convenient to use a unit vector  $\mathbf{s} = \mathbf{S}/S$ , with  $\mathbf{s} \equiv (s_x, s_y, s_z) \equiv (\sin\theta\cos\phi, \sin\theta\sin\phi, \cos\theta)$ , where  $\theta$  and  $\phi$  are the polar and azimuthal angles of the vector  $\mathbf{s}$ . To the lowest order in  $S^{-1}$  equations of motion for the spin components can be written as

$$\dot{s}_x = s_y(s_z + \mu), \qquad \dot{s}_y = -s_x(s_z + \mu) + fs_z,$$

$$\dot{s}_z = -fs_y, \qquad f = A/2SD, \qquad \mu = \delta\omega/SD.$$
(3.13)

Here, overdot implies differentiation with respect to dimensionless time  $\tau = SDt$ , that is,  $\dot{\mathbf{s}} \equiv d\mathbf{s}/d\tau = (SD)^{-1}d\mathbf{s}/dt$ . Equations (3.13) preserve the length of the vector  $\mathbf{s}$  and also the reduced Hamiltonian  $g = H/S^2D$ ,

$$g \equiv g(\theta, \phi) = -\frac{1}{2}(s_z + \mu)^2 - fs_x. \tag{3.14}$$

For convenience, we added to g the term  $-\mu^2/2$ .

The effective energy  $g(\theta, \phi)$  is shown in Fig. 3.5. Also shown in this figure are the positions of the stationary states  $\dot{\mathbf{s}} = \mathbf{0}$  and examples of the phase trajectories described by Eqs. (3.13).

An insight into the spin dynamics can be gained by noticing that g has the form of the scaled free energy of an easy axis ferromagnet [64], with s playing the role of the magnetization M/M, and with  $\mu$  and f being the reduced components of the magnetic field along the easy axis z and the transverse axis x, respectively. In the

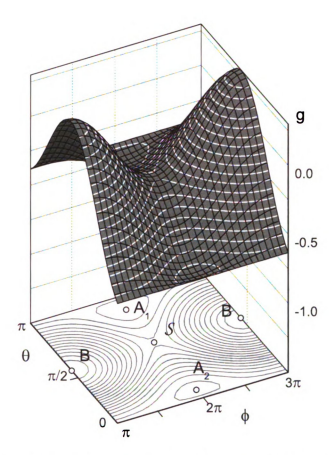


Figure 3.5: The effective energy  $g(\theta,\phi)$  as a function of the polar and azimuthal angles of the classical spin  $\theta$  and  $\phi$ . The lines  $g(\theta,\phi)=$  const describe classical spin trajectories. The points  $A_1$  and  $A_2$  are the minima of g, B is the maximum, and S is the saddle point. In the region  $g_S > g > g_{A_1}$  there are two coexisting types of trajectories. They lie on the opposite sides of the surface  $g(\theta,\phi)$  with respect to  $g_S$ . The plot refers to  $\mu=0.125$ , f=0.3.

region

$$|f|^{2/3} + |\mu|^{2/3} < 1 \tag{3.15}$$

the function g has two minima,  $A_1$  and  $A_2$ , a maximum B, and a saddle point S. We will assume that the minimum  $A_2$  is deeper than  $A_1$ , that is

$$g_B > g_S > g_{A_1} > g_{A_2}.$$
 (3.16)

As seen from Eqs. (3.13) and (3.14) and Fig. 3.5, for f > 0 the minima and the saddle

point are located at  $\phi = 0$  and the maximum is at  $\phi = \pi$ ; the case f < 0 corresponds to a replacement  $\phi \to \phi + \pi$ . On the boundary of the hysteresis region (3.15) the shallower minimum  $A_1$  merges with the saddle point  $\mathcal{S}$ .

In the case of an easy-axis ferromagnet with free energy g, the minima of g correspond to coexisting states of magnetization within the hysteresis region (3.15). For multiphoton absorption g is the scaled quasienergy, not free energy, and stability is determined dynamically by balance between relaxation and high-frequency excitation. One can show that, for relevant energy relaxation mechanisms, the system still has two coexisting stable stationary states albeit only in a part of the region (3.15). The states correspond to the shallower minimum and the maximum of g; for small damping the actual stable states are slightly shifted away from the extrema of g on the  $(\theta, \phi)$ -plane. We will not discuss relaxation effects in this chapter.

#### 3.4.1 Conformal property of classical trajectories

Dynamical trajectories of a classical spin on the plane  $(\theta, \phi)$  are the lines  $g(\theta, \phi) = \text{const.}$  They are either closed orbits around one of the minima  $A_1, A_2$  or the maximum B of g, or open orbits along the  $\phi$  axis, see Fig. 3.5. On the Bloch sphere  $\mathbf{s}^2 = 1$ , closed orbits correspond to precession of the unit vector  $\mathbf{s}$  around the points  $\mathbf{s}_{A_1}, \mathbf{s}_{A_2}$ , or  $\mathbf{s}_B$ , in which  $\mathbf{s}$  does not make a complete turn around the polar axis. Open orbits correspond to spinning of  $\mathbf{s}$  around the polar axis accompanied by oscillations of the polar angle  $\theta$ . Even though the spin has 3 components, the spin dynamics is the dynamics with one degree of freedom, the orbits on the Bloch sphere do not cross.

An important feature of the dynamics of a classical spin in the hysteresis region is that, for each g in the interval  $(g_{A_1}, g_{\mathcal{S}})$ , the spin has two coexisting orbits, see

Fig. 3.5. One of them corresponds to spin precession around  $\mathbf{s}_{A_1}$ . It can be a closed loop or an open trajectory around the point  $A_1$  on the  $(\theta, \phi)$ -plane. The other is an open trajectory on the opposite side of the g-surface with respect to the saddle point. We will classify them as orbits of type I and II, respectively.

We show in Appendix that classical equations of motion can be solved in an explicit form, and the time dependence  $\mathbf{s}(\tau)$  is described by the Jacobi elliptic functions. The solution has special symmetry. It is related to the conformal property of the mapping of  $s_z$  onto  $\tau$ . The major results of the analysis are the following features of the trajectories  $\mathbf{s}(\tau)$  of types I and II: for equal g, (i) their dimensionless oscillation frequencies  $\omega(g)$  are equal to each other, and (ii) the period averaged values of the component  $s_x(\tau)$  are equal, too,

$$\omega_I(g) = \omega_{II}(g), \qquad \langle s_x(\tau) \rangle_I = \langle s_x(\tau) \rangle_{II}.$$
 (3.17)

Here, the subscripts I and II indicate the trajectory type. The angular brackets  $\langle \ldots \rangle$  imply period averaging on a trajectory with a given g.

The quantity  $\langle s_x(\tau) \rangle$  gives the classical transverse response of the spin to the field  $\propto A$ . Equation (3.17) shows that this response is equal for the trajectories with equal values of the effective Hamiltonian function g. This result holds for any field amplitude A, it is by no means limited to small A/D where the perturbation theory in A applies.

#### 3.4.2 The WKB picture in the neglect of tunneling

In the WKB approximation, the values of quasienergy  $\varepsilon_{\nu}$  in the neglect of tunneling can be found by quantizing classical orbits  $g(\theta, \phi) = \text{const}$ , see Ref. [65] and papers cited therein. Such quantization should be done both for orbits of type I and type

II, and we classify the resulting states as the states of type I and II, respectively. The distance between the states of the same type in energy units is  $\hbar\omega(g)SD$  [66]. Transitions between states of types I and II with the same g are due to tunneling.

If we disregard tunneling, the quasienergy levels of states I and II will cross, for certain values of  $\mu$ . Remarkably, if two levels cross for a given  $\mu$ , then all levels in the range  $g_{A_1} < g < g_S$  cross pairwise. This is due to the fact that the frequencies  $\omega(g)$  and thus the interlevel distances for the two sets of states are the same, see Eq. (3.17). Such simultaneous degeneracy of multiple pairs of levels agrees with the result of the low-order quantum perturbation theory in A and with numerical calculations.

In the WKB approximation, the expectation value of an operator in a quantum state is equal to the period-averaged value of the corresponding classical quantity along the appropriate classical orbit [66]. Therefore if semiclassical states of type I and II have the same g, the expectation values of the operator  $S_x$  in these states are the same according to Eq. (3.17). Thus, the WKB theory predicts that, in the neglect of tunneling, there occurs simultaneous crossing of quasienergy levels and susceptibilities for all pairs of states with quasienergies between  $g_{A_1}$  and  $g_{S_1}$ . This is in agreement with the result of the perturbation theory in A and with numerical calculations. However, we emphasize that the WKB theory is not limited to small A, and the WKB analysis reveals the symmetry leading to the simultaneous crossing of quasienergy levels and the susceptibilities.

Tunneling between semiclassical states with equal g leads to level repulsion and susceptibility antiresonance. The level splitting  $2\Omega_R$  can be calculated by appropriately generalizing the standard WKB technique, for example as it was done in the analysis of tunneling between quasienergy states of a modulated oscillator [67]. Then the resonant susceptibility splitting can be found from Eq. (3.8). The corresponding

calculation is beyond the scope of this chapter.

### 3.5 Degeneracy lifting by higher order terms in $S_z$

The simultaneous crossing of quasienergy levels and susceptibilities in the neglect of tunneling is a feature of the spin dynamics described by Hamiltonian (3.2). Higher-order terms in  $S_z$  lift both this degeneracy and the property that many quasienergy levels are pairwise degenerate for the same values of the frequency detuning  $\delta\omega$ . The effect is seen already if we incorporate the term  $S_z^4$  in the anisotropy energy, i.e. for a spin with Hamiltonian

$$\tilde{H} = H - \frac{1}{4}GS_z^4. {(3.18)}$$

The Hamiltonian  $\tilde{H}$  is written in the rotating wave approximation, H is given by Eq. (3.2), and G is the parameter of quartic anisotropy. The terms  $S_x^2, S_y^2$  in the spin anisotropy energy do not show up in  $\tilde{H}$  even if they are present in the spin Hamiltonian  $H_0$  but the corresponding anisotropy parameters are small compared to  $\omega_0$ . In the rotating frame these terms renormalize the coefficient at  $S_z^2$  and lead to fast oscillating terms  $\propto S_{\pm}^2 \exp(\pm 2i\omega_F t)$  that we disregard.

Multiple pairwise degeneracy occurs where the condition on Zeeman quasienergies  $\varepsilon^{(0)}(m) = \varepsilon^{(0)}(m')$  is simultaneously met for several pairs (m, m'). For  $G \neq 0$  this happens only for  $\delta\omega = 0$ , that is when the modulation frequency  $\omega_F$  is equal to the Larmor frequency  $\omega_0$ . In this case the resonating Zeeman states are  $|m\rangle^{(0)}$  and  $|-m\rangle^{(0)}$  with the same m. The susceptibilities of these states are equal by symmetry with respect to reflection in the plane (x, y).

N-photon resonance for nonzero G and  $\omega_F \neq \omega_0$  occurs generally only for one pair of states  $|m\rangle^{(0)}$  and  $|m+N\rangle^{(0)}$ . This is seen from panel (a) in Fig. 3.6. With

increasing |G| the difference in the resonant values of frequency increases, as seen from panel (c) in the same figure.

The susceptibilities in resonating states are different in the weak-field limit. When the frequency  $\omega_F$  adiabatically goes through resonance, there occurs an interchange of states, for weak field A: if the state  $|\nu\rangle$  was close to  $|m\rangle^{(0)}$  on one side of resonance, it becomes close to  $|m+N\rangle^{(0)}$  on the other side. Respectively, the susceptibility  $\chi_{\nu}$  sharply switches from its value in the state  $|m\rangle^{(0)}$  to its value in the state  $|m+N\rangle^{(0)}$ .

Susceptibility switching is seen in panels (b) and (d) in Fig. 3.6. For a weak field the frequency range where the switching occurs is narrow and the switching is sharp (vertical, in the limit  $A \to 0$ ). As the modulation amplitude A increases the range of frequency detuning  $\delta \omega$  over which the switching occurs broadens. In addition, for small G the susceptibility displays spikes. They have the same nature as for G = 0. However, they are much less pronounced, as seen from the comparison of panel (d) in Fig. 3.6 and panel (f) in Fig. 3.3 which refer to the same value of A/D.

#### 3.6 Conclusions

In this chapter we have considered a large spin with an easy axis anisotropy. The spin is in a strong magnetic field along the easy axis and is additionally modulated by a transverse field with frequency  $\omega_F$  close to the Larmor frequency  $\omega_0$ . We have studied the coherent resonant transverse response of the spin. It is determined by the expectation value of the spin component transverse to the easy axis. We are interested in multiphoton resonance where  $N\omega_F$  coincides or is very close to the difference of the Zeeman energies  $E_{m+N}^{(0)} - E_m^{(0)}$  in the absence of modulation.

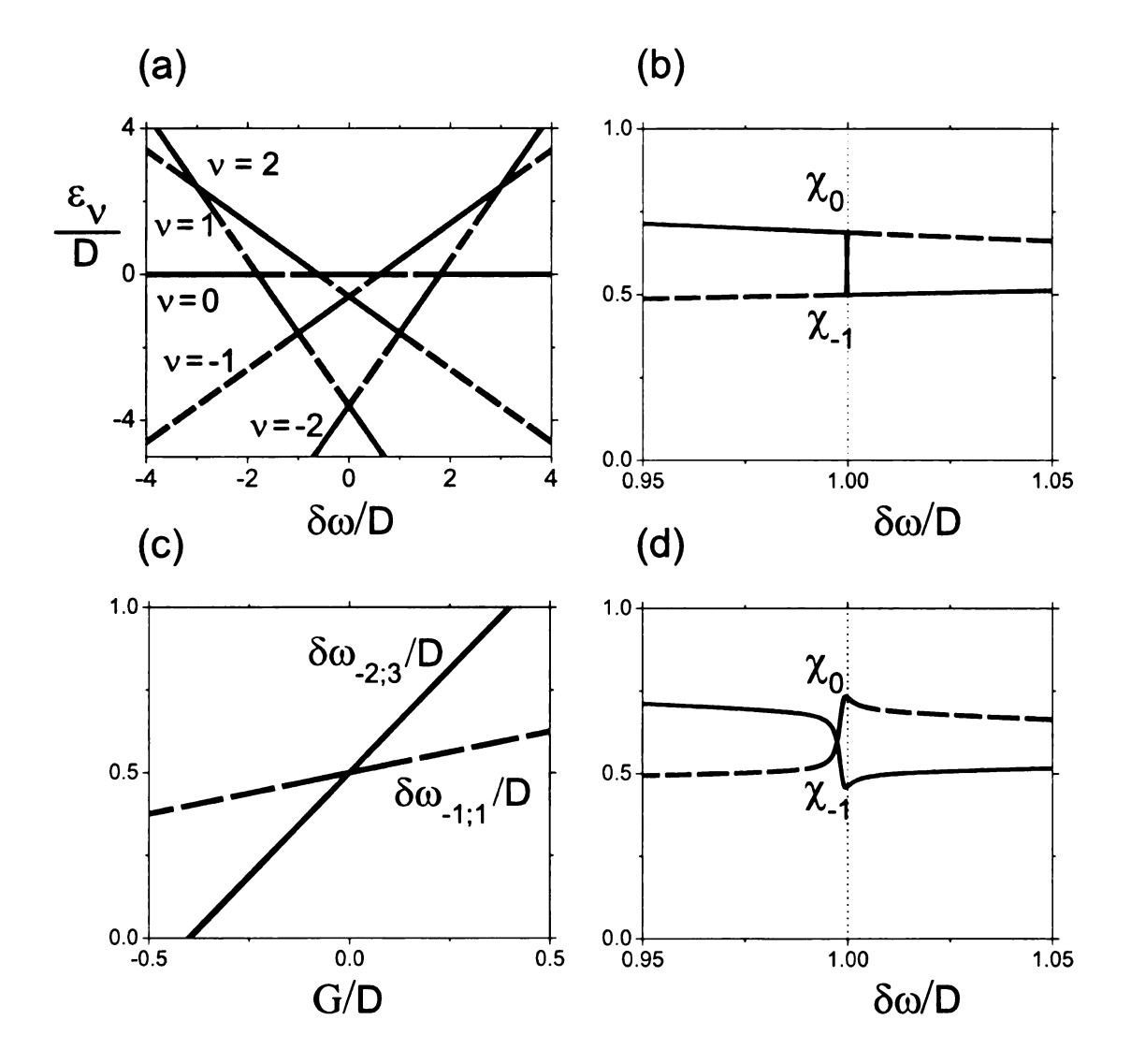


Figure 3.6: Quasienergy and susceptibility switching for a spin S=2 with quartic in  $S_z$  anisotropy. Panels (a), (b), and (d) refer to the dimensionless quartic anisotropy parameter G/D=0.4 in Eq. (3.18). Panels (b) and (d) refer to the 3-photon resonance  $|-2\rangle^{(0)} \rightarrow |1\rangle^{(0)}$  with the scaled modulation amplitude  $A/D \rightarrow 0$  and A/D=0.3, respectively; the dotted line shows the position of the resonance  $\delta\omega/D=1$ . Panel (c) shows the dependence of the resonant frequency detuning  $\delta\omega_{m;N}$  on the higher-order anisotropy parameter G in the limit  $A\rightarrow 0$ .

The major results refer to the case where the anisotropy energy is of the form  $-DS_z^2/2$ . In this case not only the quasienergies of the resonating Zeeman states  $|m\rangle^{(0)}$  and  $|m+N\rangle^{(0)}$  cross at multiphoton resonance, but the susceptibilities in these states also cross, in the weak-modulation limit. Such crossing occurs simultaneously for several pairs of Zeeman states. As the modulation amplitude A increases, the levels are Stark-shifted and the susceptibilities are also changed. However, as long as the Rabi splitting due to resonant multiphoton transitions (tunneling) can be disregarded, for resonant frequency the quasienergy levels remain pairwise degenerate and the susceptibilities remain crossing. We show that this effect is nonperturbative in A, it is due to the special conformal property of the classical spin dynamics.

Resonant multiphoton transitions lift the degeneracy of quasienergy levels, leading to a standard level anticrossing. In contrast, the susceptibilities as functions of frequency cross each other. However, near resonance they display spikes. The spikes of the involved susceptibilities point in the opposite direction, leading to decrease (antiresonance) or increase (resonance) of the transverse response. They have a profoundly non-Lorentzian shape (3.11), with width and height that strongly depend on A. The spikes can be observed by adiabatically sweeping the modulation frequency through a multiphoton resonance. If the spin is initially in the ground state, a sequence of such sweeps allows one to study the susceptibility in any excited state provided the relaxation time is long enough.

The behavior of the susceptibilities changes if terms of higher order in  $S_z$  in the anisotropy energy are substantial. In this case crossing of quasienergy levels is not accompanied by crossing of the susceptibilities in the limit  $A \to 0$ . Resonant multiphoton transitions lead to step-like switching between the branches of the susceptibilities of the resonating Zeeman states. Still, the susceptibilities display spikes

as functions of frequency for a sufficiently strong modulating field.

The results of the chapter can be applied also to molecular magnets in a static magnetic field. The spin Hamiltonian in the rotating wave approximation (3.2) is similar to the Hamiltonian of a spin in a comparatively weak static field, with the Larmor frequency  $\delta\omega$  of the same order as the anisotropy parameter D. The susceptibility then characterizes the response to the field component transverse to the easy axis. Quasienergies  $\varepsilon^{(0)}(m)$  are now spin energies in the absence of the transverse field, and instead of multiphoton resonance we have resonant tunneling. Our results show that a transverse field does not change the value of the longitudinal field for which the energy levels cross, in the neglect of tunneling. This explains the experiment [16] where such behavior was observed. Fig. 3.7 shows this independence for the case of switching steps in magnetization hysteresis loops of  $Mn_{12}$ , where switching occurs because of tunneling through the anisotropy barrier.

In conclusion, we have studied multiphoton resonance in large-spin systems. We have shown that the coherent nonlinear transverse response of the spin displays spikes when the modulation frequency goes through resonance. The spikes have non-Lorentzian shape which strongly depends on the modulation amplitude. The results bear on the dynamics of molecular magnets in a static magnetic field and provide an explanation of the experiment.



Fig. Versa field the last

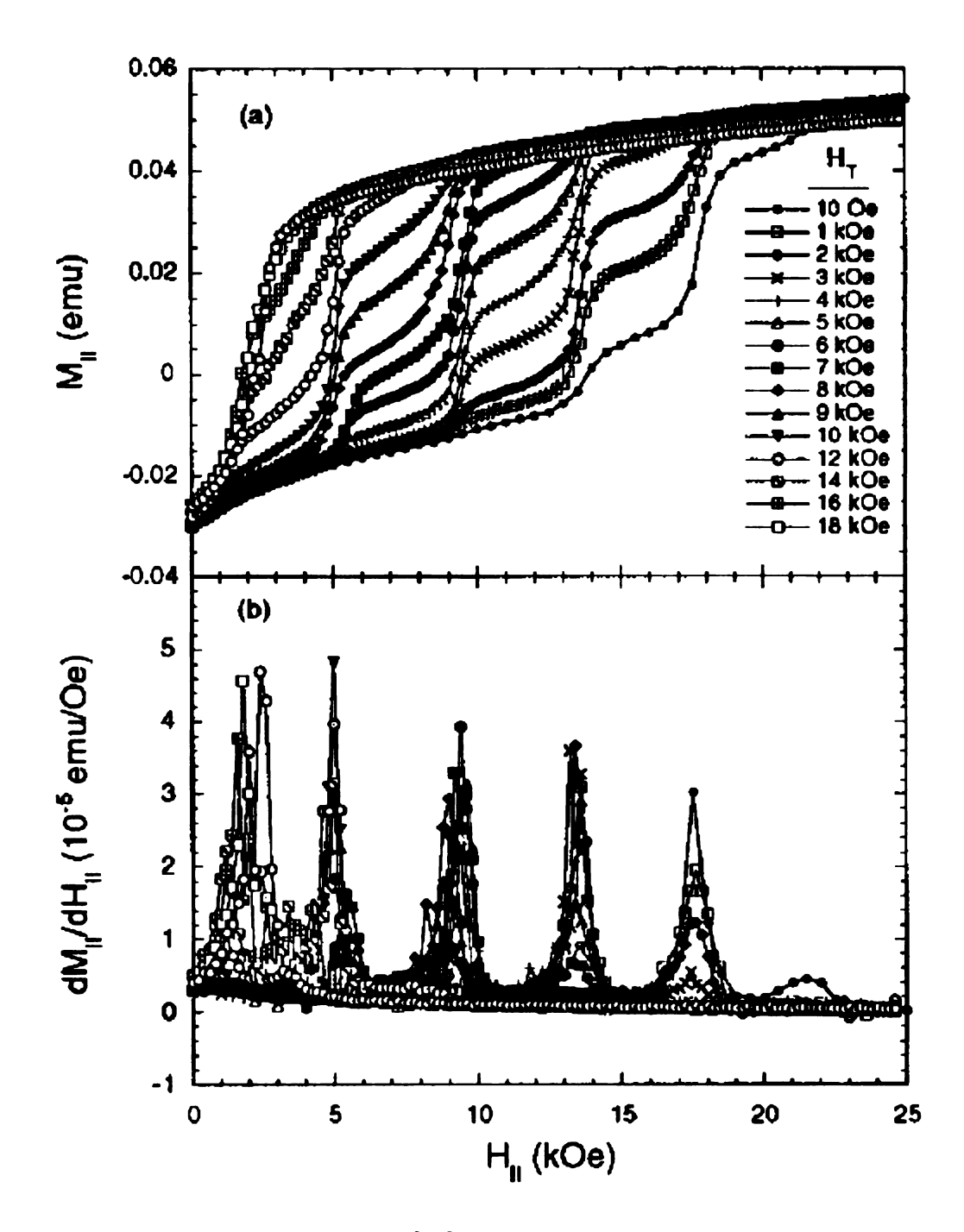


Figure 3.7: (Reproduced from Ref. [16]. Independence of hysteresis steps on transverse field. (a) Magnetic moment of  $Mn_{12}$  as a function of the external longitudinal field at 2.0 K for several values of the transverse field. Note that this is one quarter of the hysteresis loops. The steps always occur at the same values of longitudinal field. (b) The derivative of the curves in (a).

## Chapter 4

Hysteresis, Transient Oscillations, and Nonhysteretic Switching in Resonantly Modulated Large-Spin Systems

#### 4.1 Introduction

Large-spin systems have a finite but comparatively large number of quantum states. Therefore a single system can be used to study a broad range of phenomena, from purely quantum to semiclassical where the spin behaves almost like a classical top. One of the interesting features of large-spin systems is that, in a strong static magnetic field, their energy levels become almost equidistant, with level spacing close to  $\hbar\omega_0$ , where  $\omega_0$  is the Larmor frequency. As a result, radiation at frequency  $\approx \omega_0$  is resonant simultaneously for many interlevel transitions. This leads to new quantum

and classical nonlinear resonant effects.

An important class of large-spin systems is single-molecule magnets (SMMs). SMMs display an extremely rich behavior and have been attracting much attention in recent years. A variety of SMMs has already been discovered and investigated, see Refs. [22, 23, 24] for a review, and new systems are being found [25, 26]. Another example of large-spin systems is provided by large nuclear spins, the interest in which has renewed in view of their possible use in quantum computing [11].

In this paper we study the dynamics of large-spin systems,  $S \gg 1$ , in the classical limit. We assume that the system is in a strong static magnetic field along the easy magnetization axis and in an almost resonant transverse field. For a small relaxation rate, even a weak transverse resonant field can lead to hysteresis of the response. As we show, the hysteresis is quite unusual.

It is convenient to describe the dynamics of a resonantly modulated spin in the rotating wave approximation (RWA). The corresponding analysis in the absence of relaxation has revealed a special quantum feature, an antiresonance of the response which accompanies anticrossing of quasienergy levels [68]. Quantum spin dynamics in the rotating frame bears also on the dynamics of the Lipkin-Meshkov-Glick model [27, 28, 29, 30].

One may expect that the features of the coherent quantum dynamics should have counterparts in the classical spin dynamics in the presence of dissipation. As we show, this is indeed the case. The system displays an unusual behavior in a certain range of modulation parameters. This behavior is due to a special symmetry. It leads to specific features of hysteresis and to discontinuous (in the neglect of fluctuations) switching between different response branches even in the absence of hysteresis.

Classical dynamics of a large-spin system in a resonant field would be expected to

have similarities with the dynamics of a modulated magnetic nanoparticle near ferromagnetic resonance. It was understood back in the 1950's [35, 36] that the response near ferromagnetic resonance becomes strongly nonlinear already for comparatively weak radiation strength due to the magnetization dependence of the effective magnetic field. Resonant response may become multivalued as a function of the modulating field amplitude [37, 38]. A detailed analysis of nonlinear magnetization dynamics in uniaxial nanoparticles modulated by a strong circularly polarized periodic field was done recently [39]. These studies as well as many other studies of magnetization dynamics in ferromagnets were based on the Landau-Lifshitz-Gilbert equation.

In contrast to magnetic nanoparticles, for large-spin systems quantum effects are substantial. A distinction which remains important in the classical limit concerns relaxation mechanisms. Spin relaxation occurs via transitions between discrete energy levels with emission, absorption, or inelastic scattering of excitations of a thermal reservoir to which the spin is coupled. Relevant relaxation mechanisms depend on the specific system but as we show, even in the classical limit relaxation is not described, generally, by the Landau-Lifshitz damping. As a result the classical spin dynamics strongly differs from the dynamics of a magnetic nanoparticle.

The microscopic analysis of relaxation is simplified in the presence of a strong static magnetic field. Here, all spin energy levels are almost equidistant. Therefore excitations of the thermal bath emitted, for example, in transitions within different pairs of neighboring levels have almost the same energies. As a consequence, relaxation is described by a small number of constants independent of the form of the weighted with the interaction density of states of the bath, and the analysis applies for an arbitrary ratio between the level nonequidistance and their relaxational broadening [40].

We consider three relaxation mechanisms. Two of them correspond to transitions between neighboring and next neighboring spin levels, with the coupling to bosonic excitations quadratic in the spin operators. Such coupling is important, in particular, for SMMs where energy relaxation is due to phonon scattering. The theory of relaxation of SMMs was developed earlier [17, 69] and has been tested experimentally, see Refs. [70, 71] and papers cited therein. We also consider coupling to a bosonic bath linear in spin operators. It leads to relaxation that in the classical limit has the form of the Landau-Lifshitz damping provided the modulation field is weak compared to the static field, as assumed in the RWA.

The typical duration of scattering events that lead to spin relaxation is often  $\sim \omega_0^{-1}$ . In the RWA they appear instantaneous. The operator that describes relaxation has a simple functional form, with no retardation in the "slow" time. This is advantageous for studying the classical limit and allows us to obtain analytical results.

In the classical limit, a spin is characterized by two dynamical variables, for example, azimuthal and polar angles. In the RWA, they satisfy autonomous equations of motion, the coefficients in these equations do not depend on time. A two-variable nonlinear dissipative system can have both stationary and periodic states [72]. As we show, such states indeed emerge for a resonantly modulated spin. They were predicted also for a magnetic nanoparticle with Landau-Lifshitz damping in the case of a generally nonresonant modulation [39].

For a spin, the occurrence of periodic states in the rotating frame critically depends on the interrelation between the relaxation parameters. In particular, these states do not emerge for a resonantly modulated spin with microscopic relaxation that reduces to the Landau-Lifshitz damping in the RWA. Moreover, quantum fluctuations lead to phase diffusion which results in decay of periodic states in the rotating frame, making the corresponding vibrations transient.

This chapter is organized as follows. In Sec. 4.2 we introduce a model of the spin and its interaction with a thermal bath and derive the quantum kinetic equation with account taken of different relaxation mechanisms. In Sec. 4.3 we obtain classical equations of motion and discuss the symmetry of the system. We find analytically, for weak damping, the positions of the bifurcation curves where the number of stationary states in the rotating frame changes (saddle-node bifurcations) and where periodic states are split off from stationary states (Hopf bifurcations). Sec. 4.4 describes the specific and, perhaps, most unusual feature of the system, the occurrence of Hamiltonian-like dynamics in the presence of dissipation. In Sec. 4.5 spin dynamics and hysteresis are described for the relation between relaxation parameters where the system does not have periodic states in the rotating frame. In Sec. 4.6 we consider the opposite case. The onset of periodic states and their stability are analyzed and the features of the hysteresis related to the occurrence of periodic states are studied. Details of the calculations are outlined in Appendix. Sec. 4.7 contains concluding remarks.

#### 4.2 The model

We consider a large spin,  $S \gg 1$ , in a strong stationary magnetic field along the easy axis z. The spin is modulated by a transverse magnetic field with frequency  $\omega_F$  close to the Larmor frequency  $\omega_0$ . The Hamiltonian of the spin has the form

$$H_0 = \omega_0 S_z - \frac{1}{2} D S_z^2 - S_x A \cos \omega_F t \qquad (\hbar = 1)$$
 (4.1)

This Hamiltonian well describes many single-molecule magnets, including  $Mn_{12}$  crystals; D characterizes the magnetic anisotropy and A is the modulation amplitude. It also describes a nuclear spin, with D characterizing the quadrupolar coupling energy to an electric field gradient in the crystal with an appropriate symmetry.

We assume that the Zeeman energy levels in the absence of modulation are almost equidistant. We also assume that the resonant modulation is not too strong. These conditions are met provided

$$|\omega_0 - \omega_F|, DS, A \ll \omega_0. \tag{4.2}$$

For many SMMs the inequality  $DS \ll \omega_0$  is fairly demanding and requires strong static magnetic fields; for example  $D \approx 0.6$  K for Fe<sub>8</sub> (where S = 10) [24]. On the other hand, for more isotropic SMMs the anisotropy is much smaller; for example,  $D \approx 0.04$  K for Fe<sub>17</sub> where S = 35/2, see Ref. [26] (our definition of D differs by a factor of 2 from the definition used in the literature on SMMs). The anisotropy is usually much weaker for large-S nuclei and the condition (4.2) is not restrictive.

The quantum dynamics of an isolated spin with Hamiltonian Eq. (4.1) was considered earlier [68]. Here we are interested in the spin dynamics in the presence of dissipation. Different dissipation mechanisms are important for different systems. For single-molecule magnets, energy dissipation is due primarily to transitions between spin energy levels accompanied by emission or absorption of phonons. The transitions between both nearest and next nearest spin levels are important [17, 69, 73]. The corresponding interactions are

$$H_i^{(1)} = \sum_k V_k^{(1)} \left[ (S_+ S_z + S_z S_+) b_k + \text{h.c.} \right]$$

$$H_i^{(2)} = \sum_k V_k^{(2)} \left( S_+^2 b_k + \text{h.c.} \right), \qquad S_{\pm} = S_x \pm i S_y,$$

$$(4.3)$$

where k enumerates phonon modes,  $b_k$  is the annihilation operator for the k-th mode,

and  $V_k^{(1)}$  and  $V_k^{(2)}$  are the coupling parameters responsible for transitions between nearest and next nearest Zeeman levels. The phonon Hamiltonian is

$$H_{ph} = \sum_{k} \omega_k b_k^+ b_k. \tag{4.4}$$

A similar interaction Hamiltonian describes the coupling of a nuclear spin to phonons, cf. Ref. [74] and the early work [75, 76].

Along with the interaction (4.3) we will consider the interaction that is linear in the spin operators.

$$H_i^{(3)} = \sum_k V_k^{(3)} (S_+ b_k + \text{h.c.}).$$
 (4.5)

Such interaction is allowed by time-reversal symmetry in the presence of a strong static magnetic field, with the coupling constants  $V_k^{(3)}$  proportional to the off power of the field. It can be thought of as arising from phonon-induced modulation of the spin g-factor. The interaction Eq. (4.5) is also important for impurity spins in magnetic crystals, in which case  $b_k$  is the annihilation operator of a magnon [77, 78].

#### 4.2.1 Rotating wave approximation

The dynamics of a periodically modulated spin can be conveniently described in the rotating wave approximation. To do this we make a canonical transformation  $U(t) = \exp(-i\omega_F S_z t)$ . The transformed Hamiltonian  $H_0$  then becomes  $\tilde{H}_0 = U^{\dagger} H_0 U - i U^{\dagger} \dot{U}$ ,

$$\tilde{H}_0 = -\delta \omega S_z - \frac{1}{2}DS_z^2 - \frac{1}{2}AS_x,$$

$$\delta \omega = \omega_F - \omega_0. \tag{4.6}$$

Here we disregarded fast-oscillating terms  $\propto A \exp(\pm 2i\omega_F t)$ .

We note that the Hamiltonian (4.6) has the form of the free energy of a magnetic moment in an easy axis ferromagnet, with **S** playing the role of the magnetization and  $\delta\omega$  and A giving the components of the effective magnetic field (in energy units) along the z and x axes, respectively.

It is convenient to change to dimensionless variables and rewrite the Hamiltonian as  $\tilde{H}_0 = S^2 D(\hat{g} + \mu^2/2)$ , with

$$\hat{g} = -\frac{1}{2}(s_z + \mu)^2 - fs_x,$$

$$\mathbf{s} = \mathbf{S}/S, \qquad \mu = \delta\omega/SD, \qquad f = A/2SD. \tag{4.7}$$

The Hamiltonian  $\hat{g}$  describes the dynamics of an isolated spin in "slow" dimensionless time  $\tau = SDt$ . It gives dimensionless quasienergies of a periodically modulated spin in the RWA. From Eq. (4.7), the spin dynamics is determined by the two dimensionless parameters,  $\mu$  and f, which depend on the interrelation between the frequency detuning of the modulating field  $\delta\omega$ , the anisotropy parameter DS, and the modulation amplitude A. The spin variables  $\hat{\mathbf{s}}$  are advantageous for describing large spins, since the commutators of their components are  $\propto S^{-1}$ , which simplifies a transition to the classical limit for  $S \gg 1$ .

### 4.2.2 Quantum kinetic equation

We will assume that the interaction with phonons (magnons) is weak. Then under standard conditions the equation of motion for the spin density matrix  $\rho$  is Markovian in slow time  $\tau$ , i.e., on a time scale that largely exceeds  $\omega_F^{-1}$  and the typical correlation time of phonons (magnons). We will switch to the interaction representation with respect to the Hamiltonian  $\omega_F S_z + H_{\rm ph}$ . Then to leading order in the spin to bath coupling the quantum kinetic equation can be written as

$$S^{-1}\dot{\rho} = i[\rho, g] - \hat{\Gamma}^{(1)}\rho - \hat{\Gamma}^{(2)}\rho - \hat{\Gamma}^{(3)}\rho, \tag{4.8}$$

where  $\dot{A} \equiv \partial A/\partial \tau$ .

The operators  $\hat{\Gamma}^{(j)}$  describe relaxation due to the interactions  $H_i^{(j)}$ , with j=1,2,3. They can be written schematically as

$$\hat{\Gamma}\rho = \Gamma[(\bar{n}+1)(L^{+}L\rho - 2L\rho L^{+} + \rho L^{+}L) + \bar{n}(LL^{+}\rho - 2L^{+}\rho L + \rho LL^{+})]$$
(4.9)

Here we have taken into account that all transitions between spin states with emission or absorption of phonons (magnons) involve almost the same energy transfer  $\Delta E$ , with  $\Delta E \approx \omega_F$  for terms  $\propto \Gamma^{(1)}, \Gamma^{(3)}$  and  $\Delta E \approx 2\omega_F$  for the term  $\propto \Gamma^{(2)}$ . In this sense, equation for spin relaxation (4.9) resembles the quantum kinetic equation for a weakly nonlinear oscillator coupled to a bosonic bath [40]. Respectively,  $\bar{n}$  is the Planck number of the emitted/absorbed phonons,  $\bar{n} = [\exp(\Delta E/kT - 1)]^{-1}$ . Because of the same transferred energy, different transitions are characterized by the same rate constants, which for the interactions  $H_i^{(1)-(3)}$  have the following form, in dimensionless time:

$$\Gamma^{(1)} = \pi D^{-1} S^{2} \sum_{k} \left| V_{k}^{(1)} \right|^{2} \delta \left( \omega_{F} - \omega_{k} \right),$$

$$\Gamma^{(2)} = \pi D^{-1} S^{2} \sum_{k} \left| V_{k}^{(2)} \right|^{2} \delta \left( 2\omega_{F} - \omega_{k} \right),$$

$$\Gamma^{(3)} = \pi D^{-1} \sum_{k} \left| V_{k}^{(3)} \right|^{2} \delta \left( \omega_{F} - \omega_{k} \right).$$
(4.10)

The operators L for the interactions  $H_i^{(1)-(3)}$  are

$$L^{(1)} = s_- s_z + s_z s_-, \quad L^{(2)} = s_-^2, \quad L^{(3)} = s_-,$$
 (4.11)

where  $s_{\pm} = S_{\pm}/S$ .

It is important to note that, along with dissipation, coupling to phonons (magnons) leads to a polaronic effect of renormalization of the spin energy. A standard analysis shows that renormalization due to  $H_i^{(3)}$ , to second order in  $H_i^{(3)}$  comes

to a change of the anisotropy parameter D and the Larmor frequency. A similar change comes from nonresonant terms  $\propto S_+ b_k^\dagger + H.c.$ . In contrast, renormalization from  $H_i^{(1),(2)}$ , along with terms  $\propto S_z, S_z^2$ , leads to terms of higher order in  $S_z$  in the spin Hamiltonian, in particular to terms  $\propto S_z^4$ . The condition that they are small compared to the anisotropy energy  $DS_z^2$  imposes a constraint on the strength of the coupling  $H_i^{(1),(2)}$ . Respectively, we will assume that the dimensionless decay rates  $\Gamma^{(1),(2)}$  are small,  $\Gamma^{(1),(2)} \ll 1$ . It is not necessary to impose a similar condition on the dimensionless rate  $\Gamma^{(3)}$ . Still we will be interested primarily in the spin dynamics in the underdamped regime, where  $\Gamma^{(1)-(3)}$  are small.

# 4.3 Classical motion of the modulated spin

The analysis of spin dynamics is significantly simplified in the classical, or meanfield limit. Classical equations of motion for the spin components can be obtained by multiplying Eq. (4.8) by  $s_i$  (i = x, y, z), taking the trace, and decoupling  $\text{Tr}(s_{i_1}s_{i_2}\rho) \to s_{i_1}s_{i_2}$ . The decoupling should be done after the appropriate commutators are evaluated; for example,  $\text{Tr}([s_z, \hat{g}] \rho) \to -ifs_y$ . From Eqs. (4.7), (4.8), (4.11) we obtain

$$\dot{\mathbf{s}} = -\mathbf{s} \times \partial_{\mathbf{s}} g + (\dot{\mathbf{s}})_d, \quad (\dot{\mathbf{s}})_d = \Gamma_d(s_z) \mathbf{s} \times (\mathbf{s} \times \hat{\mathbf{z}}),$$

$$\Gamma_d(s_z) = 2 \left( 4\Gamma^{(1)} s_z^2 + 2\Gamma^{(2)} (1 - s_z^2) + \Gamma^{(3)} \right), \tag{4.12}$$

where  $\hat{\mathbf{z}}$  is a unit vector along the z-axis, which is the direction of the strong dc magnetic field.

We have assumed in Eq. (4.12) that  $S \gg \bar{n}$ . Note that, in dimensional units,  $S = |\mathbf{L}|/\hbar$ , where  $\mathbf{L}$  is the angular momentum, whereas in the classical temperature limit  $\bar{n} = kT/\hbar\omega_F$  or  $kT/2\hbar\omega_F$  depending on the scattering mechanism. Therefore

the condition  $S\gg \bar{n}$  imposes a limitation on temperature.

Equation (4.12) is reminiscent of the Landau-Lifshitz equation for magnetization of a ferromagnet. However, in contrast to the Landau-Lifshitz equation a retardation-free equation of motion for a classical spin could be obtained only in the rotating frame, that is, in slow time  $\tau$ . The term with  $\partial_{\bf s} g$  describes precession of a spin with energy (quasienergy, in the present case) g. The term  $(\dot{\bf s})_d$  describes the effective friction force. It is determined by the instantaneous spin orientation, but its form is different from that of the friction force in the Landau-Lifshitz equation.

We emphasize that Eq. (4.12) is not phenomenological, it is derived for the microscopic model of coupling to the bath (4.3), (4.5). We now consider what would happen if we start from the Landau-Lifshitz equation and switch to the rotating frame using the RWA in the assumption that the resonant driving is comparatively weak,  $A \ll \omega_0$  [cf. Eq. (4.2)]. In this case one should keep in the expression for the friction force only the leading term in the effective magnetic field, i.e., assume that  $\mathbf{H} \parallel \hat{\mathbf{z}}$ . The result would be Eq. (4.12) with a dissipative term of the same form as the term  $\propto \Gamma^{(3)}$  but without dissipative terms that have the structure of the terms  $\propto \Gamma^{(1)}, \Gamma^{(2)}$ . However, these latter terms play a major role for SMMs [17, 69, 70, 71] and for phonon scattering by nuclear spins.

As mentioned in the Introduction, the dynamics of a single-domain magnetic nanoparticle in a circularly polarized field was studied using the Landau-Lifshitz-Gilbert equation in a series of papers [39, 79, 80, 81]. It is clear from the above comment that the results of this analysis do not generally describe resonant behavior of SMMs. Moreover, periodic states in the rotating frame predicted in Ref. [39] do not arise in resonantly excited spin systems with relaxation  $\propto \Gamma^{(3)}$ , as shown below.

# 4.3.1 Stationary states in the rotating frame for weak damping

A classical spin is characterized by its azimuthal and polar angles,  $\phi$  and  $\theta$ , with  $s_z = \cos \theta, s_x = \sin \theta \cos \phi, s_y = \sin \theta \sin \phi$ . In canonically conjugate variables  $\phi, s_z$  equations of motion (4.12) take the form

$$\dot{\phi} = \partial_{s_z} g, \tag{4.13}$$

$$\dot{s}_z = -\partial_{\phi} g - \Gamma_d(s_z)(1 - s_z^2),$$

where g as a function of  $s_z$ ,  $\phi$  has the form  $g = -(s_z + \mu)^2/2 - f(1 - s_z^2)^{1/2} \cos \phi$ , cf. Eq. (4.7). We note that the dissipation term is present only in the equation for  $\dot{s}_z$ .

In the absence of relaxation, precession of a spin with given g corresponds to moving along orbits on the  $(\phi, s_z)$ -plane. The orbits can be either closed or open; in the latter case  $\phi$  varies by  $2\pi$  over a period, cf. Fig. 4.1. There are also stationary states where the spin orientation does not vary in time. Generally, relaxation breaks this structure. If it is weak it makes some of the stationary states asymptotically stable or unstable and can also transform some of the orbits into stable or unstable limit cycles, which correspond to periodic oscillations of  $s_z$  and  $\phi$  in the rotating frame. The frequency of these oscillations is determined by the system nonlinearity and is not immediately related to a combination of the modulation frequency and the Larmor frequency, for example.

Stationary states of Eq. (4.13), which is written in the rotating frame, correspond to the states of forced vibrations of the spin components  $s_x$ ,  $s_y$  at frequency  $\omega_F$  in the laboratory frame. Periodic states in the rotating frame correspond, in the laboratory frame, to periodic vibrations of  $s_z$  and to vibrations of  $s_x$ ,  $s_y$  at combination frequencies equal to  $\omega_F$  with added and subtracted multiples of the oscillation frequency in

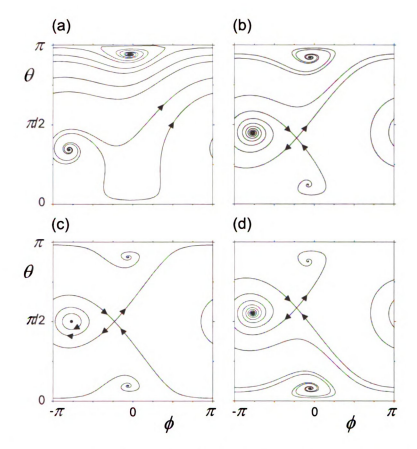


Figure 4.1: Phase portraits of the spin on  $(\theta,\phi)$ -plane  $(s_z=\cos\theta)$ . The data refer to  $\Gamma^{(1)}=\Gamma^{(2)}=0$ ,  $\Gamma^{(3)}=0.1$ , and f=0.3. In panels (a)-(d)  $\mu=-0.6,-0.2,0,0.2$ , respectively.

the rotating frame (which is small compared to  $\omega_F$ ). In what follows we keep this correspondence in mind, but the discussion refers entirely to the rotating frame.

The analysis of stability of stationary states is based on linearizing the equations of motion near these states and looking at the corresponding eigenvalues  $\lambda_1, \lambda_2$  [72]. In the absence of damping the stationary states are either hyperbolic points (saddles) with real  $\lambda_{1,2}$  or elliptic points (centers) with imaginary  $\lambda_{1,2}$ . From Eq. (4.13), a fixed point is hyperbolic if  $\lambda_1\lambda_2 = \mathcal{D} < 0$ , where

$$D = \partial_{\phi}^{2} g \partial_{s_{z}}^{2} g - (\partial_{\phi} \partial_{s_{z}} g)^{2} \qquad (4.14)$$

(the derivatives are calculated at the stationary state). On the other hand, if  $\mathcal{D} > 0$ 

the stationary state corresponds to an elliptic point, orbits g = const are circling around it.

For weak damping, hyperbolic points remain hyperbolic. On the other hand, a center becomes asymptotically stable (an attractor) or unstable (a repeller) for  $\mathcal{T} < 0$  or  $\mathcal{T} > 0$ , respectively. Here  $\mathcal{T} = -\partial [\Gamma_d(s_z)(1-s_z^2)]/\partial s_z$ , or in explicit form

$$\mathcal{T} = -4s_z \left[ 4\Gamma^{(1)}(1 - 2s_z^2) - 4\Gamma^{(2)}(1 - s_z^2) - \Gamma^{(3)} \right], \tag{4.15}$$

where  $s_z$  is taken for the appropriate center;  $\lambda_1 + \lambda_2 = \mathcal{T}$ . The sign of  $\mathcal{T}$  determines stability of a stationary state also where dissipation is not small.

The quasienergy g has symmetry properties that the change  $f \to -f$  can be accounted for by replacing  $\phi \to \phi + \pi, s_z \to s_z$ . This replacement preserves the form of equations of motion (4.13) also in the presence of damping. Therefore in what follows we will concentrate on the range  $f \geq 0$ . On the other hand, the change  $\mu \to -\mu$  would not change g if we simultaneously replace  $\phi \to \phi, s_z \to -s_z$ . In equations of motion one should additionally change  $\tau \to -\tau$ . Therefore, if for  $\mu = \mu^{(0)} < 0$  the system has an attractor located at a given  $(\phi^{(0)}, s_z^{(0)})$ , then for  $\mu = -\mu_0$  it has a repeller located at  $\phi^{(0)}, -s_z^{(0)}$ . This behavior is illustrated in Fig. 4.1, where panels (b) and (d) refer to opposite values of  $\mu$ .

#### 4.3.2 Saddle-node bifurcations

The function  $g(\mathbf{s})$  has a form of the free energy of a magnetic moment of an easy axis ferromagnet, as mentioned earlier, with  $\mu$  and f corresponding to the components of the magnetic field along and transverse to the easy axis, respectively. It is well known that g may have either two or four extreme points where  $\partial g/\partial s_z = \partial g/\partial \phi = 0$ . The region where there are four extrema lies inside the Stoner-Wohlfarth astroid

[82]  $|f|^{2/3} + |\mu|^{2/3} = 1$  on the plane of the dimensionless parameters  $\mu$  and f, see Fig. 4.2(a). The extrema of g outside the astroid are a minimum and a maximum, whereas inside the astroid g additionally has a saddle and another minimum or maximum. All of them lie at  $\phi = 0$  or  $\phi = \pi$ .

In the presence of weak damping, the minima and maxima of g become stable or unstable stationary states. We note that there are no reasons to expect that the stable states lie at the minima of g, because g is not an energy but a quasienergy of the spin. The number of stable/unstable stationary states changes on the saddle-node bifurcation curve on the  $(f, \mu)$ -plane. The condition that two stationary states merge [72] has the form

$$\mathcal{D} + \mathcal{T}\partial_{\phi}\partial_{s_z}g = 0. \tag{4.16}$$

For weak damping a part of the curve given by this equation is close to the astroid. On the astroid  $s_z = -\operatorname{sgn}(\mu)|\mu|^{1/3}$ . Then from Eq. (4.15) for the merging saddle and node

$$\mathcal{T} = -4\operatorname{sgn}(\mu)\sqrt{1 - |f|^{2/3}} \times \left(4\Gamma^{(1)}(1 - 2|f|^{2/3}) + 4\Gamma^{(2)}|f|^{2/3} + \Gamma^{(3)}\right). \tag{4.17}$$

If damping  $\propto \Gamma^{(1)}$  is weak, the node is stable for  $\mu > 0$  and unstable for  $\mu < 0$ . On the other hand, if  $\Gamma^{(1)}$  is large, the stability depends on the value of f.

The most significant difference between the saddle-node bifurcation curve and the Stoner-Wohlfarth astroid is that the bifurcation curve consists of two curvilinear triangles, that is, the astroid is "split", see Fig. 4.2(b) and Fig. 4.5 below. This is also the case for a modulated magnetic nanoparticle [39]. The triangles are obtained from Eqs. (4.13) and (4.16). After some algebra we find that the "bases" of the bifurcation

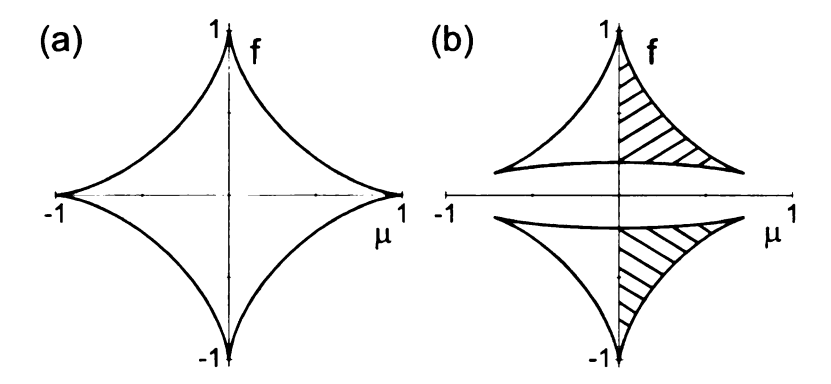


Figure 4.2: Saddle-node bifurcation lines. Panel (a): zero-damping limit, the lines have the form of the Stoner-Wolfarth astroid in the variables of reduced amplitude f and frequency detuning  $\mu$  of the resonant field. Panel (b): nonzero damping,  $\Gamma^{(3)} = 0.1$ ,  $\Gamma^{(1)} = \Gamma^{(2)} = 0$ . In the dashed region the spin has two coexisting stable equilibria in the rotating frame.

triangles are given by expression

$$f_B \approx \pm \Gamma_d(\mu)(1 - \mu^2)^{1/2},$$
 (4.18)

to leading order in  $\Gamma_d$ . This expression applies not too close to the vertices of the triangles. We note, however, that Eq. (4.18) gives the exact bifurcational value of  $f_B$  for  $\mu = 0$  and arbitrary  $\Gamma_d(0)$ .

The shape of the gap between the upper and lower curvilinear bifurcation triangles depends on the damping mechanism. In particular, the damping  $\propto \Gamma^{(1)}$  does not contribute to the gap for small  $|\mu|$  (cf. Fig. 4.5), whereas the damping  $\propto \Gamma^{(2)}$  does not contribute to the gap at small  $1 - |\mu|$ . The damping-induced change of the sides of the triangles compared to the astroid is quadratic in  $\Gamma_d$ , far from the small-f range.

The positions of the small-f vertices of the bifurcation triangles  $f_C$ ,  $\mu_C$  for small damping can be found from Eqs. (4.13) and the condition that Eq. (4.16) has a

degenerate root, which gives

$$\mu_C \approx \pm \left[ 1 - \sqrt{3} \left( -\Gamma_d^2 + \mathcal{T} \Gamma_d \right)^{1/2} \right],$$

$$f_C \approx \pm (64/27)^{1/4} \Gamma_d^{3/4} \left( \Gamma_d + (1/2)\mathcal{T} \right)^{1/2} \left( -\Gamma_d + \mathcal{T} \right)^{1/4},$$

where  $\Gamma_d$  and  $\mathcal{T}$  are calculated for  $s_z = 1$ .

#### 4.3.3 Periodic states and Hopf bifurcations

An important property of the modulated classical spin is the possibility to have periodic states in the rotating frame. Such states result from Hopf bifurcations in which a stationary state transforms into a limit cycle [72]. A Hopf bifurcation occurs if

$$T=0, \quad \mathcal{D}>0$$

in the stationary state. Besides the special case  $s_z=0$  discussed in Sec. 4.4, the corresponding stationary state is at  $s_z=s_{zH}$ , where

$$s_{zH} = \alpha \frac{1}{2} \left( \frac{4\Gamma^{(1)} - 4\Gamma^{(2)} - \Gamma^{(3)}}{2\Gamma^{(1)} - \Gamma^{(2)}} \right)^{1/2},$$

$$\alpha = \pm 1, \qquad \Gamma^{(1)} \ge \Gamma^{(2)} + \frac{1}{4}\Gamma^{(3)}$$
(4.19)

(the inequality on the damping parameters follows from the condition  $(s_z^2)_H \leq 1$ )

The field  $f_H$  on the Hopf bifurcation lines as a function of the reduced detuning  $\mu$  is given by a particularly simple expression for weak damping. In this case, from second equation (4.13) the phase  $\phi_H$  for the bifurcating stationary state is close to either 0 or  $\pi$  with the additional constraint  $\partial_{s_z}^2 g \, \partial_{\phi}^2 g > 0$ . Then from first equation (4.13) and Eq. (4.19) we find that Hopf bifurcation curves are straight lines, in the

limit of vanishingly small damping.

$$f_H = \pm \left[1 - s_{zH}^2\right]^{1/2} \left[1 + \mu s_{zH}^{-1}\right],$$
 (4.20)

$$|f_{II}| \ge \left[1 - s_{zH}^2\right]^{3/2} \quad \text{or} \quad |\mu| \ge |s_{zII}|.$$
 (4.21)

The structure of these lines is seen in Fig. 4.5 below. They end on the saddle-node bifurcation curves and are tangent to these curves at the end points. A detailed analysis is presented in Sec. 4.6.

### 4.4 Hamiltonian-like motion at exact resonance

The spin dynamics (4.12) displays an unusual and unexpected behavior where the modulation frequency  $\omega_F$  coincides with the Larmor frequency  $\omega_0$ , in which case  $\mu = 0$ . This is a consequence of the symmetry of the quasienergy and the dissipation operator. In a certain range of dynamical variables  $\phi$ ,  $s_z$ , the spin behaves as if there were no dissipation, even though dissipation is present. This behavior is seen in the pattern of phase trajectories of the spin. An example of the pattern is shown in Fig. 4.1(c) for the case  $\Gamma^{(2)} = \Gamma^{(3)} = 0$ , but the behavior is not limited to this case. As seen from Fig. 4.1(c), phase trajectories form closed loops, typical for Hamiltonian systems.

For |f| lying inside the bifurcation triangles, the Hamiltonian-like dynamics occurs only in a part of the phase plane. This region of f corresponds to  $\Gamma_d(0) < |f| < [1 + \Gamma_d^2(0)]^{1/2}$  [the upper bound on |f| for  $\mu = 0$  can be easily obtained from Eqs. (4.13), (4.16)]. Here, the spin has four stationary states. For small  $|\mu|$  two of them have small  $|s_z|$ ,  $s_z \approx -\mu/(1 - f\cos\phi)$  where  $\sin\phi \approx -\Gamma_d(0)/f$ . One of these states is a saddle point  $[\phi \approx -\arcsin[\Gamma_d(0)/f]]$  and the other is a focus  $[\phi \approx \pi + \arcsin[\Gamma_d(0)/f]]$ .

For  $\mu = 0$  there occurs a global bifurcation, a homoclinic saddle-saddle bifurcation

(saddle loop [72]) where the separatrix coming out from the saddle goes back into it, forming a homoclinic orbit. Simultaneously, the focus inside the loop becomes a center,  $\mathcal{T} = 0$  for  $s_z = 0$ . All trajectories inside the homoclinic orbit are closed loops. In contrast to the case of the vicinity of the double-zero eigenvalue bifurcation [72], the pattern persists throughout a broad region of f.

We show how a Hamiltonian-like region in phase space emerges first for weak damping. For  $\mu = 0$  the quasienergy g corresponds to the Hamiltonian of a spin with anisotropy energy  $\propto S_z^2$ , which is in a transverse field  $\propto f$ . Such spin in quantum mechanics has special symmetry, it can be mapped onto a particle in a symmetric potential [28, 29]. A part of the classical g = const orbits are closed loops on the  $(\phi, s_z)$ -plane. They surround the center  $(s_z = 0, \phi = \pi)$ . The orbits are symmetric with respect to the replacement

$$s_z \to -s_z, \ \phi \to \phi,$$
 (4.22)

which leads to  $\dot{\phi} \rightarrow -\dot{\phi}, \ \dot{s}_z \rightarrow \dot{s}_z$ .

Weak damping would normally cause drift of quasienergy. The drift velocity averaged over the period  $\tau_p(g)$  of motion along the orbit is

$$\langle \dot{g} \rangle = -\tau_p^{-1} \int_0^{\tau_p} d\tau \partial_{s_z} g \, \Gamma_d(s_z) (1 - s_z^2). \tag{4.23}$$

From the symmetry (4.22) and the relation  $\Gamma_d(s_z) = \Gamma_d(-s_z)$ , we have  $\langle \dot{g} \rangle = 0$  on a closed orbit for  $\mu = 0$ . Therefore a closed orbit remains closed to first order in  $\Gamma_d$ . Of course, for open orbits, where  $\phi$  is incremented by  $2\pi$  over a period,  $\langle \dot{g} \rangle \neq 0$ . These orbits become spirals in the presence of damping.

Spirals and closed orbits should be separated by a separatrix, which must be a closed orbit itself. Since the separatrix must start and end at the saddle point,

we understand that at  $\mu=0$  for small  $\Gamma_d$  there occurs a saddle-saddle homoclinic bifurcation.

The topology discussed above persists as  $\Gamma_d$  increases. The symmetry (4.22) is not broken by  $\Gamma_d$ . Indeed, from equations of motion (4.13), any orbit that crosses  $s_z = 0$  twice per period for  $\mu = 0$  has the property (4.22) and therefore is closed. The closed orbits surround the center  $s_z = 0$ ,  $\phi = \pi - \arcsin(\Gamma_d(0)/f)$  and fill out the whole interior of the separatrix loop.

The Hamiltonian-like behavior is displayed also for  $\mu = 0$  and f lying outside the bifurcation triangles. Here, the system has two stationary states, both with  $s_z = 0$  but with different  $\phi$ . From Eq. (4.15), for both of them  $\mathcal{T}$  changes sign as  $\mu$  goes through zero. Because there is no saddle point, for small  $|\mu|$  there is no separatrix, trajectories spiral toward or away from stationary states and possibly limit cycles. It follows from the arguments above that for  $\mu = 0$  all trajectories become closed orbits. This is confirmed by numerical calculations for different relaxation mechanisms.

It is convenient to analyze the overall dynamics of the spin system for  $\mu \neq 0$  separately for the cases where the system does or does not have stable periodic states in the rotating frame. In turn, this is determined by the interrelation between the damping parameters, cf. Eq. (4.19). Such analysis is carried out in Secs. 4.5 and 4.6.

# 4.5 Spin dynamics in the absence of limit cycles

We start with the case where the system does not have limit cycles. It corresponds to the situation where the damping parameter  $\Gamma^{(1)}$  is comparatively small and the interrelation between the damping parameters (4.19) does not hold. To simplify the analysis we set  $\Gamma^{(1)} = \Gamma^{(2)} = 0$ , i.e., we assume that the coupling to the bath is

linear in the spin operators and is described by the interaction Hamiltonian  $H_i^{(3)}$ . The qualitative results of this Section apply also for nonzero  $\Gamma^{(1)}$ ,  $\Gamma^{(2)}$  as long as  $\Gamma^{(3)} + 4\Gamma^{(2)} > 4\Gamma^{(1)}$ . The bifurcation diagram for this case is shown in Fig. 4.2.

From the form of the function  $\mathcal{T}$ , Eq. (4.15), it follows that the damping  $\propto \Gamma^{(3)}$  transforms centers of conservative motion with  $s_z > 0$  into unstable foci (repellers), whereas centers with  $s_z < 0$  are transformed into stable foci (attractors). Therefore for  $\mu < 0$  the spin has one stable state. It also has one stable state in the unshaded region of the half-plane  $\mu > 0$  (outside the bifurcation triangles in Fig. 4.2). Inside the shaded regions within the triangles the spin has two coexisting stable states.

Examples of the phase portrait are shown in Fig. 4.1. As expected, for weak damping the system has a stable and an unstable focus outside the bifurcation triangles, Fig. 4.1(a). In the shaded region inside the triangle it has two stable foci, an unstable focus, and a saddle point, Fig. 4.1(d). In the unshaded region inside the triangle there is one stable and two unstable foci, Fig. 4.1(b) (the values of  $\mu$  in panels (b) and (d) differ just by sign).

# 4.5.1 Hysteresis of spin response in the absence of limit cycles

The presence of two coexisting stable states leads to hysteresis of the spin response to the external field. Such hysteresis with varying dimensionless parameter  $\mu$ , which is proportional to the detuning of the field frequency, is shown in Fig. 4.3. For large negative  $\mu$  the system has one stable state with negative  $s_z$ , cf. Fig. 4.1(a). As  $\mu$  increases the system stays on the corresponding branch (the lowest solid line in Fig. 4.3) until the stable state merges with the saddle point (the saddle-node

bifurcation). This happens for  $\mu > 0$  as  $\mu$  reaches the bifurcation triangle. As  $\mu$  further increases the system switches to the branch with larger  $s_z$  and then moves along this branch. If  $\mu$  decreases starting with large values where the system has only one stable state, the switching to the second branch occurs for  $\mu = 0$ .

The hysteresis pattern in Fig. 4.3 differs from the standard S-shape characteristic. This is the case for any f lying between the minimum and maximum of the bifurcation triangle for  $\mu=0$ , i.e., for  $2\Gamma^{(3)}<|f|<\left(1+4\Gamma^{(3)}^2\right)^{1/2}$ . It is a consequence of the fact that the bifurcation at  $\mu=0$  is not a saddle-node bifurcation, whereas a most frequently considered S-shape hysteresis curve arises if both bifurcations are of the saddle-node type. In our case, for  $\mu=0$  the branch which is stable in the range of large positive  $\mu$  (the upper stable branch in Fig. 4.3) becomes unstable as a result of the motion becoming Hamiltonian-like. The value of  $s_z$  on this branch for  $\mu=0$  is  $s_z=0$ , it coincides with the value of  $s_z$  at the saddle (but the values of  $s_x$  are different). Therefore when  $s_z$  is plotted as a function of  $\mu$  the branch, which is stable for large positive  $\mu$  crosses with the branch that corresponds to the saddle point. For negative  $\mu$  the branch, which is stable for large positive  $\mu$ , becomes unstable, cf. Fig. 4.1. As  $\mu$  decreases and reaches the bifurcation triangle for  $\mu<0$ , the saddle merges with an unstable equilibrium as seen in Fig. 4.3.

The spin components display hysteresis also if the shaded area of the bifurcation triangle in Fig. 4.2(b) is crossed in a different way, for example, by varying f. If the crossing occurs so that the line  $\mu = 0$  is not crossed, the hysteresis curves have a standard S shape. We note that hysteresis of  $s_x, s_y$  corresponds to hysteresis of amplitude and phase of forced vibrations of the spin.

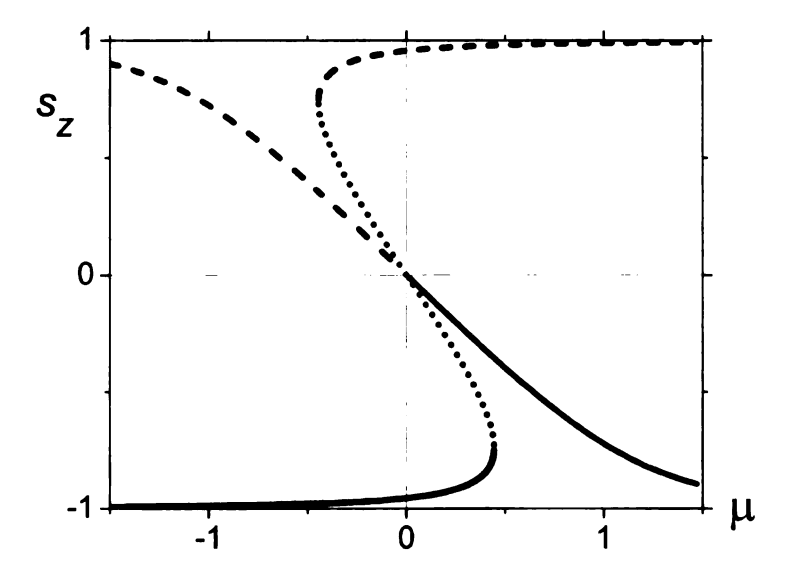


Figure 4.3: Hysteresis of spin response in the absence of periodic states in the rotating frame. The data refer to  $\Gamma^{(1)} = \Gamma^{(2)} = 0$ ,  $\Gamma^{(3)} = 0.1$ , and f = 0.3. The solid and dashed lines show, respectively, stable and unstable stationary states, the dotted line shows the saddle point.

### 4.5.2 Interbranch switching without hysteresis

The occurrence of Hamiltonian dynamics for  $\mu=0$  leads to an interesting and unusual behavior of the system even outside the bifurcation triangles, i.e. in the region where the system has only one stable state. In the small damping limit and for |f|>1 and  $|\mu|\ll 1$  the stationary states are at  $\phi=0$  and  $\phi=\pi$ , with  $s_z=\mu/(f\cos\phi-1)$ . The stable state is the one with  $s_z<0$ , whereas the one with  $s_z>0$  is unstable. As  $\mu$  goes through zero the states with  $\phi=0$  and  $\phi=\pi$  interchange stability. This means that  $s_x\approx\cos\phi$  jumps between -1 and 1. Such switching is seen in Fig. 4.4.

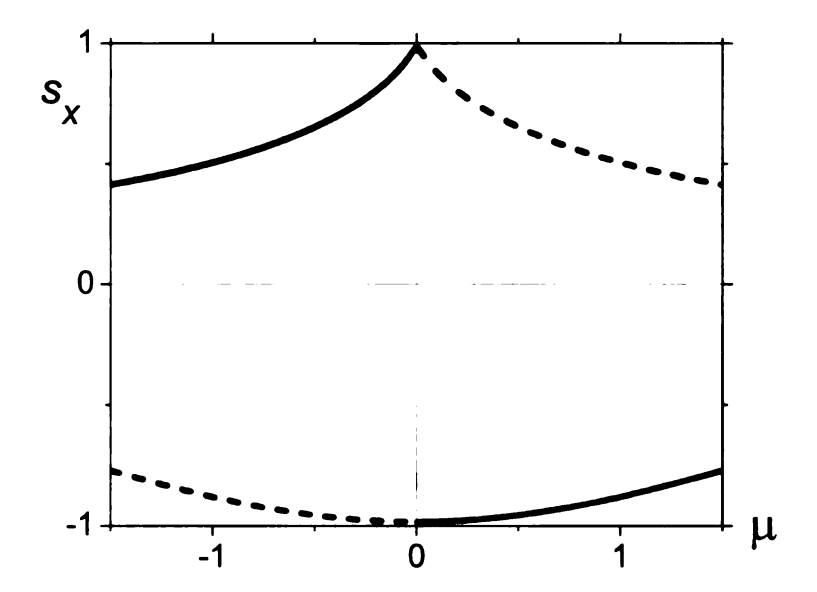


Figure 4.4: Frequency dependence of the transverse spin component for field amplitudes f where the system has one stable state. The solid and dashed lines show the stable and unstable values of  $s_x$  in the rotating frame. The data refer to  $\Gamma^{(1)} = \Gamma^{(2)} = 0$ ,  $\Gamma^{(3)} = 0.1$ , and f = 1.1. As the scaled frequency detuning  $\mu$  goes through  $\mu = 0$  the value of  $s_x$  changes to almost opposite in sign.

# 4.6 Spin dynamics in the presence of limit cycles

The classical dynamics of the spin changes significantly if the spin has stable periodic states in the rotating frame. This occurs where condition (4.19) on the damping parameters is met. The features of the dynamics can be understood by setting  $\Gamma^{(2)} = \Gamma^{(3)} = 0$ ,  $\Gamma^{(1)} > 0$ , i.e., by assuming that damping is due primarily to coupling to a bath  $H_i^{(1)}$ , which is quadratic in spin components, with elementary scattering processes corresponding to transitions between neighboring Zeeman levels. This model is of substantial interest for single-molecule magnets [17, 71].

The saddle-node bifurcation curves for weak damping  $\propto \Gamma^{(1)}$  are shown in Fig. 4.5. Inside the curvilinear triangles the spin has four stationary states, whereas outside the triangles it has two stationary states. In contrast to the case of damping  $\propto \Gamma^{(3)}$ 

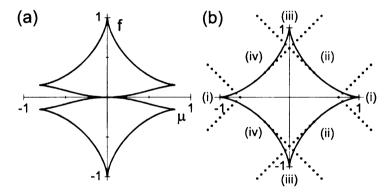


Figure 4.5: (a) Saddle-node bifurcation lines for  $\Gamma^{(1)} = 0.05$ ,  $\Gamma^{(2)} = \Gamma^{(3)} = 0$ . (b) Saddle-node (solid lines) and Hopf bifurcation (dotted lines) in the limit of small damping  $\propto \Gamma^{(1)}$ . Not too close to the astroid (see Sec. 4.6.2) for weak damping the system has the following states: (i) a stable and an unstable focus; (ii) two unstable foci and a stable limit cycle; (iii) a stable and an unstable focus and a stable and an unstable limit cycle; (iv) two stable foci and an unstable limit cycle.

shown in Fig. 4.2, in the present case the bases of the triangles touch at  $\mu = 0$ . From Eq. (4.17), one of the states emerging on the sides of the triangles is stable for  $\mu > 0$ ,  $|f| < 2^{-3/2}$  and is unstable otherwise; note that the stability changes in the middle of the bifurcation curves.

The occurrence of periodic oscillations of the spin is associated with Hopf bifurcations. In the present case, from Eq. (4.19) the Hopf bifurcational values of  $s_z$  are  $s_{zH} = \pm 1/\sqrt{2}$ . Therefore Eq. (4.20) for the Hopf bifurcation lines for weak damping takes a simple form

$$f_H = 2^{-1/2} \pm \mu, \quad f_H \notin (0, 2^{-3/2});$$
 (4.24)  
 $f_H = -2^{-1/2} \pm \mu, \quad f_H \notin (-2^{-3/2}, 0).$ 

These lines are shown in Fig. 4.5(b). For  $|f| \sim 1$  and far from the end points of the bifurcation lines, the typical frequency of the emerging oscillations is  $\sim 1$  in dimensionless units, or  $\sim DS/\hbar$  in dimensional units.

#### 4.6.1 Phase portrait far from the astroid

Evolution of the spin phase portrait with varying parameters far away from the astroid,  $|\mu| \gg 1$ , can be understood by looking at what happens as the Hopf bifurcation curves are crossed, for example by varying f. The result is determined by two characteristics. One is stability of the stationary state for f close to the bifurcational value  $f_H$ . The stability depends on the sign of  $\mathcal{T}$  for small  $f - f_H$  (note that  $\mathcal{T}$  changes sign for  $f = f_H$ ). The other characteristic is the sign of the quasienergy drift velocity  $\langle \dot{g} \rangle$  for  $f = f_H$  and for g close to its bifurcational value  $g_H$  at the stationary state. It is given by Eq. (4.23) [note that, generally,  $\langle \dot{g} \rangle \propto (g - g_H)^2$  for  $f = f_H$ ]. A combination of these characteristics tells on which side of the bifurcation point there emerges a limit cycle and whether this cycle is stable or unstable.

We write the value of  $s_z$  at the Hopf bifurcation point as  $s_{zH} = \alpha/\sqrt{2}$ , where  $\alpha = \pm 1$ , cf. Eq. (4.19). The bifurcational value of the field (4.24) is  $f_H = \pm \left(2^{-1/2} + \alpha\mu\right)\cos\phi_H$ , where  $\phi_H$  is the phase of the bifurcating stationary state. Linearizing Eq. (4.15) in  $s_z - s_{zH}$  and using the explicit form of the determinant  $\mathcal{D}$  one can show that, for small  $f - f_H$ , in a stationary state  $\operatorname{sgn}[\mathcal{T}/(f - f_H)] = -\operatorname{sgn}[\alpha f_H]$ . Then

$$\operatorname{sgn} \mathcal{T} = -(\alpha \operatorname{sgn} f_H) \operatorname{sgn} (f - f_H). \tag{4.25}$$

The analysis of the quasienergy drift velocity near a Hopf bifurcation point is done in Appendix B. It follows from Eqs. (B.1), (B.2) that

$$\langle \dot{g} \rangle = C\alpha \Gamma^{(1)} (g - g_H)^2 \left( \beta |f_H| - \sqrt{2} \right),$$

$$\operatorname{sgn} \left[ \langle \dot{g} \rangle / (g - g_H) \right] = \alpha \beta \operatorname{sgn} \left( \beta |f_H| - \sqrt{2} \right), \tag{4.26}$$

where C > 0 is a constant and  $\beta = \operatorname{sgn}(f_H \cos \phi_H) \equiv \operatorname{sgn}(2^{-1/2} + \alpha \mu) = \pm 1$  [ $\mu$  is related to  $f_H$  by Eq. (4.24)].

The sign of  $\langle \dot{g} \rangle/(g-g_H)$  shows whether g approaches  $g_H$  as a result of damping or moves away from  $g_H$ . If sgn  $[\langle \dot{g} \rangle(g-g_H)] < 0$ , the vicinity of the stationary state and the nascent limit cycle attracts phase trajectories. Therefore at a Hopf bifurcation a stable focus becomes unstable and a stable limit cycle emerges. On the other hand, if sgn  $[\langle \dot{g} \rangle(g-g_H)] > 0$ , at a Hopf bifurcation an unstable focus transforms into a stable one and an unstable limit cycle emerges.

Equation (4.25) allows one to say on which side of  $f_H$ , i.e., for what sign of  $f - f_H$  the stationary state is stable, since for a stable state  $\mathcal{T} < 0$ . Therefore together Eqs. (4.25) and (4.26) fully determine what happens as f crosses the bifurcational value.

We are now in a position to describe which states exist far from the astroid in different sectors (i)-(iv) in Fig. 4.5(b). For small |f| and large  $|\mu|$ , regions (i) in Fig. 4.5(b), the system is close to a spin in thermal equilibrium, it has one stable and one unstable stationary state. We now start changing f staying on the side of large positive  $\mu$ . When f crosses one of the bifurcation curves  $f_H = \pm \left(2^{-1/2} - \mu\right)$ , the system goes to one of the regions (ii) in Fig. 4.5(b). On the both bifurcation curves  $\alpha = \beta = -1$ . Therefore, from Eqs. (4.25), (4.26), when one of these curves is crossed as |f| increases, there emerges a stable limit cycle, and the stable focus becomes unstable. As |f| further increases it crosses the bifurcation curves  $\pm (2^{-1/2} + \mu)$  and the system goes to one of the regions (iii) in Fig. 4.5(b) (we assume that the crossing occurs in the region  $|f_H| > 2^{1/2}$ ). On these bifurcation curves  $\alpha = \beta = 1$ . Therefore, from Eqs. (4.25), (4.26), when they are crossed with increasing |f| there emerges an unstable limit cycle and the unstable focus becomes stable.

We now start from the range of large negative  $\mu$  and small |f|. As we increase |f| and cross the bifurcation curves  $f_H = \pm (\mu + 2^{-1/2})$  the system goes from region (i) to

one of the regions (iv) in Fig. 4.5(b). From Eqs. (4.25), (4.26), in this case an unstable focus goes over into a stable focus and an unstable limit cycle emerges. Further crossing into one of the regions (iii) with increasing |f| leads to a transformation of a stable focus into an unstable focus and an onset of a stable limit cycle. These arguments were used to establish the nomenclature of states in regions (i)-(iv) in Fig. 4.5(b). They agree with the results of direct numerical calculations.

#### 4.6.2 Other bifurcations of limit cycles

#### Merging of stable and unstable limit cycles

The number of periodic states in the rotating frame may change not only through Hopf bifurcations, but also through other bifurcations, where the radius of the bifurcating limit cycle does not go to zero. The simplest is a bifurcation where a stable limit cycle merges with an unstable limit cycle (saddle-node bifurcation of limit cycles). The onset of such bifurcations is clear already from Eq. (4.26). Indeed, at a Hopf bifurcation point the equation for the period-averaged quasienergy has a form  $\langle \dot{g} \rangle = c(g-g_H)^2 + \dots$  with  $c \propto \beta |f_H| - \sqrt{2}$ . For  $|f_H| = \sqrt{2}$  on the bifurcation curves (4.24) with  $\beta = 1$  [the top and bottom dotted lines in Fig. 4.5(b)] the coefficient c = 0. This is a generalized Hopf bifurcation [72], see Fig. 4.6.

At the generalized Hopf bifurcation, in phase space  $(\phi, s_z)$  a stationary state merges simultaneously with a stable and an unstable limit cycle. In parameter space  $(\mu, f)$ , the Hopf bifurcation curve coalesces with the curve where stable and unstable limit cycles are merging, and the latter curve ends. The bifurcation curves are tangent, the distance between them scales as a square of the distance to the end point  $\beta |f_H| = \sqrt{2}$  if the latter distance is small. This is seen in Fig. 4.6. In the comparatively narrow region between the Hopf bifurcation curve and the corresponding limit-cycle merging

curve the system has three limit cycles. One of these cycles disappears on the Hopf bifurcation curve, so that in regions (iii) in Fig. 4.5(b) there are two limit cycles and deeper in regions (ii) and (iv) there is one limit cycle. On its opposite end, the curve of merging limit cycles coalesces with the saddle-loop bifurcation curve.

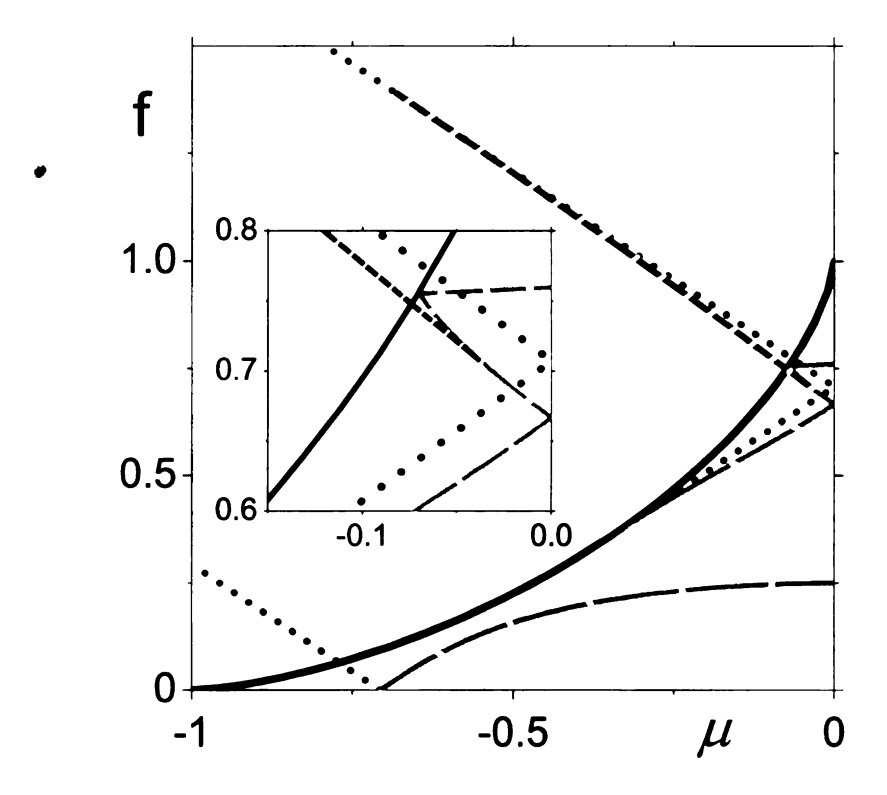


Figure 4.6: Bifurcation diagram in the limit  $\Gamma^{(1)} \to 0$ . The diagram is symmetric with respect to  $\mu = 0$  and f = 0 axes, and therefore only the quadrant  $f \ge 0, \mu \le 0$  is shown. Saddle-node, Hopf, and saddle-loop bifurcation curves are shown by the solid, dotted, and long-dash lines, respectively, whereas the short-dash line shows the curve on which stable and unstable limit cycles merge.

#### Saddle loops

Spin dynamics for damping  $\propto \Gamma^{(1)}$  is characterized also by global bifurcations of the type of saddle loops. This is clear already from the analysis of the end points of the Hopf bifurcation curves. These points lie on the curves of saddle-node bifurcations. The corresponding equilibrium point has double-zero eigenvalue, and the behavior of

the system near this point is well-known [72]. The Hopf bifurcation curve is tangent to the saddle-node bifurcation curve at the end point. In addition, there is a saddle-loop bifurcation curve coming out of the same end point and also tangent to the saddle-node bifurcation curve at this point. At a saddle-loop bifurcation the system has a homoclinic trajectory that starts and ends at the saddle point.

The structure of vicinities of the end points of the Hopf bifurcation curves is shown in Figs. 4.6 and 4.7 for the curves ending on the sides and the bases of the saddle-node bifurcation triangles, respectively. Note that the Hopf bifurcation curves that crossed at f = 0 in the limit  $\Gamma^{(1)} \to 0$  are separated for finite  $\Gamma^{(1)}$ . They end on the saddle-node bifurcation curves.

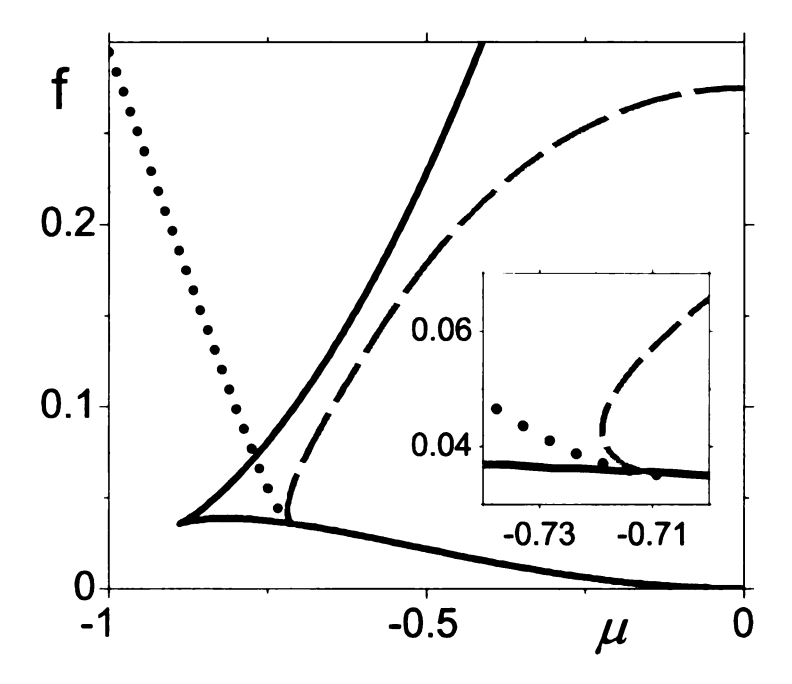


Figure 4.7: Bifurcation diagram near the end point of the Hopf bifurcation line which in the limit  $\Gamma^{(1)} \to 0$  has the form  $f_H = -\mu - 2^{-1/2}$ . For nonzero  $\Gamma^{(1)}$  this bifurcation line ends on the saddle-node bifurcation line (4.18). The plot refers to  $\Gamma^{(1)} = 0.0125$ . The inset shows a close vicinity of the end point. Hopf, saddle-node, and saddle-loop bifurcation curves are shown by dotted, solid, and long-dashed lines, respectively. Other Hopf bifurcation curves that go to  $f_H = 0$  for  $\Gamma^{(1)} \to 0$  display a similar behavior near their end points.

We have found numerically a fairly complicated pattern of saddle-loop bifurcation curves. Full analysis of this pattern is beyond the scope of this paper chapter.

# 4.6.3 Hysteresis of spin response in the presence of limit cycles

Coexistence of stable stationary states and stable limit cycles in the rotating frame leads to hysteresis of the response of a spin when the modulating field parameters are slowly varied. Examples of such hysteresis with varying scaled frequency detuning  $\mu$  and the characteristic phase portraits are shown in Fig 4.8.

The hysteretic behavior is unusual. This is a consequence of the feature of the spin dynamics for  $\mu=0$  where either all phase trajectories are closed loops (for f outside the curvilinear saddle-node bifurcation triangles in Fig. 4.5) or all trajectories in a part of the phase plane are closed loops (for f inside the triangles in Fig. 4.5). As a result two or more states (stationary or periodic) simultaneously loose or acquire stability as  $\mu$  goes through 0. This leads to an ambiguity of switching, a "Buridan's ass" type situation. Where a stable branch looses stability for  $\mu=0$ , the system has more than one stable state to switch to. Also, in contrast to the situation of Sec. 4.5 where the system had no limit cycles, hysteresis emerges whether the varying field parameter does or does not cross the saddle-node bifurcation lines.

Figures 4.8(a) and (b) show the behavior of the system with varying  $\mu$  for f inside and outside the saddle-node bifurcation triangles, respectively. It should be noted that we chose f in Fig. 4.8(a) so that the saddle-loop bifurcation line is not encountered, which provides an insight into the most basic features of the hysteresis. In addition, in Fig. 4.8(b) we do not show an extremely narrow region near Hopf bifurcation lines  $\mu \approx \pm (f - 2^{-1/2})$  where the system has small-radii stable and unstable cycles which

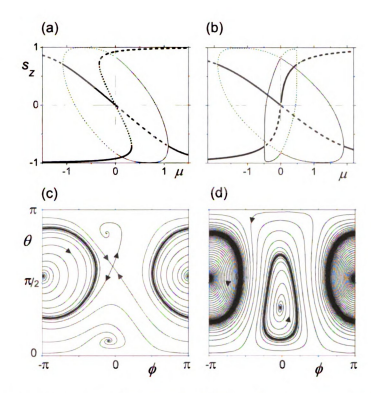


Figure 4.8: Panels (a) and (b): hysteresis of the spin dynamics with varying scaled detuning of the modulating field frequency  $\mu$ . In (a) f=0.4, so that  $\mu$  goes through the curvilinear bifurcation triangle in Fig. 4.5. In (b) f=1.2, it lies above the triangles. Bold solid lines, long dashed lines, and dotted line show stable and unstable equilibria and the saddle stationary state, respectively. Pairs of thin solid lines and short dashed lines show the boundaries (with respect to  $s_z$ ) of stable and unstable limit cycles. Panels (c) and (d): phase portraits for  $\mu=0.2$ . In (c) and (d) f=0.4 and 1.2, respectively. The arrows show the direction of motion along the trajectories. The data refer to  $\Gamma^{(1)}=0.05$ .

merge on the short-dash bifurcation line in Fig. 4.6.

In Fig. 4.8(a), for large negative  $\mu$  the system has one stable state (with negative  $s_z$ ). As  $\mu$  increases this state disappears via a saddle-node bifurcation and the system switches to a stable limit cycle. For chosen f=0.4 this happens for  $\mu\approx 0.33$ . With further increase of  $\mu$  the limit cycle shrinks and ultimately disappears via a Hopf bifurcation, and then the stationary state inside the cycle becomes stable.

On the other hand, if we start in Fig. 4.8(a) from large positive  $\mu$  and decrease

 $\mu$ , the stable stationary state via a supercritical Hopf bifurcation becomes a stable limit cycle. The cycle looses stability at  $\mu = 0$ , and as  $\mu$  becomes negative the system can switch either to the stable stationary state inside the cycle (with  $s_z \to +0$  for  $\mu \to -0$ ) or to a stable stationary state outside the cycle with negative  $s_z$ . The stable state with  $s_z \to +0$  for  $\mu \to -0$ , ultimately looses stability with decreasing  $\mu$  via a Hopf bifurcation (at  $\mu \approx -f - 2^{-1/2}$ , for small damping, cf. Fig. 4.5). If the system is in this state, it switches to the stable equilibrium with negative  $s_z$ .

A typical phase portrait for  $f = 0.4, 0 < \mu < 0.33$  is shown in Fig. 4.8(c). It gives an insight into the behavior described above. The system has a stable limit cycle with an unstable focus inside and with stable and unstable equilibria and a saddle point outside the limit cycle. For  $\mu = 0$  the system has a homoclinic saddle connection, and all trajectories inside the homoclinic trajectory are closed loops, cf. Fig. 4.1(c)

In Fig. 4.8(b), for large negative  $\mu$  the system also has one stable state (with negative  $s_z$ ). As  $\mu$  increases this state looses stability via a Hopf bifurcation (at  $\mu \approx -f + 2^{-1/2}$ , for small damping). The emerging state of stable oscillations looses stability for  $\mu = 0$ . For larger  $\mu$  the system switches either to the stationary state inside the limit cycle (with  $s_z \to +0$  for  $\mu \to +0$ ) or to another stable periodic state. The coexistence of stable and unstable limit cycles with stationary states inside of them is seen in Fig. 4.8(d).

As  $\mu$  becomes positive and further increases, the stable stationary state inside the unstable cycle looses stability by merging with this cycle, and the system switches to the periodic state corresponding to the stable limit cycle in Fig. 4.8(d). For still larger  $\mu$  ( $\mu \approx f + 2^{-1/2}$ , for weak damping) this state experiences a Hopf bifurcation and becomes a stable stationary state. The behavior with  $\mu$  decreasing from large positive values can be understood from Fig. 4.8 in a similar way.

#### 4.7 Conclusions

We have developed a microscopic theory of a resonantly modulated large spin in a strong static magnetic field and studied spin dynamics in the classical limit. We have taken into account relaxation processes important for large-spin systems of current interest. They correspond to transitions between neighboring and next-neighboring Zeeman levels with emission or absorption of excitations of a bosonic thermal bath. Classical spin dynamics depends significantly on the interrelation between the rates of different relaxation processes. Generally it is not described by the Landau-Lifshitz equation for magnetization in a ferromagnet, although one of the coupling mechanisms that we discuss leads to the Landau-Lifshitz damping in the rotating frame.

We found that the spin dynamics has special symmetry at exact resonance where the modulation frequency is equal to the Larmor frequency,  $\omega_F = \omega_0$ . This symmetry leads to a Hamiltonian-like behavior even in the presence of dissipation. In the rotating frame, phase trajectories of the spin form closed loops in a part of or on the whole phase plane. Therefore when  $\omega_F$  goes through  $\omega_0$  several states change stability at a time.

The simultaneous stability change leads to unusual observable features. Where the system has only one stable state for a given parameter value, as  $\omega_F$  goes through  $\omega_0$  there occurs switching between different states that leads to an abrupt change of the magnetization. The behavior is even more complicated where several stable states coexist for  $\omega_F$  close but not equal to  $\omega_0$ . Here, where  $\omega_F - \omega_0$  changes sign, the state into which the system will switch is essentially determined by fluctuations or by history (if  $\omega_F$  is changed comparatively fast).

We found the conditions where the spin has more than one stable stationary state in the rotating frame. Such stable states correspond to oscillations of the transverse magnetization at the driving frequency in the laboratory frame. Multistability leads to magnetization hysteresis with varying parameters of the modulating field. If the fastest relaxation process is transitions between neighboring states due to coupling quadratic in spin operators, the resonantly modulated spin can have periodic nonsinusoidal states in the rotating frame with frequency  $\propto DS/\hbar$ , where D is the anisotropy energy. In the laboratory frame, they correspond to oscillations of the transverse magnetization at combinations of this frequency (and its overtones) and the Larmor frequency.

Quantum fluctuations of the spin lead to phase diffusion of the classical periodic states in the rotating frame. As a result, classical oscillations decay. The intensity of quantum fluctuations and the related decay rate depend on the value of  $S^{-1}$ . We have found [83] that the oscillations decay comparatively fast even for S = 10. Therefore they are transient. Still the classically stable vibrations lead to pronounced features of the full quantum spin dynamics.

The present analysis can be immediately extended to a more general form of the spin anisotropy energy, in particular to the case where along with  $DS_z^2$  this energy has a term  $E(S_x^2 - S_y^2)$ , which is important for some types of single-molecule magnets [24]. In the RWA, the corresponding term renormalizes D and  $\omega_0$ . The analysis applies also to decay due to two-phonon or two-magnon coupling, which often plays an important role in spin dynamics and leads to energy relaxation via inelastic scattering of bath excitations by the spin. Another important generalization is that the results are not limited to linearly polarized radiation. It is easy to show that they apply for an arbitrary polarization as long as the radiation is close to resonance.

In conclusion, starting from a microscopic model, we have shown that the classical dynamics of a resonantly modulated large spin in a strong magnetic field displays several characteristic features. They include abrupt switching between magnetization branches with varying parameters of the modulating field even where there is no hysteresis, as well as the occurrence of hysteresis and an unusual pattern of hysteretic inter-branch switching. These features are related to the Hamiltonian-like behavior of the dissipative spin for modulation frequency equal to the Larmor frequency in the neglect of spin anisotropy. Along with forced vibrations at the modulation frequency, the transverse spin components can display transient vibrations at a combination of the modulation frequency and a slower frequency  $\propto DS/\hbar$  and its overtones. They emerge if the fastest relaxation mechanism corresponds to transitions between neighboring Zeeman levels with the energy of coupling to a thermal bath quadratic in the spin operators.

# Chapter 5

# Quantum-Classical Transition and Quantum Activation in Modulated Large-Spin Systems

### 5.1 Introduction

Large-spin systems are of great interest for the study of quantum to classical transitions. The inverse size of the spin, 1/S, can be seen as an effective Planck number which controls the "quantumness" of the system. Of particular interest in that context is the effect of hysteresis in a modulated large spin system. As detailed in chapter 4, a modulated large spin system can have several coexisting stable states in the semiclassical limit. In the quantum regime for a given set of parameters, even at zero temperature, all of these states but one become metastable. This leads to switching between the states and hence hysteresis.

For classical systems in thermal equilibrium switching is often described by the

activation law, with the switching probability being  $W \propto \exp(-\Delta U/kT)$ , where  $\Delta U$  is the activation energy. As temperature decreases, quantum fluctuations become more and more important, and below a certain crossover temperature switching occurs via tunneling [41, 42, 43]. The behavior of systems away from thermal equilibrium is far more complicated. Still, for classical systems switching is often described by an activation type law, with the temperature replaced by the characteristic intensity of the noise that leads to fluctuations [44, 45, 46, 47, 48, 49, 50, 51, 52]. Quantum nonequilibrium systems can also switch via tunneling between classically accessible regions of their phase space [32, 53, 33, 54].

Besides classical activation and quantum tunneling, nonequilibrium systems have another somewhat counterintuitive mechanism of transitions between stable states. This mechanism is called quantum activation and has been explained recently for the cases of a parametrically driven oscillator [55] and a nonlinear oscillator [56]. It describes escape from a metastable state due to quantum fluctuations that accompany relaxation of the system [57]. These fluctuations lead to diffusion away from the metastable state and, ultimately, to transitions over the classical "barrier", that is, the boundary of the basin of attraction of the metastable state.

Quantum activation in periodically modulated systems can be understood by noting that metastable states are formed as a result of the balance between external driving and dissipation due to coupling to a thermal bath. Dissipation corresponds to transitions to lower energy states with emission of excitations of the bath. Because energy of modulated systems is not conserved even without dissipation, it is more convenient to describe them by the Floquet (quasienergy) states rather than the energy eigenstates. Emission of bath excitations may result in transitions to both higher and lower quasienergies, albeit with different probabilities [57, 55, 56]. The higher-

probability transitions lead to relaxation towards a metastable state, whereas the lower-probability transitions lead to effective diffusion away from it, a finite-width distribution over quasienergy, and metastable decay even in the zero temperature limit.

Because of the similarities of a modulated spin system with a non-linear oscillator it can be expected that the dynamics of the spin is also governed by quantum activation.

In this chapter we extend the analysis of the previous chapter 4 of a modulated large spin system from the semiclassical limit to the the quantum regime. In section 5.2 we introduce spin coherent states and reformulate the quantum kinetic equation in the spin coherent state representation. This helps us to obtain a better understanding of the dynamics of the system in the presence of limit cycles. In section 5.3 we investigate the stationary quasienergy distribution of the system which enables us to get insight into various phenomena such as switching between coexisting stable states through quantum activation as well as abrupt switching between magnetization branches even in the absence of hysteresis, and Hamiltonian-like motion in the quantum regime.

# 5.2 Dynamics of modulated large-spin systems

To investigate the dynamics of large-spin systems and their transition from the quantum to the semiclassical limit it is beneficial to express the density matrix of the system in the overcomplete basis of spin coherent states.

#### 5.2.1 Some properties of spin coherent states

A spin coherent state is uniquely defined by relating it to a point on the surface of a sphere with integer or half integer radius S [84],

$$|\xi\rangle = (1 + \xi \xi^*)^{-S} \exp(\xi S_-) |S\rangle$$

$$= (1 + \xi \xi^*)^{-S} \sum_{m=-S}^{S} {2S \choose s-m}^{1/2} \xi^{s-m} |m\rangle, \qquad (5.1)$$

where  $S_z |m\rangle = m |m\rangle$  and  $\xi = e^{i\phi} \tan \theta/2$ . The azimuthal and polar angles,  $\phi$  and  $\theta$ , parameterize the spin coherent state and determine its average direction,

$$\langle \xi | S_x | \xi \rangle = S \sin \phi \sin \theta, \tag{5.2}$$

$$\langle \xi | S_y | \xi \rangle = S \cos \phi \sin \theta,$$
 (5.3)

$$\langle \xi | S_z | \xi \rangle = S \cos \theta. \tag{5.4}$$

Another important property of spin coherent states is that they satisfy the minimum Heisenberg uncertainty relation in the sense that spin components orthogonal to the mean spin vector have equal and minimal dispersion [85, 86, 87],

$$\Delta S_{x'} \Delta S_{y'} = \frac{1}{2} \left| \left\langle S_{z'} \right\rangle \right|, \tag{5.5}$$

where  $\Delta S = \sqrt{\langle S^2 \rangle - \langle S \rangle^2}$ , z' is the direction of the mean spin vector, and x', y' are the directions of the respective orthogonal spin components. Because of this property spin coherent states are states that come closest to the classical points in phase space of the system in the large spin limit. The use of spin coherent states is therefore appropriate to analyze the transition from quantum to classical behavior.

Spin coherent states form an overcomplete set in Hilbert space; they are generally non-orthogonal to each other [84]. The overlap probability between two states is given by

$$|\langle \xi_1 | \xi_2 \rangle|^2 = \left(\frac{1 + \mathbf{n}_1 \mathbf{n}_2}{2}\right)^{2S}, \tag{5.6}$$

where  $\mathbf{n}_1$  and  $\mathbf{n}_2$  are unit vectors in the directions specified by  $(\phi_1, \theta_1)$  and  $(\phi_2, \theta_2)$ , respectively. Hence, more distant states have smaller overlaps. The completeness relation includes a weight factor and has the form

$$\frac{2S+1}{\pi} \int \frac{d^2 \xi}{\left(1+\xi \xi^*\right)^2} \left|\xi\right\rangle \left\langle \xi\right| = \mathbf{1}.\tag{5.7}$$

If integrating over  $\theta$  and  $\phi$  the completeness relation transforms into

$$\frac{2S+1}{4\pi} \int \sin(\theta) d\phi d\theta |\phi, \theta\rangle \langle \phi, \theta| = \mathbf{1}.$$
 (5.8)

# 5.2.2 The master equation in the spin coherent state representation and its semiclassical limit

Starting from the quantum kinetic equation (4.8), we will now demonstrate an alternative way of deriving the classical equations of motion as they are presented in Eq. (4.13). For that purpose we switch to a representation of the system's density matrix in terms of spin coherent states. For us it is sufficient to consider the expectation value of the density matrix  $\rho$  for a given spin coherent state  $|\xi\rangle$ . This expectation value is the probability to find the system at time t in the state  $|\xi\rangle$ ,

$$p(\xi, t) = \langle \xi | \rho(t) | \xi \rangle. \tag{5.9}$$

In the semiclassical large spin limit,  $S \to \infty$ , this quantity becomes the delta function  $\delta(\phi - \phi(t))\delta(\theta - \theta(t))$ . To proceed we introduce the unnormalized spin coherent state

$$\left|\tilde{\xi}\right\rangle = \left(1 + \xi \xi^*\right)^S \left|\xi\right\rangle \tag{5.10}$$

and make the following observations:

$$S_{z} \left| \tilde{\xi} \right\rangle = \left( S - \xi \frac{\partial}{\partial \xi} \right) \left| \tilde{\xi} \right\rangle,$$

$$S_{-} \left| \tilde{\xi} \right\rangle = \frac{\partial}{\partial \xi} \left| \tilde{\xi} \right\rangle, \qquad (5.11)$$

$$S_{+} \left| \tilde{\xi} \right\rangle = \left( 2S\xi - \xi^{2} \frac{\partial}{\partial \xi} \right) \left| \tilde{\xi} \right\rangle,$$

which can be verified directly by plugging in the sum from Eq. (5.1). Note that for a sequence of spin operators the sequence of their respective differential operator expressions must be in reverse order, e.g.  $S_z S_- \left| \tilde{\xi} \right\rangle = \frac{\partial}{\partial \xi} \left( S - \xi \frac{\partial}{\partial \xi} \right) \left| \tilde{\xi} \right\rangle$ .

As a consequence and if we treat  $\xi$  and  $\xi^*$  as two independent variables the following expressions hold true:

$$\left\langle \tilde{\xi} \middle| \rho S_z \middle| \tilde{\xi} \right\rangle = \left( S - \xi \frac{\partial}{\partial \xi} \right) \tilde{p}, 
\left\langle \tilde{\xi} \middle| \rho S_- \middle| \tilde{\xi} \right\rangle = \frac{\partial}{\partial \xi} \tilde{p}, 
\left\langle \tilde{\xi} \middle| \rho S_+ \middle| \tilde{\xi} \right\rangle = \left( 2S\xi - \xi^2 \frac{\partial}{\partial \xi} \right) \tilde{p}, \tag{5.12}$$

where  $\tilde{p} = \tilde{p}(\xi, \xi^*, t) = \left\langle \tilde{\xi} \middle| \rho \middle| \tilde{\xi} \right\rangle$ . Note that in expressions where a spin operator is positioned to the left of the density matrix its hermitian conjugate acts on the bra component of the scalar product, e.g.  $\left\langle \tilde{\xi} \middle| S_{+} \rho \middle| \tilde{\xi} \right\rangle = \frac{\partial}{\partial \xi^*} \tilde{p}$  or as another example  $\left\langle \tilde{\xi} \middle| S_{+} \rho S_z \middle| \tilde{\xi} \right\rangle = \frac{\partial}{\partial \xi^*} \left( S - \xi \frac{\partial}{\partial \xi} \right) \tilde{p}$ . Since  $\left\langle \tilde{\xi} \middle| \rho \middle| \tilde{\xi} \right\rangle = \sum_{m=-S}^{S} c_m \binom{2S}{s-m}^{1/2} \xi^{s-m}$ , where  $c_m = \sum_{n=-S}^{S} \binom{2S}{s-n}^{1/2} (\xi^*)^{s-n}$ , this formalism allows us to express all relevant quantities by differential operators which act on polynomials of order 2S in  $\xi$  or  $\xi^*$ , respectively.

In order to relate expressions (5.12) to normalized spin coherent states we note that  $\langle \xi | S_1 \rho S_2 | \xi \rangle = (1 + \xi \xi^*)^{-2S} \left\langle \tilde{\xi} \left| S_1 \rho S_2 \right| \tilde{\xi} \right\rangle$  and  $\tilde{p} = (1 + \xi \xi^*)^{2S} p$ . This leads to the following replacement rules for Eqs. (5.12):

$$\frac{\partial}{\partial \xi} \to \frac{\partial}{\partial \xi} + \frac{2S\xi^*}{1 + \xi\xi^*}, \qquad \left| \tilde{\xi} \right\rangle \to \left| \xi \right\rangle, \qquad \tilde{p} \to p$$
 (5.13)

With these results we are now prepared to transform the master equation (4.8) to a differential equation. We will here rewrite the master equation in a slightly different form:

$$\dot{\rho} = i[\rho, H_0/SD] - S\hat{\Gamma}^{(1)}\rho - S\hat{\Gamma}^{(2)}\rho - S\hat{\Gamma}^{(3)}\rho, \tag{5.14}$$

where  $H_0/SD = -\mu S_z - \frac{1}{2S}S_z^2 - fS_x$  and  $\dot{\rho}$  denotes the partial derivative of the system's density matrix with respect to the slow dimensionless time  $\tau = SDt$ ,  $\dot{\rho} \equiv \frac{\partial \rho}{\partial \tau}$ .

Starting with the coherent part of the equation we obtain the following second order partial differential equation:

$$\dot{p}_{H_0} = i\langle \xi | [\rho, H_0/SD] | \xi \rangle$$

$$= i \left( \left( \mu - \frac{1}{2S} + \frac{1 - \xi \xi^*}{1 + \xi \xi^*} \right) \xi + \frac{f}{2} \left( \xi^2 - 1 \right) \right) \frac{\partial p}{\partial \xi} - i \frac{\xi^2}{2S} \frac{\partial^2 p}{\partial \xi^2} + c.c.$$
(5.15)

Terms of order 1/S are quantum corrections to the semiclassical equations of motion. In the semiclassical limit,  $S \to \infty$ , we can neglect these terms which leaves us with the first order differential equation

$$\dot{p}_{H_0} = i \left( \left( \mu + \frac{1 - \xi \xi^*}{1 + \xi \xi^*} \right) \xi + \frac{f}{2} \left( \xi^2 - 1 \right) \right) \frac{\partial p}{\partial \xi} + c.c., \qquad S \gg 1.$$
 (5.16)

Using the method of characteristics or simply by comparing coefficients with  $\dot{p} = \frac{\partial p}{\partial \tau} = \frac{dp}{d\tau} - \frac{\partial p}{\partial \xi} \frac{d\xi}{d\tau} - \frac{\partial p}{\partial \xi^*} \frac{d\xi^*}{d\tau}$  we finally obtain an ordinary differential equation for  $\xi$ :

$$\dot{\xi}_{H_0} \equiv \frac{d\xi_{H_0}}{d\tau} = -i\left(\left(\mu + \frac{1 - \xi\xi^*}{1 + \xi\xi^*}\right)\xi + \frac{f}{2}\left(\xi^2 - 1\right)\right), \qquad S \gg 1.$$
 (5.17)

For brevity, we analyze the dissipation terms (4.9) only for the case of zero temperature.

$$S\hat{\Gamma}^{(1)}\rho = \frac{1}{S^3}\Gamma^{(1)}\left(L^{\dagger}L\rho - 2L\rho L^{\dagger} + \rho L^{\dagger}L\right), L = S_-S_z + S_zS_-$$

$$S\hat{\Gamma}^{(2)}\rho = \frac{1}{S^3}\Gamma^{(2)}\left(S_+^2S_-^2\rho - 2S_-^2\rho S_+^2 + \rho S_+^2S_-^2\right)$$

$$S\hat{\Gamma}^{(3)}\rho = \frac{1}{S}\Gamma^{(3)}\left(S_+S_-\rho - 2S_-\rho S_+ + \rho S_+S_-\right)$$
(5.18)

In order to determine the contributions of the dissipation terms to the ordinary differential equation in  $\xi$  we follow the same steps as above, i.e. calculate the coefficient of  $\frac{\partial p}{\partial \xi}$  in  $\dot{p}_{\Gamma^{(1,2,3)}} = -\left\langle \xi \left| S \hat{\Gamma}^{(1,2,3)} \rho \right| \xi \right\rangle$  and drop terms of order 1/S or smaller.

In the large spin limit we obtain the following first order partial differential equations (the full equations which contain higher order terms in 1/S are presented in Appendix C; there it is shown that in fact  $\dot{p}_{\Gamma(3)}$  and  $\dot{p}_{\Gamma(1,2)}$  are partial differential equations of second and fourth order, respectively):

$$\dot{p}_{\Gamma^{(1)}} = -8\Gamma^{(1)} \left( \frac{2(1 - \xi\xi^*)(1 - \xi\xi^*(6 - \xi\xi^*))}{(1 + \xi\xi^*)^3} p + \left( \frac{1 - \xi\xi^*}{1 + \xi\xi^*} \right)^2 \left( \xi \frac{\partial p}{\partial \xi} + \xi^* \frac{\partial p}{\partial \xi^*} \right) \right), \quad S \gg 1,$$
(5.19)

$$\dot{p}_{\Gamma^{(2)}} = -16\Gamma^{(2)} \left( \frac{4\xi\xi^*(1-\xi\xi^*)}{(1+\xi\xi^*)^3} p + \frac{\xi\xi^*}{(1+\xi\xi^*)^2} \left( \xi \frac{\partial p}{\partial \xi} + \xi^* \frac{\partial p}{\partial \xi^*} \right) \right), \quad S \gg 1,$$

$$(5.20)$$

$$\dot{p}_{\Gamma^{(3)}} = -2\Gamma^{(3)} \left( \frac{2(1-\xi\xi^*)}{1+\xi\xi^*} p + \xi \frac{\partial p}{\partial \xi} + \xi^* \frac{\partial p}{\partial \xi^*} \right), \quad S \gg 1.$$
 (5.21)

Hence,

$$\dot{\xi}_{\Gamma^{(1)}} = 8\Gamma^{(1)}\xi \left(\frac{1-\xi\xi^*}{1+\xi\xi^*}\right)^2, 
\dot{\xi}_{\Gamma^{(2)}} = 16\Gamma^{(2)}\frac{\xi^2\xi^*}{(1+\xi\xi^*)^2}, \qquad S \gg 1 
\dot{\xi}_{\Gamma^{(3)}} = 2\Gamma^{(3)}\xi.$$
(5.22)

The resulting complete classical equation of motion is

$$\dot{\xi} = \dot{\xi}_{H_0} + \dot{\xi}_{\Gamma(1)} + \dot{\xi}_{\Gamma(2)} + \dot{\xi}_{\Gamma(3)}. \tag{5.23}$$

In order to compare this result with Eq. (4.13) we have to replace  $\xi(t)$  by  $\phi(t)$  and  $\theta(t)$ . Therefore, with

$$\dot{\xi} = ie^{i\phi} \tan(\theta/2)\dot{\phi} + \frac{e^{i\phi}}{\cos^2 \theta/2}\dot{\theta}$$
 (5.24)

and equating real and imaginary part of Eqs. (5.23) and (5.24) we finally obtain

$$\dot{\phi} = -\mu - \cos\theta + f\cos\phi\cot\theta, \qquad (5.25)$$

$$\dot{\theta} = f\sin\phi + 2\sin\theta \left(4\Gamma^{(1)}\cos^2\theta + 2\Gamma^{(2)}\sin^2\theta + \Gamma^{(3)}\right).$$

These two equations are identical with Eqs. (4.13) as one can see by substituting  $s_z$  by  $\cos \theta$  in Eq. (4.13).

Note that in order to check the validity of Eqs. (5.16) and (5.19-5.21) one can for example inspect whether  $Tr(\rho)$  is conserved. Using the completeness relation (5.7) we obtain that

$$Tr(\rho) = \frac{2S+1}{\pi} \int \frac{d\xi d\xi^*}{(1+\xi\xi^*)^2} p.$$
 (5.26)

Plugging in Eqs. (5.16) and (5.19-5.21), integrating by parts, and making use of the periodic boundary conditions one can easily show that indeed  $\frac{\partial}{\partial \tau} \text{Tr}(\rho) = 0$ .

### 5.2.3 Dynamics of the system in the presence of limit cycles

Of particular interest is the quantum-classical transition of limit cycles in the system. Limit cycles can occur in the semiclassical limit if the relaxation parameters in Eqs. (5.14) and (5.18) satisfy the condition  $\Gamma^{(1)} \geq \Gamma^{(2)} + \frac{1}{4}\Gamma^{(3)}$ , as has been derived in 4.3.3. In order to describe limit cycles in the quantum regime it is useful to switch to a new set of real local coordinates,  $\xi_{\parallel}$  and  $\xi_{\perp}$ . In the vicinity of the limit cycle,  $\xi_{\parallel}$  describes the length along a path on the classical limit cycle, whereas  $\xi_{\perp}$  measures the distance locally perpendicular to that path. Therefore, on the limit cycle it is  $\xi_{\perp} = 0$ .

A similar analysis has been done for the case of limit cycles in arbitrary dimensional classical Markovian systems described by the Fokker-Planck equation [88]. There the dynamics results in a stationary probability distribution in the shape of a

nearly circular crater where the ridge of the crater corresponds to the deterministic trajectory of the limit cycle. Here, we are interested in analyzing the stationary

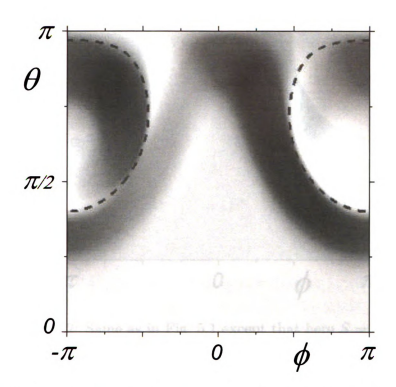


Figure 5.1: Spin density distribution,  $p_{st}$ , as a function of the azimuthal angle  $\phi$  and polar angle  $\theta$ . S=10,  $\Gamma^{(1)}=0.01$ ,  $\Gamma^{(2)}=\Gamma^{(3)}=0$ ,  $\mu=0.6$ , and f=0.4. The dotted line indicates the position of the corresponding classical stable limit cycle which coincides with the maximum of  $p_{st}$ .

solution of the system's density matrix. In order to relate the properties of the density matrix,  $\rho$ , to the classical language of limit cycles we investigate its corresponding spin coherent state probability density distribution  $p = \langle \phi, \theta | \rho | \phi, \theta \rangle$ .

We now assume that p is expressed in form of two real coordinates,  $(x_1,x_2)$  which are locally orthogonal to each other, e.g.  $(\phi,\theta)$  or  $(\text{Re}(\xi),\text{Im}(\xi))$ . The transformation to the new coordinates  $\xi_1 \equiv \xi_{\parallel}$  and  $\xi_2 \equiv \xi_{\perp}$  is then a unitary transformation given by

$$B_{ij} = \frac{\partial x_i}{\partial \xi_j} \quad (i, j = 1, 2), \qquad \text{where} \quad B^{-1} = B^T$$
 (5.27)

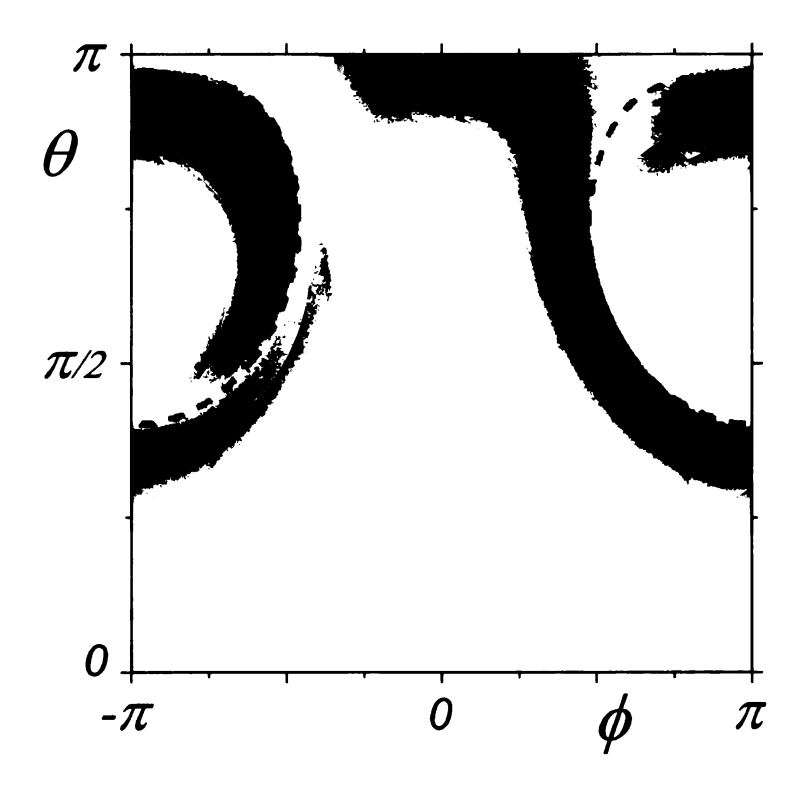


Figure 5.2: Same as in Fig. 5.1 except that here S = 30.

In the large spin limit,  $S \gg 1$ ,  $x_1$  and  $x_2$  are state variables and we know how to obtain their deterministic equations of motion (cf., for example, derivation of Eq. (5.25))

$$\frac{dx_i}{d\tau} = A_i(x_1, x_2), \qquad i = 1, 2. \tag{5.28}$$

The dynamic equations of the new variables are therefore

$$\frac{d\xi_i}{d\tau} = \sum_j \frac{\partial \xi_i}{\partial x_j} \frac{dx_i}{d\tau} = \sum_j B_{ij}^{-1} A_j = \sum_j B_{ji} A_j, \qquad i = 1, 2.$$
 (5.29)

For motion directly on the limit cycle the first coordinate,  $\xi_{\parallel}$ , changes with velocity V along the cycle and the second coordinate is zero

$$\frac{d\xi_{\parallel}}{d\tau} = V = \sqrt{A_1^2 + A_2^2}, \qquad \xi_{\perp} = 0. \tag{5.30}$$

From Eqs. (5.27) - (5.30) we obtain the matrix elements

$$B_{11} = \frac{A_1}{V}, \quad B_{12} = -\frac{A_2}{V}, \quad B_{11} = \frac{A_2}{V}, \quad B_{22} = \frac{A_1}{V}.$$
 (5.31)

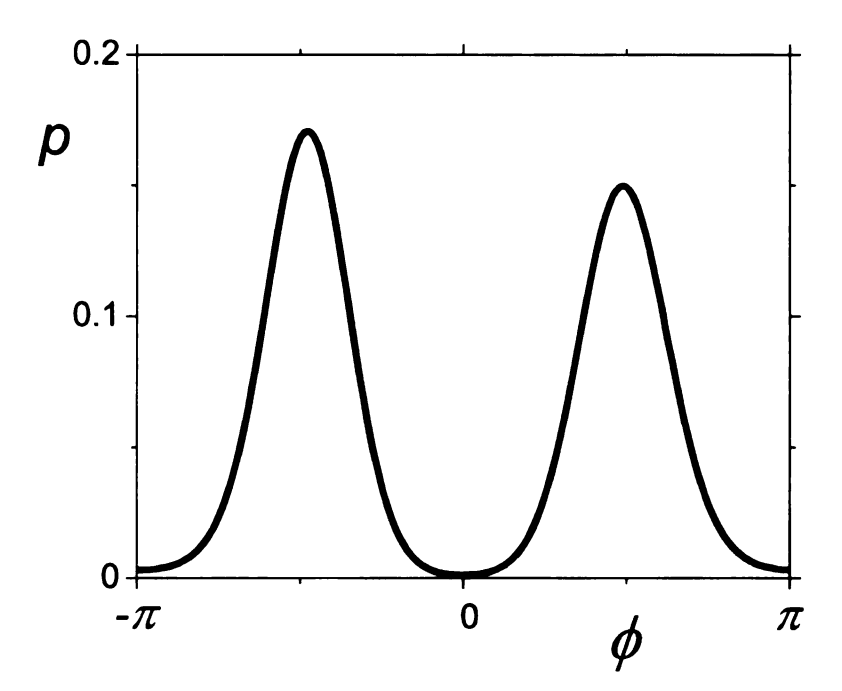


Figure 5.3: Cross section through spin density distribution,  $p_{sl}(\phi, \theta = 2)$ . S = 10,  $\Gamma^{(1)} = 0.01$ ,  $\Gamma^{(2)} = \Gamma^{(3)} = 0$ ,  $\mu = 0.6$ , and f = 0.4. The two peaks have the shape of a normal distribution.

In a close vicinity to the limit cycle,  $|\xi_{\perp}|$  is small and we can approximate  $d\xi_{\perp}/d\tau$  by a term that is proportional to  $\xi_{\perp}$ . To calculate this term we carry out the following Taylor expansion:

$$\frac{d\xi_{\perp}}{d\tau} = \sum_{j=1,2} B_{j,2} A_j = \sum_{j=1,2} B_{j,2} \frac{\partial A_j}{\partial \xi_{\perp}} \xi_{\perp} = \sum_{j,l=1,2} B_{j,2} B_{l,2} \frac{\partial A_j}{\partial x_l} \xi_{\perp}, \tag{5.32}$$

where the derivatives are evaluated on the limit cycle. Therefore,

$$\frac{d\xi_{\perp}}{d\tau} = -L\xi_{\perp},\tag{5.33}$$

where

$$L = -\sum_{j,l=1,2} B_{j,2} B_{l,2} \frac{\partial A_j}{\partial x_l}.$$
 (5.34)

The system's master equation (C.2) which has the schematic form of

$$\dot{p} = A_0 p - \sum_{i=1,2} A_i \frac{\partial p}{\partial x_i} + O(1/S)$$
(5.35)

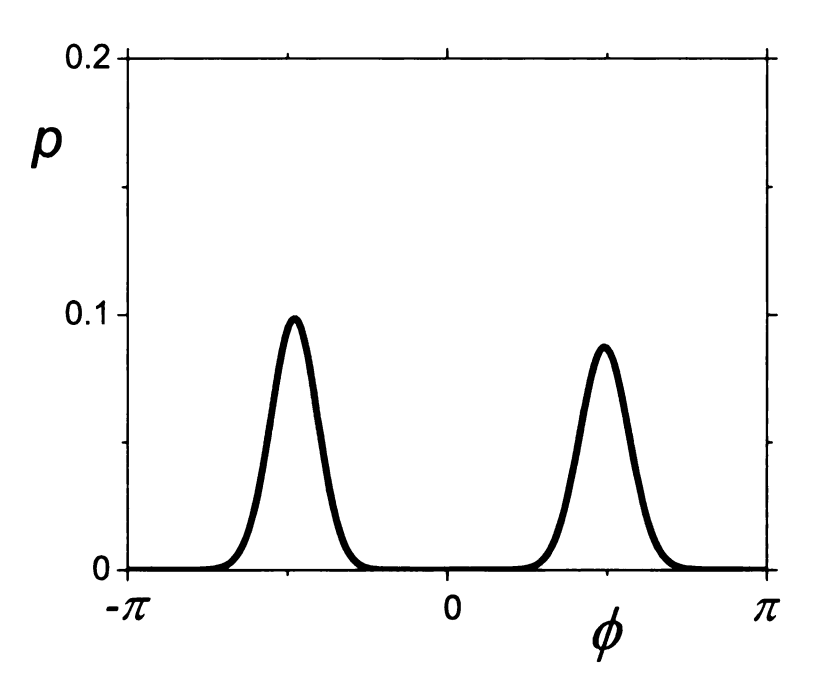


Figure 5.4: Same as in Fig. 5.3 except that here S=30. The peaks are smaller in width and height by a factor of  $\sqrt{3}$  than those in Fig. 5.3.

can now be expressed in  $\xi_{\parallel}$  and  $\xi_{\perp}$  coordinates for small values of  $|\xi_{\perp}|$  and brought into the form

$$\dot{p} = A_0 p - V \frac{\partial p}{\partial \xi_{\parallel}} + L \xi_{\perp} \frac{\partial p}{\partial \xi_{\perp}} + O(1/S)$$
(5.36)

The solution of

$$\dot{p} = 0 \tag{5.37}$$

is the spin density distribution of the system in the stationary limit,  $p_{st}$ . If terms of order 1/S and higher are disregarded Eq. (5.37) leads, in the vicinity of the limit cycle, to a delta function that is zero everywhere but on the limit cycle itself. Quantum corrections, i.e. terms proportional to powers of 1/S in (5.37), include higher order derivatives of p which lead to a smearing of the delta function. Applying the general theory that has been developed in [88], one sees that the delta function becomes a distribution that is maximal on the limit cycle. Its cross section perpendicular to

the cycle has a Gaussian peak which has a width that scales as  $1/\sqrt{S}$ . These results are illustrated in Fig. 5.1-5.4 where  $p_{st}$  is plotted as a function of  $\theta$  and  $\phi$  for two different sizes of the spin system, S=10 and S=30. The graphs show clearly that the maximum of the distribution coincides with the location of the classical limit cycle. Fig. 5.3 and 5.4 display the cross sections  $p_{st}$  ( $\phi$ ,  $\theta=2$ ), for the cases S=10 and S=30 respectively. Indeed, these are normal distributions and the width of the Gaussian peak of the spin 10 system is  $\sqrt{30/10}=\sqrt{3}$  times larger than the width of the normal distribution of the spin 30 system.

# 5.3 The stationary limit of modulated large-spin systems

We will now show that an almost resonantly driven large spin system can, even at zero temperature and in the absence of tunneling, switch from a metastable to a globally stable state. We will see that this feature is due to the mechanism of quantum activation.

For not too large values of the relaxation parameter, the system can be conveniently described in its quasienergy representation. There, relaxation is described by transitions between nearest and next nearest quasienergy levels. As explained in chapter 3, in the semiclassical limit, quasienergy levels correspond to contours on the quasienergy surface which are orbits of motion in the limit of zero damping. Therefore, in addition to the spin coherent state representation also the quasienergy representation of the system is very suitable to investigate the quantum to classical transition of a modulated large spin.

# 5.3.1 The stationary distribution in the quasienergy representation

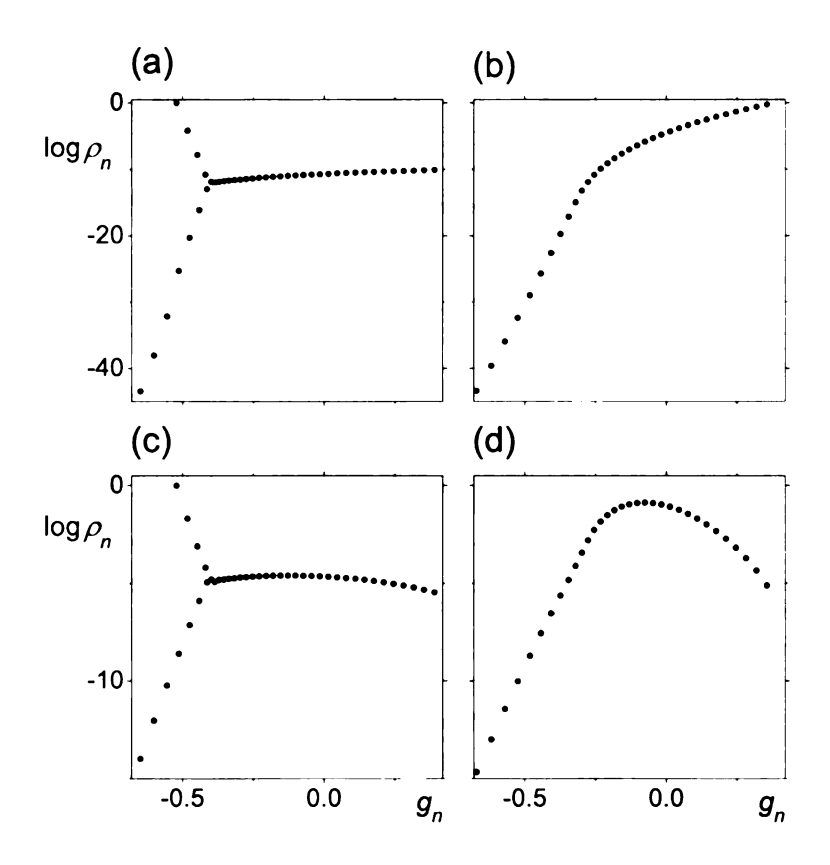


Figure 5.5: Stationary distribution over quasienergy levels,  $\rho_n = \langle n|\rho_{st}|n\rangle$ , as a function of quasienergy,  $\langle n|\hat{g}|n\rangle$ , for f=0.4 in the weak damping limit for S=20 and T=0. In panels (a),(c) and (b),(d) it is  $\mu=0.07,0.5$ , respectively. In panels (a) and (b)  $\Gamma^{(1)}=\Gamma^{(2)}=0$ ,  $\Gamma^{(3)}\to 0$  and in panel (c) and (d) it is  $\Gamma^{(1)}\to 0$ ,  $\Gamma^{(2)}=\Gamma^{(3)}=0$ . In panel (a) the position of the globally stable state corresponds to the position of the local minimum in g. The maximum of g coincides with the metastable state of the system. In panel (b) the system has only one stable state which corresponds to the maximum of g. Panel (c) shows the emerging metastable limit cycle. In panel (d) the maximum of the distribution corresponds to the position of the classical limit cycle. In panel (a) and (c) the position of the classical saddle point coincides with the position where the two quasienergy branches meet each other.

In chapter 3 we calculated the distance between quasienergy levels,  $\Omega_{m,m+1} \equiv \Omega(g)$  of the spin. To analyze the stationary distribution of the system we start with the case where relaxation is slow so that the broadening of quasienergy levels is much

smaller than the distance between them,  $\Gamma \ll \Omega$ . Then off-diagonal matrix elements of  $\rho$  in the basis of quasienergy states  $|m\rangle$  are small. We note that, at the same time, off-diagonal matrix elements of  $\rho$  in the basis of Zeeman spin states in the laboratory frame do not have to be small.

To the lowest order in  $\Gamma/\Omega$  relaxation of the diagonal matrix elements  $\rho_m \equiv \langle m|\rho|m\rangle$  is described by the balance equation

$$\frac{\partial \rho_m}{\partial \tau} = -2\Gamma \sum_{m'} \left( W_{mm'} \rho_m - W_{m'm} \rho_{m'} \right) \tag{5.38}$$

with the dimensionless transition probabilities

$$W_{mm'} = (\bar{n} + 1) \left| \left\langle m' \middle| S_{-} \middle| m \right\rangle \right|^{2} + \bar{n} \left| \left\langle m \middle| S_{-} \middle| m' \right\rangle \right|^{2}. \tag{5.39}$$

From the explicit expression of  $W_{mm'}$  and in accordance with the semiclassical results in chapter 4, it follows that, even for T=0, the spin can make transitions to states with both higher and lower quasienergy g, with probabilities  $W_{mm'}$ , where m'>m and m'< m, respectively.

Depending on the values of the driving field strength, f, and the detuning,  $\mu$ , the probability of a transition to a lower level of g is either larger or smaller than the probability of a transition to a higher level, that is,  $W_{n'n} > W_{nn'}$  or  $W_{n'n} < W_{nn'}$  for n' > n, respectively. This agrees with the classical limit in the underdamped regime in which the stable states of a modulated large spin can be both in minima and maxima of the quasienergy surface  $g(\phi,\theta)$  or, in the case of limit cycles, even somewhere in between. However, along with the drift down or up the quasienergy g, even for T=0, there is also diffusion over quasienergy away from the stable states on g, due to nonzero transition probabilities  $W_{n,n'}$  with n' > n. This diffusion leads to a quasienergy distribution which has maxima at stable points or stable limit cycles on g and falls of rapidly if moved away from them. In the range of multistability,

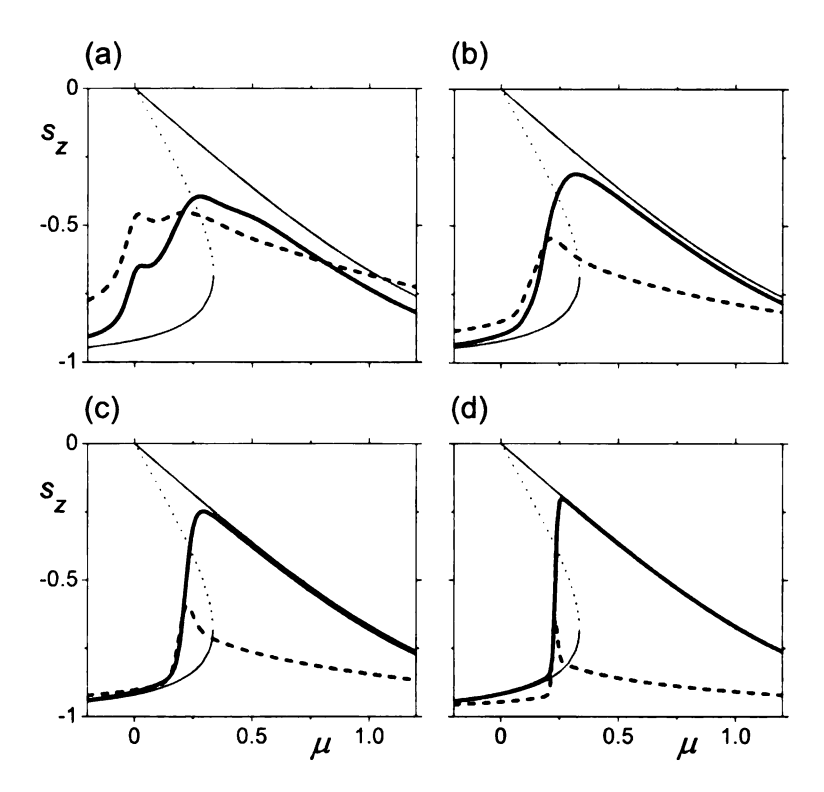


Figure 5.6: Hysteresis of the magnetization for different values of S and T=0. The thick solid line shows the normalized expectation value,  $\langle S_z \rangle / S$ , as a function of the detuning parameter,  $\mu$ , for the system in the stationary limit for f=0.4 and  $\Gamma^{(1)}=\Gamma^{(2)}=0, \Gamma^{(3)}=0.1$ . Thin solid lines show the position of classically stable states (cf. Fig. 4.3). The dashed thick line shows the uncertainty in the magnetization,  $\sqrt{\langle S_z^2 \rangle - \langle S_z \rangle^2}/S-1$ . In panels (a)-(d) it is S=2,5,10,30, respectively. In the range where the system switches between the two stable states the uncertainty in  $S_z$  has a peak. The width of the transition region depends sensitively on S.

generally, only one of the stable states is predominantly occupied. This state plays the role of the globally stable state, all other maxima in the quasienergy distribution correspond to metastable states.

In order to analyze the stationary limit in the case of finite damping the full master equation 5.14 needs to be solved:

$$\dot{\rho} = 0. \tag{5.40}$$

Fig. 5.5 shows examples of the quasienergy distribution for the cases of relaxation

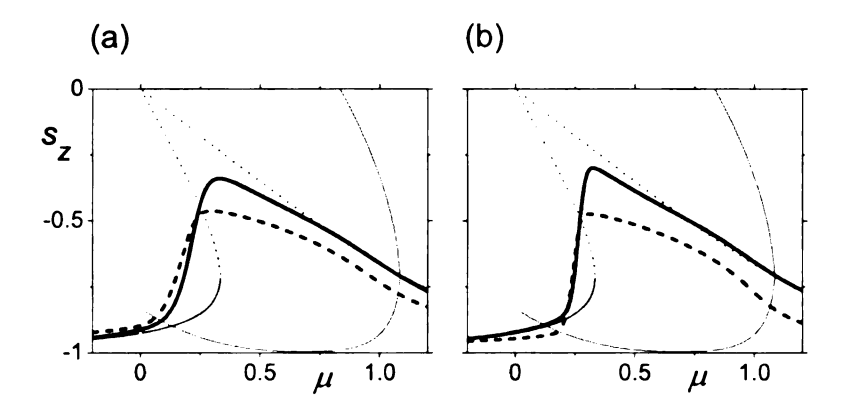


Figure 5.7: Hysteresis of the magnetization for different values of S in the presence of limit cycles. T=0. The thick solid line shows the normalized expectation value,  $\langle S_z \rangle / S$ , as a function of the detuning parameter,  $\mu$ , for the system in the stationary limit for f=0.4 and  $\Gamma^{(1)}=0.05$ ,  $\Gamma^{(2)}=\Gamma^{(3)}=0$ . Thin solid lines show the position of classically stable states (cf. Fig. 4.8). The dashed thick line shows the uncertainty in the magnetization,  $\sqrt{\langle S_z^2 \rangle - \langle S_z \rangle^2}/S - 1$ . In panels (a) and (b) it is S=10 and S=30, respectively. There where the system changes from a stable fixed point to a stable limit cycle a step in the uncertainty in  $S_z$  can be observed.

of type  $\Gamma^{(1)}$  and  $\Gamma^{(3)}$ , respectively. From there it can be seen that the distribution coincides with the positions of stable stationary states in the semiclassical limit.

It can be seen that while the distribution falls off exponentially in the vicinity of stable fixed points it only falls off subexponentially in the vicinity of limit cycles.

If the parameter pair  $(\mu, f)$  is located inside the astroid curve the quasienergy surface, g, has a separate well which is connected to the rest of the system via a saddle point (cf. Fig. 3.5 and chapter 4.3.2). In the zero damping limit, contours on g inside and outside the well correspond to different states. In the quantum regime, in the stationary limit, levels inside the well around the stable state at the minimum of the well are much stronger populated than levels with the same quasienergy outside the well.

#### 5.3.2 Switching and hysteresis

If the system is in the basin of attraction of a metastable state it will first decay towards this state on the time scale of the relaxation time,  $1/\Gamma$ . Quantum diffusion over quasienergy described by Eq. (5.38) eventually leads to switching to the globally stable state of the spin. The switching rate  $W_{\rm sw}$  is determined by the probability to reach the top of the barrier which is located at the boundary of the basin of attraction, i.e. the saddle point of  $g(\phi, \theta)$ .

$$W_{\rm sw} = C_{\rm sw} \times \exp\left(-S\,R_A\right) \tag{5.41}$$

The parameter  $C_{\rm sw}$  is of the order of the relaxation rate  $\Gamma$ .  $R_A$  plays the role of the activation energy of escape in the process of quantum activation. It originates from quantum fluctuations that accompany relaxation of the spin. Note that  $R_A$  is not the difference in quasienergies but the difference of the logarithms of populations of the metastable state and the state close to the classical saddle point.

For large enough values of the relaxation rate,  $\Gamma$ , the switching between stable states occurs via quantum activation and not via tunneling. Because of this fact the dynamics for a modulated large spin is fundamentally different of the dynamics of a large spin in a static magnetic field where tunneling and thermal activation play the major role.

There are narrow parameter ranges where there occurs switching from one globally stable state to another. These parameter ranges are analogs of first order phase transitions. In Fig. 5.6 and 5.7 it can be seen that these transitions are sharp even for comparatively small values of S. If the detuning parameter,  $\mu$ , is swept non-adiabatically through this region one can observe hysteresis in the magnetization of the spin. Fig. 5.8 shows the spin density distribution of the system in a case where

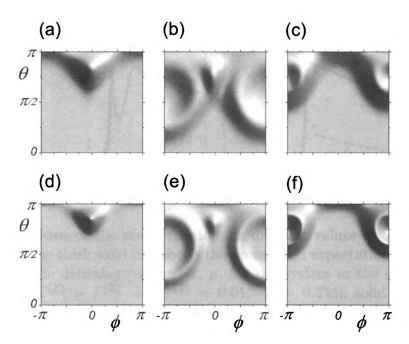


Figure 5.8: Switching in the presence of hysteresis. Panels (a)-(c) and (d)-(f) show the spin density distribution for S=10 and S=30, respectively. For all panels T=0, f=0.4 and  $\Gamma^{(1)}=0.01$ ,  $\Gamma^{(2)}=\Gamma^{(3)}=0$ . In panels (a) and (d), (b) and (e), (c) and (f) the detuning has the value of  $\mu=0.1,0.23$ , and 1.0, respectively. In panel (a) and (b) the system is inside the Stoner-Wohlfarth astroid where there are two classical stable solutions. The dominant stable branch in panel (a) is a fixed point centered roughly at  $\phi=0$ . In panel (b) the system is in its switching region; the second metastable stable branch in form of a limit cycle becomes populated and the population of the fixed point is reduced. In panel (c) the system is outside the astroid; the limit cycle remains as the only stable solution. It has a relatively small radius because the system is close to the Hopf bifurcation where the limit cycle transforms into a fixed point.

both stable states are nearly equally populated.

For small spin systems quantum tunneling effects become prominent. In Fig. 5.9 the hysteresis of a spin 10 system is compared for two different values of the relaxation parameter,  $\Gamma^{(3)}$ . Close to multiphoton resonance, if the relaxation parameter becomes of the order of the multiphoton Rabi splitting (3.4),  $\Omega_R$ , tunneling effects play a dominant role. They are expressed as sharp spikes in in the hysteresis curve. The width of the spikes depends sensitively on the order of the multiphoton resonance.

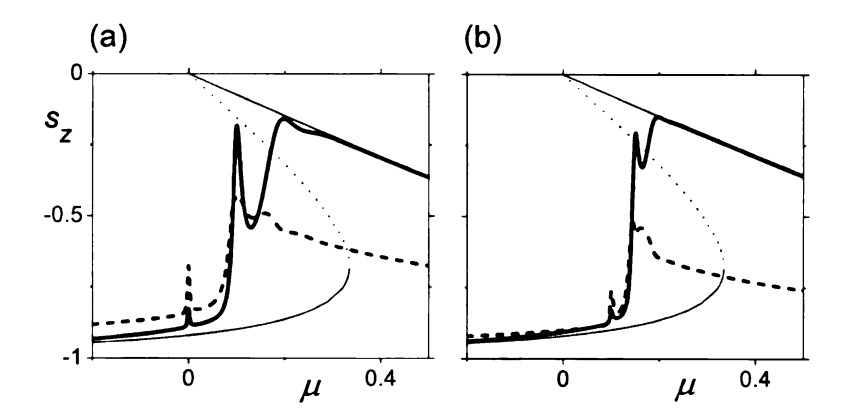
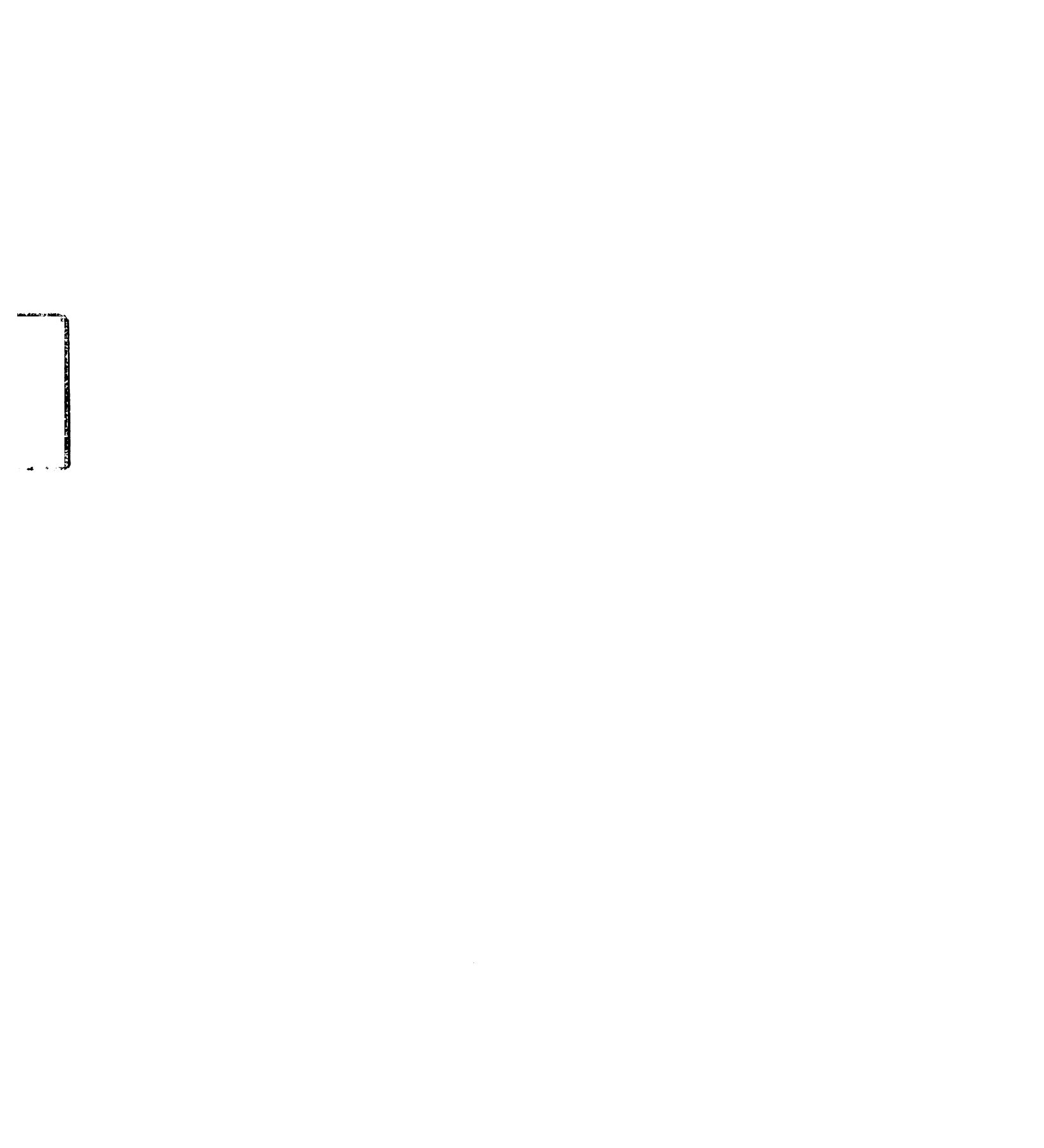


Figure 5.9: Hysteresis of the magnetization for different values of S in the case of small damping. The thick solid line shows the normalized expectation value,  $\langle S_z \rangle / S$ , as a function of the detuning parameter,  $\mu$ , for the system in the stationary limit for f=0.4 and  $\Gamma^{(1)}=\Gamma^{(2)}=0$ ,  $\Gamma^{(3)}=0.01$ . T=0.Thin solid lines show the position of classically stable states (cf. Fig. 4.3). The dashed thick line shows the uncertainty in the magnetization,  $\sqrt{\langle S_z^2 \rangle - \langle S_z \rangle^2}/S - 1$ . In panels (a) and (b) it is S=5 and S=10, respectively. Close to multiphoton resonances tunneling effects become prominent. There, the system forms superpositions of states inside and outside the well of the quasienergy surface g. As a consequence, the magnetization and its standard deviation display peaks.

### 5.3.3 Uniform distribution of quasienergy levels and nonhysteretic switching

Another interesting feature of the quasienergy distribution can be seen at the symmetry line  $\mu = 0$ . There the distribution is uniform in a range of quasienergy states which correspond to the part of phase space where in the semiclassical limit a Hamiltonian-like behavior can be observed (cf. chapter 4.4). Fig. 5.10b and 5.10d show such distributions in the region of monostability and bistability, respectively.

As shown in chapter 4.5.2, for  $\mu = 0$  and for values of the driving strength f outside the astroid region, there occurs non-hysteretic switching between two different solution branches. Quantum corrections, similar to the case of hysteretic switching, lead to a narrow parameter range where the two different branches of classical so-



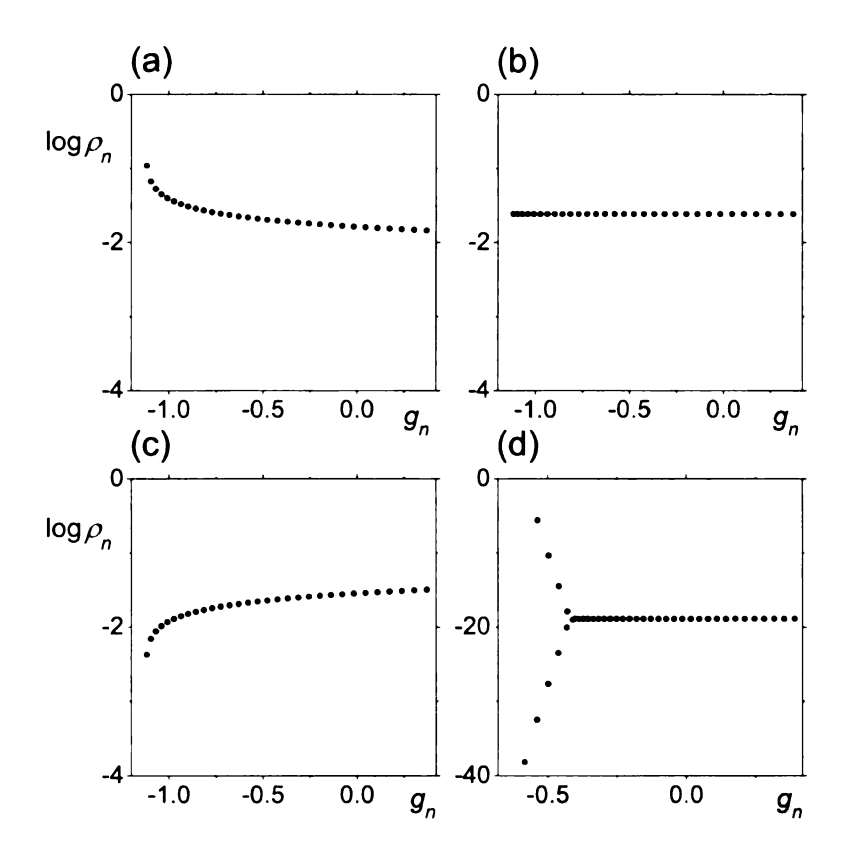


Figure 5.10: Stationary distribution over quasienergy levels,  $\rho_n = \langle n|\rho_{st}|n\rangle$ , as a function of quasienergy,  $\langle n|\hat{g}|n\rangle$ , in the weak damping limit,  $\Gamma^{(1)} = \Gamma^{(2)} = 0$ ,  $\Gamma^{(3)} \to 0$ , for S=20 and T=0. In panels (a)-(d) it is  $\mu=-0.01,0,0.01,0.001$ , respectively. In panels (a)-(c) it is f=1.1 whereas in panel (d) it is f=0.4. Panels (a)-(c) show non-hysterestic switching from one stable state to another. Panels (b) and (d) show a completely or partially flat distribution which corresponds to the part of the quasienergy surface g where the system displays Hamiltonian-like motion in the semiclassical limit, i.e. either over the whole phase plane as in panel (b) or from the maximum in g down to the saddle as in panel (d). In panel (d)  $\mu=0.001$  instead of  $\mu=0$  was chosen in order to avoid multiphoton resonance.

lutions have almost equal population. However, as shown in Fig. 5.10 for any given value of the detuning, there is only one maximum in the quasienergy distribution, hence only one stable state. This is made possible by the symmetry at  $\mu=0$ , where the distribution is completely uniform. Fig. 5.11 shows such a non-hysteretic switching for a component of the spin that is perpendicular to the magnetization axis. In Fig. 5.12 the switching is illustrated by plots of the spin density distribution.

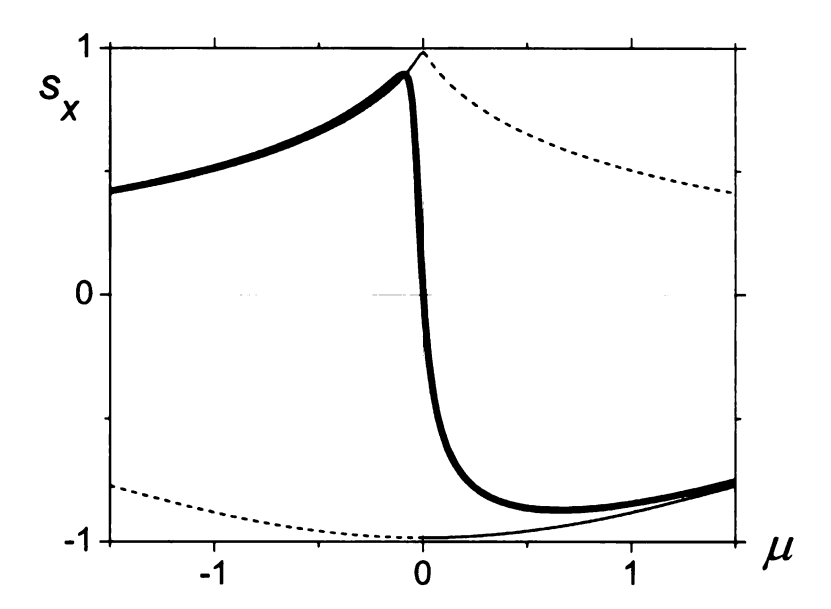


Figure 5.11: Switching in the absence of hysteresis. The thick solid line shows the normalized expectation value of the transverse magnetization in the rotating frame,  $\langle S_x \rangle / S$  as a function of the detuning parameter,  $\mu$ , for the system in the stationary limit for S=10, f=1.1 and  $\Gamma^{(1)}=\Gamma^{(2)}=0$ ,  $\Gamma^{(3)}=0.1$ . T=0. Thin solid and dashed lines show the position of classical stable and unstable states, respectively. The spin switches between the two states within a finite transition region.

### 5.4 Conclusions

In the representation of spin coherent states the state of a modulated large-spin system in the rotating wave approximation can be expressed in terms of its spin density distribution which is the expectation value of the system to be in a given spin coherent state which by itself is represented by a point on the surface of a sphere with integer or half integer radius S. Since in the large spin limit the spin density distribution becomes the classical statistical probability distribution of the system it is well suited for analyzing the transition of the spin from the quantum to the semiclassical regime. The inverse size of the spin, 1/S, plays the role of an effective Planck number which controls the "quantumness" of the system.

As an example we analyzed the role of quantum corrections for the case where

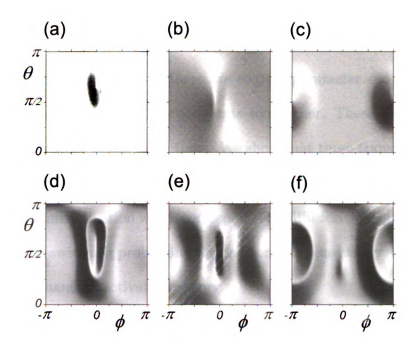


Figure 5.12: Switching in the absence of hysteresis. Panels (a)-(c) and (d)-(f) show the stationary spin density distribution for  $\Gamma(1) = \Gamma(2) = 0$ ,  $\Gamma(3) = 0.01$  and  $\Gamma(1) = 0.01$ ,  $\Gamma(2) = \Gamma(3) = 0$ , respectively. T = 0. In all panels S = 30 and f = 1.1, hence the system lies outside astroid where no coexisting stable solutions exist. In panels (a) and (d), (b) and (e), (c) and (f) the detuning has the value of  $\mu = -0.1$ , 0, and 0.1, respectively. Classically, the stable solutions in panels (a) and (d) abruptly switch to another branch at  $\mu = 0$ . In the quantum regime the sharp switching line is smeared out as can be seen from panels (b) and (e). Note that in panels (b) and (e) the system is in its Hamiltonian-like state.

the system's classical motion is along a limit cycle. We showed that in the quantum regime the spin density distribution displays a crater shaped ring with its maximum coinciding with the position of the classical limit cycle. This stationary behavior is a consequence of the diffusion of the system due to quantum fluctuations. The uncertainty property of the quantum system is manifested in a cross section of the spin density distribution that has a Gaussian peak with a width that scales as  $1/\sqrt{S}$ .

To analyze the system's stationary limit it is convenient to determine its quasienergy level distribution. In the zero damping limit, this can easily be done by solving the balance equation. We showed that the distribution coincides with the positions of stable stationary states in the semiclassical limit. The analysis has shown that in the range of multistability, generally, only one of the stable states is predominantly occupied. However, there are narrow parameter ranges where there occurs switching from one globally stable state to another. These parameter ranges are analogs of first order phase transitions. We show that these transitions are sharp even for comparatively small values of S. We established that the method of interstate switching is quantum activation which corresponds to diffusion over quasienergy levels and found that the switching probability depends on S exponentially as  $\exp\{-SR_A\}$ , where  $R_A$  is the quantum activation energy.

We demonstrated that switching in the absence of hysteresis also occurs within a sharp transition range where the two different branches of classical solutions are almost equally strongly occupied. However, here, in contrast to hysteretic switching the quasienergy distribution exhibits only one maximum for any given value of the detuning parameter.

We showed that the semiclassical feature of Hamiltonian-like behavior of a part of phase space corresponds to a flat distribution of the respective quasienergy levels.

It is interesting to note that the effect of quantum activation only requires the generic property of a system to have an almost equidistant energy spectrum where transitions to neighboring levels are caused by emission and absorption of quanta to and from the environment and pumping to higher levels is caused by an almost resonant radiation source. Because of that it is that large modulated spins behave similarly to oscillators where quantum activation has previously been observed [55, 56]. However, important differences between modulated large-spin systems and oscillators remain. Both systems follow different Lie algebras and have different symmetry properties. In contrast to the oscillator the spin has finite dimensionality and undergoes

different relaxation mechanisms. In summary, this leads to differentiating features of the spin such as limit cycles, Hamiltonian-like dynamics, multistability, and non-hysteretic switching. Interestingly, the classical character of these features is visible already for comparatively small spin systems,  $S \gtrsim 3$ .

## Chapter 6

### **Conclusions**

We have studied nonlinear resonant phenomena in two-level and multilevel quantum systems. We showed that modulated multilevel systems display new coherent and incoherent effects hat can be observed with currently available experimental techniques. The results bear on quantum control, quantum computation, and quantum measurement.

We have developed a theory of quantum gates based on Landau-Zener (LZ) pulses. In these pulses the control dc field is varied in such a way that the qubit frequency passes through the frequency of an external radiation field. We showed that an LZ gate can be expressed in a simple explicit form in terms of rotation matrices. LZ pulses allow one to implement arbitrary single qubit gate operations. One of our central results is that already a sequence of three LZ pulses can be made fault-tolerant. The duration of this error compensating pulse sequence is about 4 times the duration of the single pulse and the error of the corresponding gate  $\mathcal{E}$  scales with the error  $\varepsilon$  in the qubit energy or radiation frequency at least as  $\varepsilon^3$ . This is parametrically better than in the case of standard error compensating pulse

sequences where the gate error scales as  $\varepsilon^2$ . For typical values of frequency offsets LZ gates have errors that are at least  $10^4$  times smaller than those of conventional fault-tolerant on-resonance gates.

We have developed a microscopic theory of a resonantly modulated large spin in a strong static magnetic field. We studied coherent quantum effects, which occur on times smaller than the relaxation time, as well as the stationary and quasistationary behavior in the presence of of dissipation. We analyzed the dynamics of a large-spin system in the semiclassical limit and established a picture of the quantum to classical transition in such type of systems.

In our analysis we concentrated on the important case of a large spin with an easy axis anisotropy, where the anisotropy energy is of the form  $-DS_z^2/2$ . This is characteristic of large nuclear spins and molecular magnets. We considered the standard geometry where a static magnetic field is applied along the easy axis whereas an ac field points in the transverse direction. The ac field frequency  $\omega_F$  is close to the Larmor frequency  $\omega_0$ .

For the case where the system can be regarded as being isolated from its environment we studied the coherent resonant response of the spin.

At multiphoton resonance, in the weak-modulation limit, the quasienergies of the resonating Zeeman states cross. We found that this is also true for the susceptibilities in these states. Such crossing occurs simultaneously for several pairs of Zeeman states. Resonant multiphoton transitions lift the degeneracy of quasienergy levels, leading to level anticrossing. In contrast, near resonance, the susceptibilities as functions of frequency display spikes. The spikes of the susceptibilities point in opposite

directions, leading to a decrease (antiresonance) or an increase (resonance) of the response. They have a profoundly non-Lorentzian shape with width and height that strongly depend on the driving field amplitude A. The spikes can be observed by adiabatically sweeping the modulation frequency through a multiphoton resonance.

We showed that this effect is nonperturbative in A, it is due to a special conformal property of the classical spin dynamics. Our results bear also on the dynamics of molecular magnets in a static magnetic field and provide an explanation of a number of experiments that have been done on such systems but remained unexplained.

For the case where the system is coupled to an environment we have taken into account relaxation processes important for large-spin systems of current interest. They correspond to transitions between neighboring and next-neighboring Zeeman levels with emission or absorption of excitations of a bosonic thermal bath. Starting from the microscopic model we derived the quantum kinetic equation. This equation is simplified in the semiclassical limit, leading to classical equations of motion of the modulated spin. We showed that the classical spin dynamics depends strongly on the interrelation between the rates of different relaxation processes. Although one of the coupling mechanisms that we discuss leads formally to the Landau-Lifshitz equation for magnetization dynamics in the rotating frame, generally the dynamics in the rotating frame is not described by the Landau-Lifshitz damping.

We found that the spin dynamics has special symmetry at exact resonance where the modulation frequency is equal to the Larmor frequency,  $\omega_F = \omega_0$ . This symmetry leads to a Hamiltonian-like behavior even in the presence of dissipation. In the rotating frame, phase trajectories of the spin form closed loops in a part of or on the whole phase plane. Therefore when when  $\omega_F$  goes through  $\omega_0$  several states change

stability at a time. The simultaneous stability change leads to unusual observable features. Where the system has only one stable state for a given parameter value, as as  $\omega_F$  goes through  $\omega_0$  the state changes discontinuously, leading to an abrupt change of the transverse magnetization.

We found the conditions where the spin has more than one stable stationary state in the rotating frame. Such stable states correspond to oscillations of the transverse magnetization at the driving frequency in the laboratory frame. Multistability leads to magnetization hysteresis with varying parameters of the modulating field. If the fastest relaxation process is transitions between neighboring states due to coupling quadratic in spin operators, the resonantly modulated spin can have periodic nonsinusoidal states in the rotating frame with frequency  $\propto DS/\hbar$ , where D is the anisotropy energy. They are described by limit cycles on the spin phase plane in the rotating frame. In the laboratory frame, these states correspond to oscillations of the transverse magnetization at combinations of the limit-cycle frequency, its overtones, and the Larmor frequency.

In order to extend the analysis from the semiclassical limit to the full quantum regime and describe the effects of quantum fluctuations we developed a formalism which allows us to transform the system's quantum kinetic operator equation into a partial differential equation of motion of the system's probability density distribution in the spin coherent state representation. The spin density distribution is the expectation value of the system to be in a given spin coherent state which by itself is represented by a point on the surface of a sphere with radius S. In the large spin limit this probability density goes over into the classical statistical probability distribution of the system.

Spin coherent states are particularly convenient for the analysis of the quantum analog of a classical limit cycle. There, the spin density distribution displays a crater shaped ring with its maximum coinciding with the position of the limit cycle. The cross section of the spin density distribution has a Gaussian peak and the width of the peak scales as  $1/\sqrt{S}$ .

We showed that the full stationary distribution of the system has peaks at the positions of stable stationary states in the semiclassical limit. The analysis demonstrates that in the range of multistability, generally, only one of the stable states is predominantly occupied. However, there are narrow parameter ranges where there occurs switching from one stable state to another. These parameter ranges are analogs of first order phase transitions. We showed that these transitions are sharp even for comparatively small values of S. We established that the mechanism of interstate switching is quantum activation which corresponds to diffusion over quasienergy levels. The switching probability depends on S exponentially as  $\exp\{-SR_A\}$ , where  $R_A$  is the quantum activation energy.

We found that switching in the absence of hysteresis also occurs within a narrow transition range. However, here, in contrast to switching in the region where there are two or more classically stable states the quasienergy distribution exhibits only one maximum for any given value of the detuning parameter. We showed that the semiclassical feature of Hamiltonian-like behavior of a part of phase space corresponds to a flat distribution over the respective quasienergy levels.

APPENDICES

### Appendix A

# Symmetry of classical spin dynamics: a feature of the conformal mapping

Classical equations of motion for the spin components (3.13) can be solved in the explicit form, taking into account that  $s^2 = 1$  and that  $g(\theta, \phi) = \text{const}$  on a classical trajectory. For time evolution of the z-component of the spin we obtain

$$s_z(\tau) = \frac{r_2(r_1 - r_3) - r_3(r_1 - r_2)\operatorname{sn}^2(u; m_J)}{r_1 - r_3 - (r_1 - r_2)\operatorname{sn}^2(u; m_J)}$$
(A.1)

where  $r_1 > r_2 > r_3 > r_4$  are the roots of the equation

$$[(r+\mu)^2 + 2g]^2 + 4f^2(r^2 - 1) = 0$$
(A.2)

and  $\operatorname{sn}(u;m_J)$  is the Jacobi elliptic function. The argument u and the parameter  $m_J$  are

$$u = \tilde{\omega}\tau, \qquad \tilde{\omega} = \frac{1}{4} \left[ (r_1 - r_3)(r_2 - r_4) \right]^{1/2},$$
  

$$m_J = (r_1 - r_2)(r_3 - r_4)/(r_1 - r_3)(r_2 - r_4), \qquad (A.3)$$

Equation (A.1) describes an orbit which, for a given g, oscillates between  $s_z = r_1$  and  $s_z = r_2$ ; the corresponding oscillations of  $s_x$ ,  $s_y$  can be easily found from Eqs. (3.13), (3.14).

Oscillations of  $s_z$  between  $r_3$  and  $r_4$  for the same g are also described by Eq. (A.1) provided one replaces  $u \to u + K(m_J) + iK'(m_J)$ , where  $K(m_J)$  is the elliptic integral and  $K'(m_J) = K(1 - m_J)$ . Clearly, both types of oscillations have the same period over  $\tau$  equal to  $2K(m_J)/\tilde{\omega}$ . They correspond to the trajectories of types I and II in Fig. 3.5 that lie on different sides of  $g(\theta, \phi)$ -surface. Respectively, the vibration frequencies for the corresponding trajectories  $\omega_I(g)$  and  $\omega_{II}(g)$  are the same. This proves the first relation in Eq. (3.17).

The Jacobi elliptic functions are double periodic, and therefore  $s_z$  is also double periodic,

$$s_z(\tau) = s_z \left[ \tau + \tilde{\omega}^{-1} (2nK + 2imK') \right]$$
 (A.4)

with integer n, m. Ultimately, this is related to the fact that equations of motion (3.13) after simple transformations can be put into a form of a Schwartz-Christoffel integral that performs conformal mapping of the half-plane Im  $s_z > 0$  onto a rectangle on the u-plane. We will show now that the mapping has a special property that leads to equal period-averaged values of  $s_x(\tau)$  on trajectories of different types but with the same g. Because  $s_z(\tau)$  is double periodic, cf. Eq. (A.4), so is also the function  $s_x(\tau) = -(2f)^{-1} \left[2g + (s_z(\tau) + \mu)^2\right]$ . Keeping in mind that the transformation  $u \to u + K(m_J) + iK'(m_J)$  moves us from a trajectory with a given g of type I to a trajectory of type II, we can write the difference of the period-averaged values of  $s_x(\tau)$  on the two trajectories as

$$\langle s_x(\tau) \rangle_I - \langle s_x(\tau) \rangle_{II} = \frac{\omega(g)}{2\pi\tilde{\omega}} \oint_C s_x du$$
 (A.5)

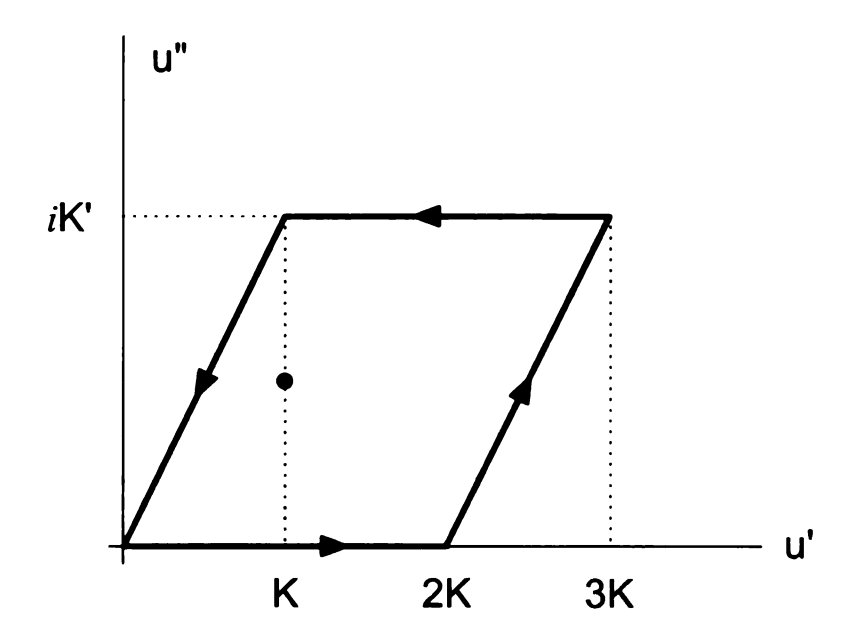


Figure A.1: The contour of integration in the  $u \propto \tau$  plane. The horizontal parts correspond to two trajectories  $\mathbf{s}(\tau)$  with the same g. The values of  $\mathbf{s}(\tau)$  on the tilted parts of the parallelogram are the same. The plot refers to  $\mu = 0.125$ , g = -0.366.

where the contour C is a parallelogram on the u-plane with vortices at 0, 2K, 3K + iK', K + iK'. It is shown in Fig. A.1.

An important property of the mapping (A.1) is that  $s_z(\tau)$  has one simple pole inside the contour C, as marked in Fig. A.1. Respectively,  $s_x(\tau)$  has a second-order pole. The explicit expression (A.1) allows one to find the corresponding residue. A somewhat cumbersome calculation shows that it is equal to zero. This shows that the period-averaged values of  $s_x$  on the trajectories with the same g coincide, thus proving the second relation in Eq. (3.17).

### Appendix B

## Energy change near a Hopf

### bifurcation

In this Appendix we outline the calculation of the relaxation of quasienergy g near a Hopf bifurcation point. For concreteness we assume that  $\Gamma^{(2)} = \Gamma^{(3)} = 0$  and the only nonzero damping parameter is  $\Gamma^{(1)}$ . For small damping a stationary state that experiences a bifurcation has phase  $\phi_H$  close to either 0 or  $\pi$ , whereas  $s_{zH} \approx \pm 2^{-1/2}$ . The dynamics is characterized by two parameters,  $\alpha = \operatorname{sgn} s_{zH}$  and  $\beta = \operatorname{sgn}[f_H \cos \phi_H]$ . The bifurcational value of the field for  $\Gamma^{(1)} \to 0$  is  $f_H = (2^{-1/2} + \alpha \mu) \cos \phi_H$  [cf. Eq. (4.24)].

At the bifurcating stationary state the quasienergy is  $g_H = g(\phi_H, s_{zH})$ ; it is easy to see that this is a local minimum of  $g(\phi, s_z)$  for  $\beta > 0$  or a maximum for  $\beta < 0$ . Respectively, on phase plane  $(\phi, s_z)$  the constant-g trajectories close to the bifurcating stationary state rotate about this state clockwise for  $\beta > 0$  and counterclockwise for  $\beta < 0$ . The angular frequency of this rotation is  $\approx 2\pi/\tau_p(g_H) = \mathcal{D}^{1/2}$ , where  $\mathcal{D}$  is given by Eq. (4.14).

We now consider dissipation-induced drift over quasienergy  $\langle \dot{g} \rangle$ . It is given by

Eq. (4.23). Noting that  $\partial_{s_z} g = \dot{\phi}$  and using the Stokes theorem we can rewrite this equation as

$$\langle \dot{g} \rangle = \beta \tau_p^{-1}(g) \int d\phi \, ds_z \mathcal{T},$$
 (B.1)

where the integral is taken over the interior of the constant-g orbit on the  $(\phi, s_z)$  plane and  $\mathcal{T} \equiv \mathcal{T}(s_z)$  is given by Eq. (4.15). At a Hopf bifurcation point  $\mathcal{T} = 0$ . Therefore  $\mathcal{T}(s_z)$  in Eq. (B.1) must be expanded in  $\delta s_z = s_z - s_{zH}$ .

It is convenient to calculate integral (B.1) by changing to integration over actionangle variables  $(I, \psi)$ , which are canonically conjugate to  $(s_z, \phi)$ , with g being the effective Hamiltonian. The angle  $\psi$  gives the phase of oscillations with given quasienergy g. The action variable  $I = (2\pi)^{-1} \oint s_z d\phi$  is related to g by the standard expression  $dI/dg = \tau_p(g)/2\pi \approx \mathcal{D}^{-1/2}$ ; we note that I becomes negative away from the stationary state for  $\beta < 0$ .

In evaluating expression (B.1) it is further convenient to start with integration over  $\psi$ . It goes from 0 to  $2\pi$  and corresponds to period averaging for a given  $I \propto \delta g = g - g_H$  (integration over I corresponds to integration over  $\delta g$ ).

If vibrations about  $(\phi_H, s_{zH})$  were harmonic, the lowest-order term in  $\delta s_z$  that would not average to zero on integration over  $\psi$  would be  $(d^2T/ds_z^2)(\delta s_z)^2/2 \propto |\delta g|$  (the derivative of  $\mathcal{T}$  is calculated at the bifurcating stationary state). However, it is easy to see that the integral over  $\psi$  of the linear in  $\delta s_z$  term in  $\mathcal{T}$  is also  $\sim \delta g$ . It can be calculated from equation of motion  $\dot{\phi} = \partial_{s_z} g$  by expanding the right-hand side to second order in  $\delta s_z$ ,  $\delta \phi$  and noting that  $\dot{\phi} = 0$ , where the overline means averaging over  $\psi$ . This gives, after some algebra,

$$\bar{\mathcal{T}} = 64\Gamma^{(1)}\alpha \left(\delta g\right) \left(2^{3/2}\beta |f_H| - 1\right)^{-2} \times \left(\beta |f_H| - 2^{1/2}\right). \tag{B.2}$$

This expression combined with Eq. (B.1) shows how the energy relaxation rate depends on the field  $f_{II}$ . It is used in Section 4.6 to establish the full bifurcation diagram.

### Appendix C

### Spin Coherent State

### Representation of the Master

### **Equation**

Eqs. (5.16) and (5.19-5.21) describe the system's master equation in the coherent state representation in the large spin limit,  $S \gg 1$ . Here, we present the full equation, including all quantum corrections, i.e. terms of order 1/S and higher.

The original operator master equation (5.14) has the form

$$\dot{\rho} = \dot{\rho}_{H_0} + \dot{\rho}_{\Gamma(1)} + \dot{\rho}_{\Gamma(2)} + \dot{\rho}_{\Gamma(3)}. \tag{C.1}$$

Switching to the coherent state representation leads to the partial differential equation

$$\dot{p} = \langle \xi | \dot{\rho} | \xi \rangle = \dot{p}_{H_0} + \dot{p}_{\Gamma(1)} + \dot{p}_{\Gamma(2)} + \dot{p}_{\Gamma(3)},$$
 (C.2)

where  $p = p(\xi, \xi^*, t)$ ,  $\dot{p} \equiv \frac{\partial p}{\partial \tau}$ , and

$$\dot{p}_{H_0} = i \left( \left( \mu - \frac{1}{2S} + \frac{1 - \xi \xi^*}{1 + \xi \xi^*} \right) \xi + \frac{f}{2} \left( \xi^2 - 1 \right) \right) \frac{\partial p}{\partial \xi} - i \frac{\xi^2}{2S} \frac{\partial^2 p}{\partial \xi^2} + c.c. \tag{C.3}$$

$$\begin{split} \dot{p}_{\Gamma(1)} &= -\Gamma^{(1)} \sum_{0 \leq i+j \leq 4} J_{i,j} \frac{\partial^{i+j}}{\partial \xi^{i} \partial (\xi^{*})^{j}} p \\ J_{0,0} &= \frac{4(2S-1)(1-\xi\xi^{*})(\xi\xi^{*}(14-\xi\xi^{*})-1+2S(1+\xi\xi^{*}(\xi\xi^{*}-6)))}{S^{2}(1+\xi\xi^{*})^{3}} \\ J_{1,0} &= \frac{2\xi(4S^{3}(\xi\xi^{*}-1)^{2}-9(1+\xi\xi^{*})^{2}-8S^{2}(\xi\xi^{*}-3)(3\xi\xi^{*}-1))}{S^{3}(1+\xi\xi^{*})^{2}} \\ &\quad + \frac{2\xi(29-\xi\xi^{*}(50+19\xi\xi^{*}))}{S^{2}(1+\xi\xi^{*})^{2}} \\ J_{1,1} &= -\frac{2(\xi\xi^{*})^{2}(4S^{2}(\xi\xi^{*}-3)^{2}+9(1+\xi\xi^{*})^{2}+4S(\xi\xi^{*}(2+3\xi\xi^{*})-9))}{S^{3}(1+\xi\xi^{*})^{2}} \\ J_{2,0} &= -\frac{\xi^{2}(57(1+\xi\xi^{*})^{2}+4S^{2}(5+\xi\xi^{*}(\xi\xi^{*}-10))+4S(\xi\xi^{*}(8+19\xi\xi^{*})-19))}{S^{3}(1+\xi\xi^{*})^{2}} \\ J_{2,1} &= -\frac{4\xi^{3}(\xi^{*})^{2}(3+3\xi\xi^{*}+2S(\xi\xi^{*}-3))}{S^{3}(1+\xi\xi^{*})} \\ J_{2,2} &= -\frac{8(\xi\xi^{*})^{3}}{S^{3}} \\ J_{3,0} &= \frac{16\xi^{3}(S-2-(2+S)\xi\xi^{*})}{S^{3}(1+\xi\xi^{*})} \\ J_{3,1} &= 0 \\ J_{4,0} &= -\frac{4\xi^{4}}{S^{3}} \\ J_{i,j} &= J_{j,i}^{*} \end{split}$$

$$\dot{p}_{\Gamma(2)} = -\Gamma^{(2)} \sum_{0 \le i+j \le 4} K_{i,j} \frac{\partial^{i+j}}{\partial \xi^{i} \partial (\xi^{*})^{j}} p \qquad (C.5)$$

$$K_{0.0} = \frac{8(2S-1)(1-\xi\xi^{*})(1-\xi\xi^{*}(2-4S-\xi\xi^{*}))}{S^{2}(1+\xi\xi^{*})^{3}}$$

$$K_{1.0} = \frac{4\xi(3+4S(S-2)+(6+2S(4+S(2S-9)))\xi\xi^{*}+3(1+S+2S^{2})(\xi\xi^{*})^{2})}{S^{3}(1+\xi\xi^{*})^{2}}$$

$$K_{1.1} = \frac{8(\xi\xi^{*})^{3}(2s(2+\xi\xi^{*})-4S^{2}-(1+\xi\xi^{*})^{2})}{S^{3}(1+\xi\xi^{*})^{2}}$$

$$K_{2.0} = \frac{2\xi^{2}(12(1+\xi\xi^{*})^{2}-2S^{2}(\xi\xi^{*}(4+\xi\xi^{*})-1)+s(\xi\xi^{*}(4+13\xi\xi^{*})-13))}{S^{3}(1+\xi\xi^{*})^{2}}$$

$$K_{2.1} = \frac{4\xi^{4}(\xi^{*})^{3}(2S-1-\xi\xi^{*})}{S^{3}(1+\xi\xi^{*})}$$

$$K_{2.2} = -\frac{2(\xi\xi^{*})^{4}}{S^{3}}$$

$$K_{3.0} = \frac{2\xi^{3}(5-2S+(5+2S)\xi\xi^{*})}{S^{3}(1+\xi\xi^{*})}$$

$$K_{3.1} = 0$$

$$K_{4.0} = \frac{\xi^{4}}{S^{3}}$$

$$K_{i,j} = K_{j,i}^{*}$$

$$\dot{p}_{\Gamma^{(3)}} = -2\Gamma^{(3)} \left( \frac{2(1-\xi\xi^*)}{1+\xi\xi^*} p + \left(1 - \frac{1}{S}\right) \left(\xi \frac{\partial p}{\partial \xi} + \xi^* \frac{\partial p}{\partial \xi^*}\right) \right)$$

$$-\frac{(\xi\xi^*)^2}{S} \frac{\partial^2 p}{\partial \xi \partial \xi^*} - \frac{\xi^2}{2S} \frac{\partial^2 p}{\partial \xi^2} - \frac{(\xi^*)^2}{2S} \frac{\partial^2 p}{\partial (\xi^*)^2} \right)$$
(C.6)

Note, that the terms  $\dot{p}_{H_0}$  and  $\dot{p}_{\Gamma^{(3)}}$  are partial differential expressions of second order whereas  $\dot{p}_{\Gamma^{(1,2)}}$  are of fourth order.

**BIBLIOGRAPHY** 

### **Bibliography**

- [1] B. E. Kane, Nature **393**(6681), 133 (1998).
- [2] L. M. K. Vandersypen and I. L. Chuang, Rev. Mod. Phys. **76**(4), 1037 (2004).
- [3] K. R. Brown, A. W. Harrow, and I. L. Chuang, Phys. Rev. A 70(5), 052318 (2004).
- [4] L. Viola, J. Mod. Opt. **51**(16-18), 2357 (2004).
- [5] P. Facchi, S. Tasaki, S. Pascazio, H. Nakazato, A. Tokuse, and D. A. Lidar, Phys. Rev. A 71(2), 022302 (2005).
- [6] P. Sengupta and L. P. Pryadko, Phys. Rev. Lett. 95(3), 037202 (2005).
- [7] H. K. Cummins, G. Llewellyn, and J. A. Jones, Phys. Rev. A 67(4), 042308 (2003).
- [8] L. Landau, Phys. Z. Sowjetunion 2, 46 (1932).
- [9] C. Zener, Proc. R. Soc. London, Ser. A 137, 696 (1932).
- [10] G. Yusa, K. Muraki, K. Takashina, K. Hashimoto, and Y. Hirayama, Nature 434(7036), 1001 (2005).
- [11] M. N. Leuenberger and D. Loss, Phys. Rev. B 68(16), 165317 (2003).
- [12] E. M. Chudnovsky and L. Gunther, Phys. Rev. Lett. **60**(8), 661 (1988).
- [13] D. A. Garanin, J. Phys. A 24(2), L61 (1991).
- [14] A. Garg, Europhys. Lett. **22**(3), 205 (1993).
- [15] J. R. Friedman, M. P. Sarachik, J. Tejada, and R. Ziolo, Phys. Rev. Lett. 76(20), 3830 (1996).
- [16] J. R. Friedman, M. P. Sarachik, J. M. Hernandez, X. X. Zhang, J. Tejada, E. Molins, and R. Ziolo, J. Appl. Phys. 81(8), 3978 (1997).
- [17] D. A. Garanin and E. M. Chudnovsky, Phys. Rev. B 56(17), 11102 (1997).

- [18] W. Wernsdorfer and R. Sessoli, Science **284**(5411), 133 (1999).
- [19] A. Garg, Phys. Rev. Lett. **83**(21), 4385 (1999).
- [20] J. Villain and A. Fort, Eur. Phys. J. B 17(1), 69 (2000).
- [21] W. Wernsdorfer, M. Murugesu, and G. Christou, Phys. Rev. Lett. 96(5), 057208 (2006).
- [22] W. Wernsdorfer, Adv. Chem. Phys. 118, 99 (2001).
- [23] J. R. Friedman, Exploring the Quantum/Classical Frontier: Recent Advances in Macroscopic and Mesoscopic Quantum Phenomena (Nova Science, Huntington, NY, 2003), chap. Resonant Magnetization Tunneling in Molecular Magnets.
- [24] D. Gatteschi, R. Sessoli, and J. Villain, *Molecular Nanomagnets* (Oxford University Press, 2006).
- [25] A. Sieber, G. Chaboussant, R. Bircher, C. Boskovic, H. U. Güdel, G. Christou, and H. Mutka, Phys. Rev. B 70(17), 172413 (2004).
- [26] M. Evangelisti, A. Candini, A. Ghirri, M. Affronte, G. W. Powell, I. A. Gass, P. A. Wood, S. Parsons, E. K. Brechin, D. Collison, and S. L. Heath, Phys. Rev. Lett. 97(16), 167202 (2006).
- [27] H. J. Lipkin, N. Meshkov, and A. J. Glick, Nucl. Phys. 62(2), 188 (1965).
- [28] V. V. Ulyanov and O. B. Zaslavskii, Phys. Rep. 216(4), 179 (1992).
- [29] D. A. Garanin, X. M. Hidalgo, and E. M. Chudnovsky, Phys. Rev. B 57(21), 13639 (1998).
- [30] P. Ribeiro, J. Vidal, and R. Mosseri, Phys. Rev. Lett. 99(5), 050402 (2007).
- [31] D. M. Larsen and N. Bloembergen, Opt. Commun. 17(3), 254 (1976).
- [32] V. N. Sazonov and V. I. Finkelstein, Doklady Akad. Nauk Sssr 231(1), 78 (1976).
- [33] A. P. Dmitriev and M. I. Dyakonov, Zh. Eksp. Teor. Fiz. 90(4), 1430 (1986).
- [34] M. I. Dykman and M. V. Fistul, Phys. Rev. B 71(14), 140508 (2005).
- [35] P. W. Anderson and H. Suhl, Phys. Rev. 100(6), 1788 (1955).
- [36] H. Suhl, J. Phys. Chem. Solids 1(4), 209 (1957).
- [37] G. V. Skrotskii and Y. I. Alimov, Sov. Phys. JETP 9(4), 899 (1959).
- [38] D. J. Seagle, S. H. Charap, and J. O. Artman, J. Appl. Phys. 55(6), 2578 (1984).
- [39] G. Bertotti, C. Serpico, and I. D. Mayergoyz, Phys. Rev. Lett. 86(4), 724 (2001).

- [40] M. I. Dykman and M. A. Krivoglaz, *Soviet Physics Reviews* (Harwood Academic, New York, 1984), vol. 5, pp. 265–441.
- [41] I. Affleck, Phys. Rev. Lett. **46**(6), 388 (1981).
- [42] H. Grabert and U. Weiss, Phys. Rev. Lett. **53**(19), 1787 (1984).
- [43] A. I. Larkin and Y. N. Ovchinnikov, J. Stat. Phys. 41(3-4), 425 (1985).
- [44] R. Landauer, J. Appl. Phys. **33**(7), 2209 (1962).
- [45] A. D. Ventcel' and M. I. Freidlin, Uspehi Mat. Nauk 25(1), 3 (1970), ISSN 0042-1316.
- [46] M. I. Dykman and M. A. Krivoglaz, Zh. Eksp. Teor. Fiz. 77(1), 60 (1979).
- [47] R. Graham and T. Tél, J. Stat. Phys. **35**(5-6), 729 (1984).
- [48] A. J. Bray and A. J. McKane, Phys. Rev. Lett. 62(5), 493 (1989).
- [49] M. I. Dykman, Phys. Rev. A **42**(4), 2020 (1990).
- [50] R. S. Maier and D. L. Stein, Phys. Rev. E 48(2), 931 (1993).
- [51] R. L. Kautz, Rep. Prog. Phys. **59**(8), 935 (1996).
- [52] O. A. Tretiakov, T. Gramespacher, and K. A. Matveev, Phys. Rev. B 67(7), 073303 (2003).
- [53] M. J. Davis and E. J. Heller, J. Chem. Phys. **75**(1), 246 (1981).
- [54] E. J. Heller, J. Phys. Chem. A **103**(49), 10433 (1999).
- [55] M. Marthaler and M. I. Dykman, Phys. Rev. A **73**(4), 042108 (2006).
- [56] M. I. Dykman, Phys. Rev. E **75**(1), 011101 (2007).
- [57] M. I. Dykman and V. N. Smelyansky, Zh. Eksp. Teor. Fiz. **94**(9), 61 (1988).
- [58] M. Dykman and P. Platzman, Quantum Inf. Comput. 1, 102 (2001).
- [59] V. Benza and G. Strini, Fortschr. Phys. **51**(1), 14 (2003).
- [60] P. Platzman and M. I. Dykman, Science **284**(5422), 1967 (1999).
- [61] K. Saito and Y. Kayanuma, Phys. Rev. B **70**(20), 201304 (2004).
- [62] I. S. Gradshteyn and I. M. Ryzhik, *Table of Integrals, Series, and Products, 6th edition* (San Diego, CA: Academic Press, 2000).
- [63] V. N. Smelyanskiy, A. G. Petukhov, and V. V. Osipov, Phys. Rev. B 72(8), 081304 (2005).

- [64] L. D. Landau and E. M. Lifshitz, *Electrodynamics of Continuous Media* (Elsevier Butterworth-Heinemann, Oxford, 2004), second ed.
- [65] A. Garg and M. Stone, Phys. Rev. Lett. **92**(1), 010401 (2004).
- [66] L. D. Landau and E. M. Lifshitz, Quantum mechanics. Non-relativistic theory (Butterworth-Heinemann, Oxford, 1981), third ed.
- [67] A. P. Dmitriev and M. I. Dyakonov, JETP Lett. 44(2), 84 (1986).
- [68] C. Hicke and M. I. Dykman, Phys. Rev. B **76**(5), 054436 (2007).
- [69] M. N. Leuenberger and D. Loss, Phys. Rev. B **61**(2), 1286 (2000).
- [70] S. Bahr, K. Petukhov, V. Mosser, and W. Wernsdorfer, Phys. Rev. Lett. 99(14), 147205 (2007).
- [71] M. Bal, J. R. Friedman, W. Chen, M. T. Tuominen, C. C. Beedle, E. M. Rumberger, and D. N. Hendrickson, arXiv.org:0706.3471 (2007).
- [72] J. Guckenheimer and P. Holmes, Nonlinear Oscillators, Dynamical Systems and Bifurcations of Vector Fields (Springer-Verlag, New York, 1997).
- [73] J. Villain, F. Hartman-Boutron, R. Sessoli, and A. Rettori, Europhys. Lett. **27**(2), 159 (1994).
- [74] R. L. Melcher, in *Proceedings of the 1970 Ultrasonics Symposium* (IEEE, San Francisco, 1971), pp. 35–47.
- [75] R. G. Shulman, B. J. Wyluda, and P. W. Anderson, Phys. Rev. 107(4), 953 (1957).
- [76] E. F. Taylor and N. Bloembergen, Phys. Rev. **113**(2), 431 (1959).
- [77] Y. Izyumov, Proc. Phys. Soc. 87, 505 (1966).
- [78] M. A. Krivoglaz and L. B. Kvashnina, Phys. Stat. Sol. 29(1), 53 (1968).
- [79] A. Magni, G. Bertotti, C. Serpico, and I. D. Mayergoyz, J. Appl. Phys. 89(11), 7451 (2001).
- [80] G. Bertotti, I. Mayergoyz, and C. Serpico, J. Appl. Phys. 95(11 II), 6598 (2004).
- [81] C. Serpico, M. d'Aquino, G. Bertotti, and I. D. Mayergoyz, J. Appl. Phys. 95(11), 7052 (2004).
- [82] E. C. Stoner and E. P. Wohlfarth, Phil. Trans.Roy. Soc. A 240(826), 599 (1948).
- [83] C. Hicke and M. I. Dykman, in preparation.
- [84] J. M. Radcliff, J. Phys. A 4(3), 313 (1971).

- [85] F. T. Arecchi, H. Thomas, R. Gilmore, and E. Courtens, Phys. Rev. A 6(6), 2211 (1972).
- [86] C. Aragone, E. Chalbaud, and S. Salamo, J. Math. Phys. **17**(11), 1963 (1976).
- [87] G. Vetri, J. Phys. A 8(6), L55 (1975).
- [88] M. I. Dykman, G. P. Golubev, D. G. Luchinsky, P. V. E. McClintock, N. D. Stein, and N. G. Stocks, Phys. Rev. E **49**(3), 1935 (1994).

MICHIGAN STATE UNIVERSITY LIB